

https://dspace.org/

The analysis of shaft voltages in a synchronous generator with various induced faults

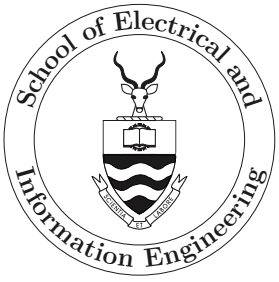
de Canha, Daniel

2012-07-19
http://hdl.handle.net/10539/11703

Downloaded from a DSpace repository. https://dspace.org/

The Analysis of Shaft Voltages in a Synchronous Generator with Various Induced Faults

Daniel de Canha



A dissertation submitted to the Faculty of Engineering and the Built Environment, University of the Witwatersrand, Johannesburg, in fulfilment of the requirements for the degree of Master of Science in Engineering.

Johannesburg, 2008

Declaration

I declare that this dissertation is my own, unaided work, except where otherwise acknowledged. It is being submitted for the degree of Master of Science in Engineering in the University of the Witwatersrand, Johannesburg. It has not been submitted before for any degree or examination in any other university.

Signed this ____ day of _____ 20__

_____

Daniel de Canha

Abstract

Axial shaft voltages have been investigated as a condition monitoring tool for turbo-generators. It was found that static air-gap eccentricity in a 20 kW, 2 pole synchronous generator, which was designed and built to mimic a larger 660 MW set, can be diagnosed using the shaft voltage. The shaft voltage in this experimental alternator has been simulated using 2D finite elements method (FEM) software. This software has been used to explain some of the causes of the shaft voltage in this generator. It was confirmed that shaft signals are primarily caused by constructional asymmetries. The FEM software has also been used to study the effects of various faults on the shaft voltage in a time efficient manner. These faults should be investigated experimentally in future work.

Acknowledgements

I wish to thank my supervisor Prof. Willie Cronje and Alan Meyer for their advice and support in all manners and forms. My predecessor on this project, Simon Hoffe, who gave me as good a start as one could hope for, also deserves my gratitude. Most of all I want to thank my family for their tremendous support during my now, much extended varsity years.

Contents

Declaration i

Abstract ii

Acknowledgements iii

Contents iv

List of Figures x

List of Tables 1

1 Introduction 3

1.1 Project Background 3

1.2 Dissertation Overview 5

2 Miniature Synchronous Generator 7

2.1 Introduction 7

2.2 Access to phase groups 7

2.3 Current Transformers 8

2.4 Circulating Currents 10

2.5 Air gap measurement and correction 11

2.6 Search Coils 12

2.7 Conclusion 14

3 FEM Model Construction Using Maxwell 2D 16

3.1 Introduction 16

3.2 Background 16

3.3 Drawing the mini-gen in 2D 17

3.4 Materials Setup 26

3.5 Boundaries 27

3.6 Sources 27

3.6.1 Stranded vs. Solid Sources 28

3.6.2 External Connections 28

3.7 Solver Setup 31

3.7.1 Mesh Setup 31

3.7.2 Motion Setup 32

3.7.3 Time Step Setup 33

3.8 Simulation Outputs 33

3.8.1 Open and Short Circuit Characteristics 33

3.8.2 Search Coils 34

3.8.3 Field Plots 35

3.8.4 Time Stamped Data 35

3.9 Conclusion 37

4 Effect of the Mesh on the Shaft Voltage **38**

4.1 Introduction 38

4.2 User Generated Meshes 39

4.2.1 Object Refinement 39

4.2.2 Using Dummy Objects as Meshing Aids 41

4.3 Automatically Generated Meshes 41

4.4 Curvilinear Mesh 44

4.5 Effect of Time Step 47

4.6 Measured Shaft Voltage 47

4.7 Conclusion 48

5 Causes of the Shaft Voltage **49**

5.1 Introduction 49

5.2 Stator Asymmetries 50

5.2.1 Weld recesses and key way 50

5.3 Rotor Asymmetries 53

5.3.1 Effect of a missing damper bar 53

5.3.2 Rotor with distorted/wrong size slots 53

5.4 Shaft based search coil 55

5.5 Conclusion 55

6 Further Investigations into Eccentricity **57**

6.1 Introduction 57

6.2 Effect of eccentricity on the shaft voltage 58

6.2.1 Simulated Shaft Voltage 58
6.2.2 Measured Shaft Voltage 59
6.3 Circulating currents and eccentricity 59
6.4 Vibrations and eccentricity 62
6.4.1 Axial vibrations 62
6.4.2 Radial Vibrations 63
6.5 Conclusion 63

7 Simulation Based Fault Study **66**

7.1 Introduction 66
7.2 Field Faults 66
7.2.1 Simulation Techniques 66
7.2.2 Effect of inter-turn shorts on the shaft voltage 68
7.2.3 Effect of a single earth fault on the shaft voltage 72
7.2.4 Inducing field winding faults in the mini-gen 72
7.3 Exciter Faults 75
7.4 Armature Faults 75
7.4.1 Earth Faults 76
7.4.2 Phase Group Open Circuit 77
7.5 Conclusion 77

8 Migrating from Maxwell to Flux **81**

8.1 Introduction 81
8.2 Geometry 83

8.3 Mesh 83
8.4 Physics 87
8.5 Solver 87
8.6 Results 87
8.7 Conclusion 89

9 Conclusion **91**

9.1 Recommendations for further work 91
9.1.1 Faults to be investigated 91
9.1.2 Signal Processing 92
9.1.3 FEM Simulations 92
9.1.4 Mini-gen Lab Setup 93
9.1.5 Shaft Signals 94
9.2 Major Outcomes 94

A Laboratory Setup Modifications **96**

A.1 Earthing Resistor 96

B Series Star Configuration **97**

C Measurement of Load Angle **101**

D Additional useful information for Maxwell **103**

D.1 Maxwell File Types 103
D.2 Simulation Times 103

E MATLAB files **105**

E.1 Introduction 105

E.2 Computing and plotting FFTs 105

E.3 Analysing circulating currents 106

E.4 Plotting graphs for publishing 108

References **111**

List of Figures

2.1 Miniature turbo generator on the test bed with driving motor, fan, and auto-transformer adjusted load 8

2.2 Current transformers used to measure the phase group currents with shunt resistors and low pass filter circuit 9

2.3 Experimental setup for CT evaluation 10

2.4 Signal conditioning circuit for the current transformers 10

2.5 Parallel star connection of the armature phase groups 11

2.6 The rotor with sections of resi-glass removed near the ends of the core to allow for a direct air gap measurement 12

2.7 Bolts in the stator supports are used to adjust the alignment of the stator relative to the rotor 13

2.8 Location of search coils 13

2.9 Location of one search coil in the stator 14

2.10 Two search coils in the grooves of the stator teeth with twisted leads 14

2.11 The two search coils at the opposite end of the core 14

2.12 Anti-aliasing filter and protection circuit used when connected to dSpace 15

2.13 PCB for search coil filter connected to a shielded cable 15

3.1 Completed 2D drawing of the generator in Maxwell's 2D Modeller . 17

3.2 Mesh generated with the quadtree seeding algorithm with a seed value of 6 18

3.3 Possible drawing planes for Maxwell 2D 18

3.4 Drawing showing dimensions of the rotor of the mini-generator . . . 19

3.5 Drawing showing dimensions of the stator of the mini-generator . . . 20

3.6 Photo of the rotor during construction with empty slots 20

3.7 Photo of the rotor during construction with field winding 21

3.8 Photo of the stator during construction with casing 21

3.9 Cross section of the mini-generator 23

3.10 (a) Casing and outer part of stator with shapes for weld recesses and keyway, (b) subtraction of shapes in (a), (c) first shape for inner part of stator 24

3.11 (a) Shapes for stator slots , (b) Shapes in (a) duplicated & first coils added for armature winding , (c) complete armature winding showing phase groups 25

3.12 (a) Round shape for rotor with cut-outs for packing and dampers, (b) subtraction of shapes in (a) also showing damper bars, (c) completed rotor with field winding 25

3.13 Location of one search coil in the 2D model 25

3.14 External SPICE circuit showing armature, shaft voltage and search coil windings 29

3.15 Open Circuit Characteristic 34

3.16 Short Circuit Characteristic 34

3.17 Simulated search coil voltage 35

3.18 Measured search coil voltage 35

3.19 Magnetic Flux Density (T) field plot 36

4.1 Mesh generated by refining each object individually - user1 39

4.2 Number of elements for the larger objects 40

4.3 Number of elements for the smaller objects 40

4.4 Dense manually refined mesh - user2 42

4.5 Mesh generated with dummy objects and individual object refinement - dummy 42

4.6 Calculated shaft voltage waveform using a manually refined mesh - user1 43

4.7 Calculated shaft voltage frequency spectrum using a user refined mesh - user1 43

4.8 Calculated shaft voltage waveform using a dense manually refined mesh - user2 43

4.9 Calculated shaft voltage frequency spectrum using a dense manually refined mesh - user2 43

4.10 Calculated shaft voltage waveform using a mesh generated with dummy objects - dummy 43

4.11 Calculated shaft voltage frequency spectrum using a mesh generated with dummy objects - dummy 43

4.12 Calculated shaft voltage waveform using a mesh generated from the quadtree 6 algorithm - qt6 43

4.13 Calculated shaft voltage frequency spectrum using a mesh generated from the quadtree 6 algorithm - qt6 43

4.14 Mesh generated using the quadtree 6 algorithm - qt6 45

4.15 Mesh generated using the quadtree 8 algorithm - qt8 45

4.16 Calculated shaft voltage waveform using a mesh generated from the quadtree 8 algorithm - qt8 46

4.17 Calculated shaft voltage frequency spectrum using a mesh generated from the quadtree 8 algorithm - qt8 46

4.18 Calculated shaft voltage waveform using a curvilinear mesh generated from the quadtree 6 algorithm - qt6cl 46

4.19 Calculated shaft voltage frequency spectrum using a curvilinear mesh generated from the quadtree 6 algorithm - qt6cl 46

4.20 Calculated shaft voltage waveform using a 0.2 ms time step - qt6ls . 46

4.21 Calculated shaft voltage frequency spectrum with a 0.2 ms time step - qt6ls 46

4.22 Measured shaft voltage waveform 46

4.23 Measured shaft voltage frequency spectrum 46

5.1 Cross section of the synchronous generator showing key way, weld recesses, missing damper and shaft based search coil 51

5.2 Simulated shaft voltage with no key way or weld recesses (note the voltage scale) 52

5.3 Simulated shaft voltage with weld recesses but no key way 52

5.4 Simulated shaft voltage with a key way but no weld recesses 52

5.5 Simulated shaft voltage with a key way and weld recesses 52

5.6 Measured shaft voltage 52

5.7 Simulated shaft voltage frequency spectrum with a key way and weld recesses 52

5.8 Measured shaft voltage frequency spectrum 52

5.9 Simulated shaft voltage frequency spectrum with a key way, weld recesses and a missing damper bar 52

5.10 Upon removal of part of the resi-glass covering on the rotor, a slot without a damper bar and various other slot distortions were discovered 54

5.11 Shaft voltage with a missing damper in a slot which is 1mm too narrow 55

5.12 Shaft voltage with a missing damper in the narrow slot and one slot which is 1mm too wide 55

5.13 Simulated voltages from the shaft based search coil and from the shaft-case based 'winding' 56

6.1 Static eccentricity where the axes of symmetry of the stator and rotor are offset but parallel 58

6.2 Simulated shaft voltage frequency spectrum with no eccentricity . . 60

6.3 Simulated shaft voltage frequency spectrum with 0.3 mm eccentricity 60

6.4 Simulated shaft voltage frequency spectrum with 0.6 mm eccentricity 60

6.5 Simulated shaft voltage frequency spectrum with 0.9 mm eccentricity 60

6.6 Measured shaft voltage frequency spectrum with no eccentricity . . . 60

6.7 Measured shaft voltage frequency spectrum with 0.3 mm eccentricity 60

6.8 Measured shaft voltage frequency spectrum with 0.6 mm eccentricity 60

6.9 Measured shaft voltage frequency spectrum with 0.9 mm eccentricity 60

6.10 Parallel star connection of armature phase groups showing path for circulating currents 61

6.11 Placement of the vibration probes to measure radial and axial vibrations on the drive end bearing 62

6.12 Measured axial vibration frequency spectrum with no eccentricity . . 64

6.13 Measured axial vibration frequency spectrum with 0.3 mm eccentricity 64

6.14 Measured axial vibration frequency spectrum with 0.6 mm eccentricity 64

6.15 Measured axial vibration frequency spectrum with 0.9 mm eccentricity 64

6.16 Measured radial vibration frequency spectrum with no eccentricity . 64

6.17 Measured radial vibration frequency spectrum with 0.3 mm eccentricity 64

6.18 Measured radial vibration frequency spectrum with 0.6 mm eccentricity 64

6.19 Measured radial vibration frequency spectrum with 0.9 mm eccentricity 64

7.1 Maxwell 2D external circuit including the field winding 69

7.2 Boundaries and Sources editor in Maxwell 2D showing how the field coils are split up to simulate an inter-turn short in the top slots of the rotor 70

7.3 Boundaries and Sources editor in Maxwell 2D showing how the field coils are split up to simulate an inter-turn short in the middle slots of the rotor 70

7.4 Maxwell 2D external circuit showing how an inter-turn short is induced in the field winding 71

7.5 Maxwell 2D external circuit showing how 2 inter-turn shorts are induced in the field winding 71

7.6 Maxwell 2D external circuit showing how a short between the field winding and the shaft (earth) is simulated 71

7.7 Shaft Voltage with the Field Winding excited by a voltage source in the winding editor 73

7.8 Shaft Voltage with the Field Winding excited by a current source in the external circuit 73

7.9 Shaft Voltage with one inter-turn short in the field winding in the 1st rotor slot 73

7.10 Shaft Voltage with one inter-turn short in the field winding in the middle rotor slot 74

7.11 Shaft Voltage with two inter-turn shorts in the field winding in the middle rotor slot 74

7.12 Shaft Voltage with a short between the field winding in the middle rotor slot and earth 74

7.13 Insulation on the outermost rotor coils in the field winding overhang was deliberately removed during construction to allow for inter-turn shorts to be induced in the mini-gen 75

7.14 Maxwell 2D circuit with phase C partially separated into individual coils and a short between the first coil and earth 78

7.15 Maxwell 2D circuit showing how an earth fault is simulated in Phase A by separating the coils into various groups and connecting an individual coil from the 4th slot to earth 79

7.16 Shaft voltage frequency spectrum with an earthing resistor placed on the star point of the armature winding 80

7.17 Shaft voltage frequency spectrum with a short to earth in the 1st slot of Phase group A1 80

7.18 Shaft voltage frequency spectrum with a short to earth in the 4th slot of Phase group A1 80

7.19 Shaft voltage frequency spectrum with a phase group open circuited 80

8.1 Comparison of Maxwell 2D and Flux 2D model creation 82

8.2 Flux 2D mesh 1 showing areas with very high element densities such as the air gap and stator teeth 85

8.3 Flux 2D mesh 1. Important mesh lines which divide the stator and rotor into segments are highlighted in yellow 85

8.4 Flux 2D mesh 2, obtained by reducing the number of mesh points on the mesh lines as highlighted 86

8.5 Flux 2D mesh 3, obtained by further reducing the number of mesh points on the mesh lines as highlighted 86

8.6 Maxwell 2D shaft voltage time and frequency signals 90

8.7 Flux 2D shaft voltage time and frequency signals using mesh 1 (dense) 90

8.8 Flux 2D shaft voltage time and frequency signals using mesh 2 . . . 90

8.9 Flux 2D shaft voltage time and frequency signals using mesh 3 (sparse) 90

8.10 Measured shaft voltage time and frequency signals 90

A.1 Armature in parallel star with an earthing resistor 96

B.1 Armature in series star 97

B.2 Armature in parallel star 98

B.3 Parallel star connection 98

B.4 Series star connection 98

B.5 Phase group winding conventions 99

B.6 Open Circuit Characteristic 100

B.7 Short Circuit Characteristic 100

C.1 Setup for load angle measurement 102

C.2 Waveform displayed on scope 102

List of Tables

2.1 Shunt resistor values and current ranges for phase group CTs 9

2.2 Circulating currents with the misaligned air gap and once the air gap had been corrected 10

3.1 Miniature Synchronous Generator Ratings 22

3.2 Table of Materials assigned to different objects in 2D Model 26

4.1 Details of various meshes and simulation times in Maxwell 2D 40

5.1 Shaft voltage with combinations of the weld recesses and key-way . . 53

5.2 Shaft RMS voltages for simulations with differently distorted rotor slots 54

6.1 Simulated shaft RMS voltages with various eccentricities 58

6.2 Measured shaft RMS voltages with various eccentricities 59

6.3 Measured circulating current in **Amperes** (A) with no load 61

6.4 Simulated **percentage** (%) circulating current on full load 61

6.5 Measured **percentage** (%) circulating current on full load 62

7.1 Shaft and Phase voltages for simulations with various field winding faults 68

7.2 Simulated shaft voltages and earth currents with various armature faults 77

8.1 Simulated Shaft and Phase RMS voltages from different meshes in Flux 88

B.1 Series and parallel Y operating conditions 99

Chapter 1

Introduction

1.1 Project Background

Axial shaft voltages in rotating machines are unavoidable and are known to cause damaging bearing currents. A great deal of work has been performed on understanding their causes and mitigating their effects or preventing them to some extent [1–4].

The most common technique used to prevent currents flowing through the bearings, is to ground the shaft using a suitable conductive brush which rides on the shaft as it rotates. In this way any shaft currents will tend to flow through the low impedance of shaft grounding system rather than through the bearings.

Shaft voltages are of particular concern in large steam driven turbo-generators such as those used by Eskom in the majority of its power stations. Electrostatic charge builds up on the shaft due to the friction between the steam and turbine. If this charge is allowed to accumulate there is a chance that it will discharge through the bearings. This is in addition to any shaft voltage which exists due to constructional asymmetries or faults in the machine. Thus proper grounding of these machines is critical [5].

The turbo-generator sets in Eskom's power stations have comprehensive online condition monitoring systems which help to ensure their high availability and safe operation. Rather than viewing shaft voltages as a nuisance, Eskom wishes to add a shaft signal measurement to their monitoring systems with the belief that shaft signals can provide information about the health of the machine.

Some researchers share this belief and have investigated shaft signals as a diagnostic

tool for rotating machines. In fact there are several patents on monitoring systems using shaft voltages and currents [6–10] for many different types of machines.

These documents are limited in the scientific explanation of shaft voltages. The data published in these patents suggests that a phenomenological approach has been taken. If a machine is known to have a certain fault and a unique signature is obtained from the shaft voltage then the patent holders have noted it and included this intelligence in a monitoring system. They offer no explanation of why the unique signature was found in the first place. This research aims to develop a model of shaft voltages from first principles.

As far as synchronous machines are concerned, there is recent work which has investigated shaft signals as a diagnostic tool.

Torlay et al [11–13] have reported success in using a 2D FEM simulation package to simulate field winding short circuits and eccentricities on small (30 kVA) and large (1300 MW) synchronous machines. Correlations between the simulations and measured data were observed. The machines investigated were four pole machines while two pole machines are of interest in this research. There were discrepancies between simulations and results which weren't accounted for and not all the claimed results were presented. Hence there is a lack of applicability to machines of interest here and a need for verification of results.

Other authors [14–18] have also investigated shaft voltages. These works have focused on salient pole machines or machines with more than 2 poles. This work distinguishes itself in that it is an investigation into using shaft voltages for fault diagnosis in a 2 pole non-salient generator.

It is not possible to perform fault studies on the type of machines in question (660 MW turbo-generators) so a much smaller generator has been designed and built for this purpose (the mini-gen). It is designed to allow for the types of faults which occur commonly in the larger sets to be easily induced in it.

A measurement system geared to measuring the shaft voltage on this generator was implemented by Hoffe and an investigation into using the shaft voltage to diagnose eccentricity was conducted by him in [5]. After the completion of Hoffe's masters when access to the parallel connected armature phase groups was made possible, large circulating currents were discovered. Therefore the goals of this research project are to:

- Determine the cause of the circulating currents in the mini-gen armature winding
- Reduce the circulating currents in the armature winding to an acceptable level so as to allow the project to continue with new fault investigations with a healthy machine
- Confirm that static eccentricity can still be diagnosed in the mini-gen once the circulating currents have been reduced
- Determine if static eccentricity can be diagnosed using vibrations or armature currents
- Improve the understanding of the causes of the shaft signals

The way in which these objectives are dealt with in the dissertation is expanded upon below.

1.2 Dissertation Overview

Chapter 2: A brief description of the mini-gen and its dSPACE based measurement system is given. Various improvements have been made to the mini-gen and its laboratory setup. The mini-gen was thought to be in perfect operating condition until circulating currents were discovered in the armature winding. The causes and reduction of these circulating currents are among the various improvements presented.

Chapter 3: A FEM model of the mini-gen, using Maxwell 2D, is described in a format which can be used as a guide for setting up similar 2D FEM models. An evaluation of the outputs of the FEM application is also provided. This section is loosely based on the work presented at a SAUPEC conference [19].

Chapter 4: Various simulations with different meshes were run and evaluated in terms of which gives an acceptably realistic shaft voltage in the least amount of time, this chapter is based on [20].

Chapter 5: It is shown that with the aid of the FEM model, some of the causes of the shaft voltage in this machine can be explained. The work in [21] is drawn upon and supplemented here.

Chapter 6: Eccentricity has be investigated again even though it was dealt with in [5], by Hoffe. Rather than looking at large static eccentricities it was decided that small eccentricities should be induced and the effect on not just the shaft voltage but vibrations and circulating armature currents should be observed. This chapter was also presented as a conference paper [22].

Chapter 7: A simulation based fault study was conducted with some of the more common turbo-generator faults and the predictions of the simulations are discussed with a view to future work.

Chapter 8: Similarly to Chapter 3, this penultimate chapter documents how the mini-gen model was simulated in Flux (the research groups new FEM package). A comparison between the two FEM applications is given and they are evaluated in terms of which has the most accurate shaft voltage. Additionally it is a useful aid to those migrating from Maxwell to Flux.

Chapter 9: Finally recommendations for further work and the main findings of the project are summarised in this, the concluding chapter.

The Appendix includes the MATLAB code which was used to calculate and plot the FFTs in this dissertation and some other useful functions for calculating phase angles and plotting graphs. There is also some information on running the generator in a series star configuration as opposed to parallel star and measurement of the load angle.

Chapter 2

Miniature Synchronous Generator

2.1 Introduction

A large part of the commissioning of the mini-gen and its supporting laboratory setup, shown in Figure 2.1, were completed by Hoffe and what were thought to be some minor improvements were suggested [5]. The most important of these suggestions was the breaking out of the armature terminals to allow access to all the parallel connected phase groups. This modification led to a number of improvements in the measurement capability of the lab setup with the addition of current transducers for each phase group. The subsequent measurements revealed a flaw in the mini-gen construction. The discovery and solution to this problem are presented in this chapter.

2.2 Access to phase groups

It was thought that it would be desirable to measure circulating currents to confirm results from simulations of static eccentricity and for other faults which could cause circulating currents. Therefore individual phase group terminals were broken out and made available on a break-out board as can be seen in Figure 2.1.

The break-out board allows one to change between series or parallel star and delta connections as well as providing access to the neutral point. Connections for series-Y and parallel-Y are provided in Appendix A with the phase group naming conventions.

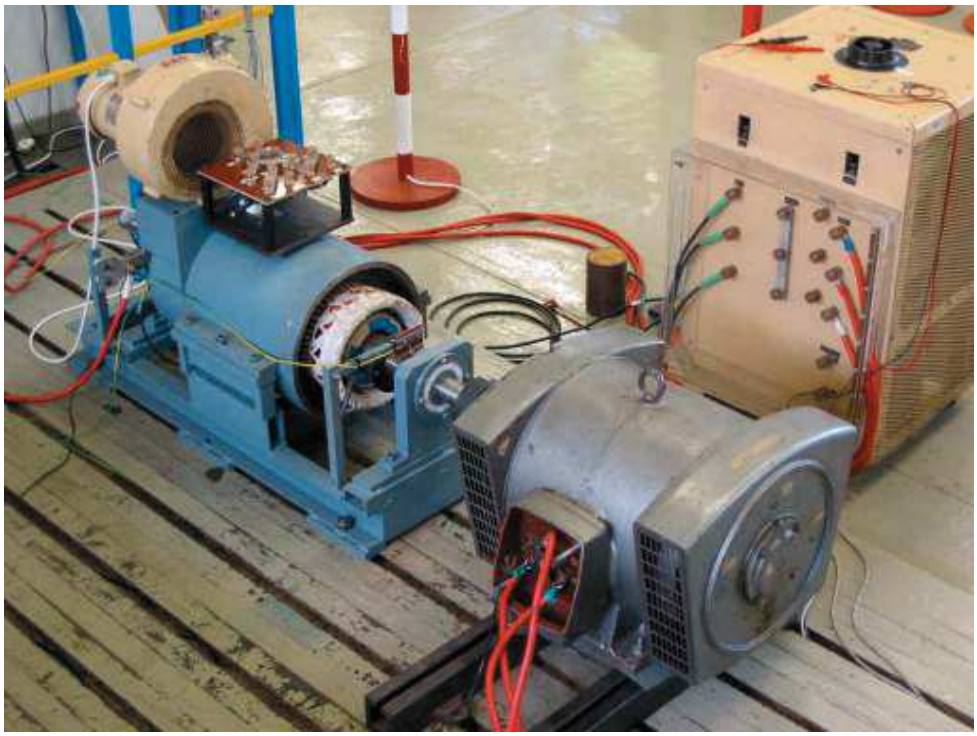


Figure 2.1: Miniature turbo generator on the test bed with driving motor, fan, and auto-transformer adjusted load

2.3 Current Transformers

Once the phase group terminals were made accessible a means of measuring all the phase group currents simultaneously was required. Rather than using several expensive Tektronix probes current transformers were bought and evaluated. There are numerous other current sensing technologies available such as hall effect sensors or shunt resistors but the current transformers provide isolation, require no power supplies, are low cost and relatively accurate at low frequencies. In terms of observing circulating currents the fundamental will be of the most interest. Some faults may have an effect on the small higher frequencies in the current waveforms but they can always be observed in one phase group with a more accurate instrument.

The current transformers are photographed in Figure 2.2 and were compared with a Tektronix probe on a resistive load supplied through a line impedance stabilisation network (LISN) as in Figure 2.3. The LISN reduces the noise from the mains which is important when trying to measure the phase angle between 2 signals. The current transformers are connected to the signal conditioning circuitry in Figure 2.2 which simply consists of a set of selectable shunt resistors and a low pass filter as can be

seen in Figure 2.4. The current ranges in which each shunt resistor should be used are tabulated in 2.1. The output from the current transformers was recorded on the 16 bit ADC channels of the dSpace system along with that of the reference probe. The captured data was analysed in Matlab using the functions in the appendix to calculate the phase and gain errors for different current magnitudes and shunt resistor selections. The maximum magnitude and phase errors were found to be 2.25% and 4°for the 4.5A→33A range relative to the Tektronix probe. The CTs produce very similar errors with maximum phase and magnitude errors between any two CTs of 1% and 0.2°respectively, allowing for circulating currents to be calculated accurately. Finally it was verified that the CTs do not pick up significant stray flux once placed around the phase group leads. They were sized for the wire dimensions of these external leads.

It would have been advisable to determine the impulse response of the current transformers so as to compensate for it using the dSpace system but given the time constraints for determining the effect of eccentricity on the parallel phase group connections it was decided that measuring the fundamental accurately was sufficient for detecting circulating currents.

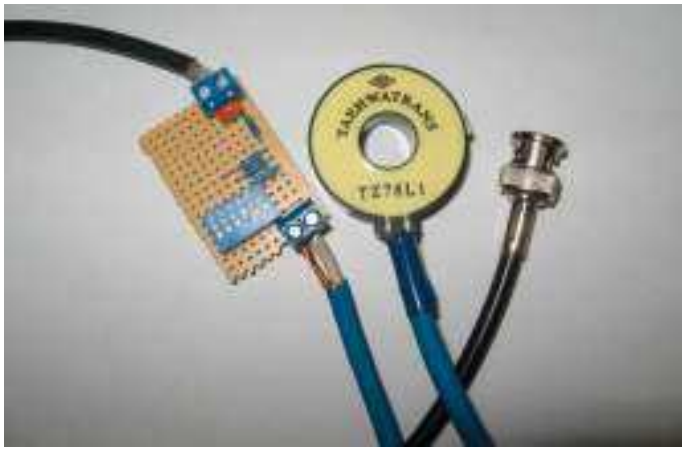


Figure 2.2: Current transformers used to measure the phase group currents with shunt resistors and low pass filter circuit

Table 2.1: Shunt resistor values and current ranges for phase group CTs

Shunt (Ω)	Current Range	dSpace scaling factor
82	33 A → 190 A	305
510	4.5 A → 33 A	49
3600	150 mA → 4.5 A	6.94

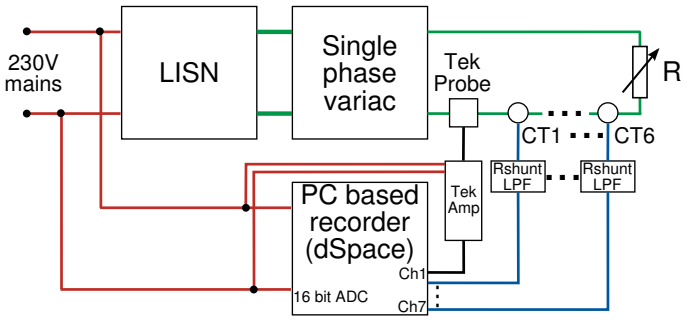


Figure 2.3: Experimental setup for CT evaluation

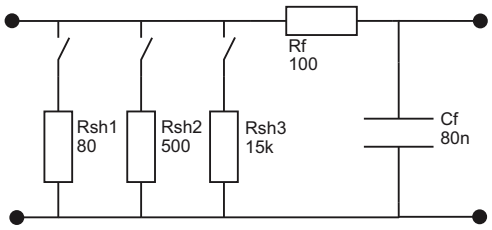


Figure 2.4: Signal conditioning circuit for the current transformers

2.4 Circulating Currents

The mini-gen is designed to be misaligned easily so that the effect of static eccentricity on the shaft voltage could be investigated as a proof of concept for the project. To our surprise I discovered that large circulating currents were present in the mini-gen in what was meant to be the aligned configuration. Table 2.2 gives the percentage circulating current and phase differences for the phase group currents with the generator on full load.

Table 2.2: Circulating currents with the misaligned air gap and once the air gap had been corrected

	Phase A		Phase B		Phase C	
Air Gap	%	ϕ	%	ϕ	%	ϕ
mis-aligned	23	-9°	27	-18°	30	-33°
corrected	2.94	4°	4.92	5°	3.97	3°

Instead of suspecting the obvious, that a static eccentricity was present, it was suspected that there was something wrong with the armature winding and numerous tests were carried out to determine if there was anything obviously at fault. The phase group resistances, inductances and impedance to earth were measured but were found to be very similar to one another and no obvious faults could be found.

Furthermore on disconnecting the phase groups from one another and leaving them each individually open circuited it was found that the phase voltages were approximately equal and in phase. Eventually it was suspected that perhaps the machine had not been aligned as well as was thought and that the air gap had to be measured to confirm this.

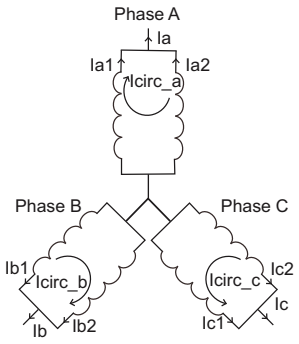


Figure 2.5: Parallel star connection of the armature phase groups

2.5 Air gap measurement and correction

The resi-glass covering of the rotor prevents a direct measurement of the air gap. Furthermore the uneven surface of the resi-glass makes it impossible to measure the air gap accurately. The most workable solution was to remove small sections so that a measurement of the air gap between the rotor and stator cores could be made. We were loathe to do this though, considering that removing sections of the resi-glass could compromise its integrity. Once it was verified that the rotor fits on one of the lathes in the workshop we went ahead and removed a section of resi-glass on either end of the rotor core without damaging the remaining parts. Figure 2.6 shows the rotor with the strips of resi-glass removed.

Upon reassembly of the machine it was found that there was indeed a static eccentricity and the positioning of the bolts which mount the stator to the frame were incorrectly positioned. Figure 2.7 shows the modifications which were made to the stator supports to adjust the alignment of the stator relative to the rotor which remains fixed. Four holes were drilled and tapped in the stator supports, two vertical and two horizontal on either side of the machine. This allows for both horizontal and vertical correction of the air gap. The misalignment was approximately 0.3 mm vertical and 0.05 mm horizontal. It is interesting to note that such large circulating currents were present with only 5% eccentricity. Table 2.2 shows the large reduction in circulating currents once the air gap is corrected. The percentage circulating

current is still not zero but is very low on full load. The circulating current is higher on high impedance loads because the internal resistance of the phase groups provides a path of comparably lower resistance than when a low impedance load is connected, so more current circulates rather than flows into the load. The effect of small static eccentricities such as this one on the shaft voltage and phase group currents is discussed further in Chapter 6.

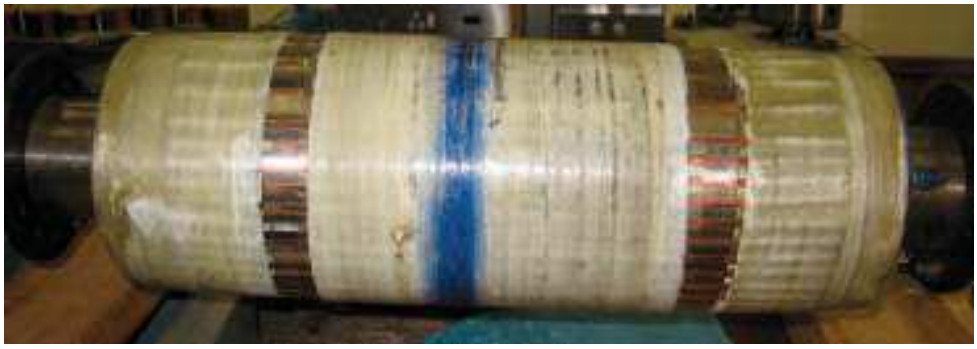


Figure 2.6: The rotor with sections of resi-glass removed near the ends of the core to allow for a direct air gap measurement

2.6 Search Coils

It was decided that it would be interesting to determine how the flux distribution in the mini-gen changes when a fault is present. Twelve single turn search coils were placed with a pitch of 30°along the grooves of the stator teeth for this purpose. Figure 2.8 shows the locations and labelling of the search coils. Figure 2.9 shows the location of a single search coil.

Figures 2.10 and 2.11 are photos showing how the search coils were placed in the stator. PVC insulated wire of 1 mm diameter is used. The wire is held in place by the slot wedges. The search coil leads were twisted before being connected to dual core shielded cables, to prevent noise pickup. The cables are routed around the outside of the winding overhangs and held in place with cable ties before they exit the machine through a hole in the end shield.

The shielded cables from the machine are connected to an anti-aliasing filter before being connected to the dSpace system. The circuit in Figure 2.12 includes a low-pass filter with a cut-off frequency of approximately 4.8 kHz and zener diodes and a fuse to clamp the voltage at 10 V to protect the dSpace system. The circuit boards use surface mount components to keep loop areas to a minimum and include a BNC



Figure 2.7: Bolts in the stator supports are used to adjust the alignment of the stator relative to the rotor

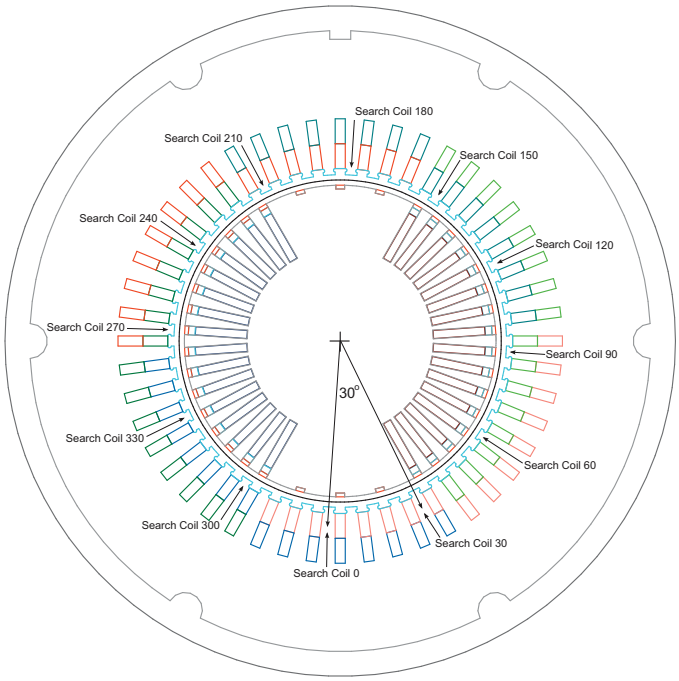


Figure 2.8: Location of search coils

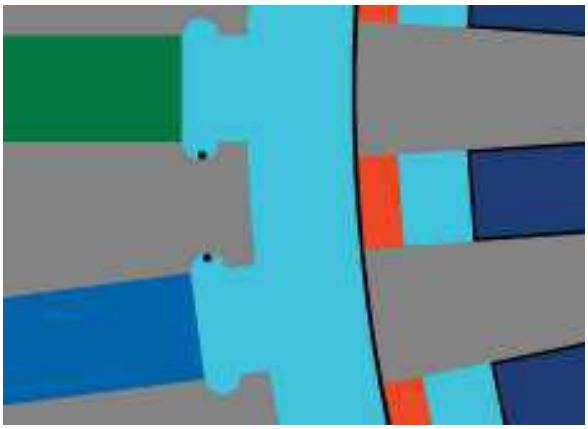


Figure 2.9: Location of one search coil in the stator



Figure 2.10: Two search coils in the grooves of the stator teeth with twisted leads



Figure 2.11: The two search coils at the opposite end of the core

connector for direct connection to the dSpace break out box. The shields of the cables are grounded at the dSpace end as can be seen in the diagram. Figure 2.13 shows the PCBs with the filter circuit. The waveforms obtained from the search coils have been measured and simulated in Maxwell 2D and are presented in Chapter 3 although they were not used to aid in diagnosing faults or for measuring the air gap flux due to the time constraints of the project. It is hoped that future work will make better use of this capability.

2.7 Conclusion

The misaligned air gap was an unacceptable fault that came about during manufacture but it has been corrected and the levels of circulating currents are acceptable.

The addition of the current transformers and search coils provides extra measurement capability which may help with future investigations into various faults.

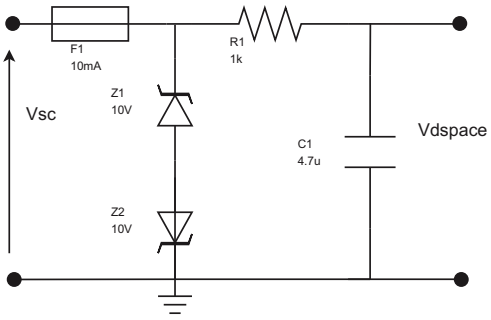


Figure 2.12: Anti-aliasing filter and protection circuit used when connected to dSpace

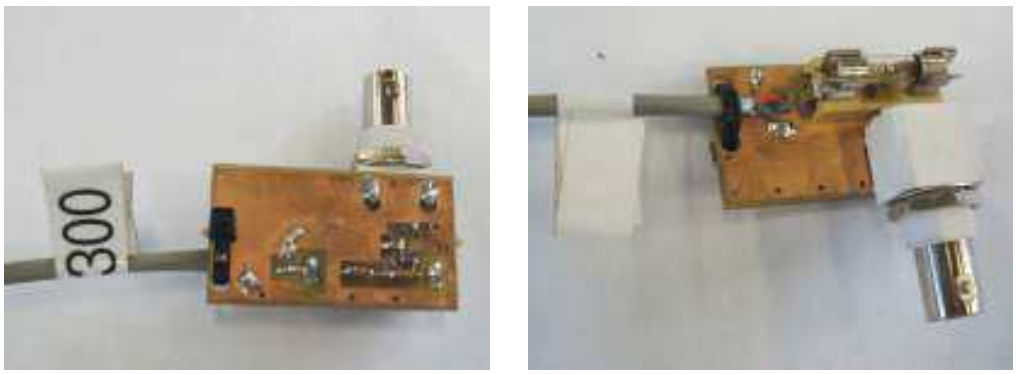


Figure 2.13: PCB for search coil filter connected to a shielded cable

Chapter 3

FEM Model Construction Using Maxwell 2D

3.1 Introduction

Being able to simulate the shaft voltage has proved extensively useful for investigating faults and for discovering the causes of the shaft voltage in the mini-gen.

This chapter documents how this FEM model of the mini-gen was created using Maxwell 2D [23]. In this way the chapter also serves as a tutorial for the transient solver in Maxwell 2D.

It is not necessary to have an in depth knowledge of the theory behind the FEM for electro-magnetics, as described in [24], to use Maxwell 2D. This detail is hidden, so as to allow the user to solve a wide range of field problems from first principles which would be difficult to solve by hand.

It is assumed that the reader has performed the tutorials available on the Maxwell website [25, 26] or has some experience using Maxwell and wants to learn how to create a transient model.

3.2 Background

The first step in any Maxwell 2D simulation is to choose the type of solver. The transient solver is selected as discussed above. Next a cross section of the problem

region is drawn as in Figure 3.1, materials, electromagnetic boundaries and sources are defined and a mesh is created as in Figure 3.2. As can be seen the cross section of the machine is divided into many small triangles of various sizes. These triangles are the finite elements and together form the mesh. The magnetic components of Maxwell's equations are solved at the vertices of these triangles. The field solutions between the vertices are interpolated using shape functions [24]. From the field solutions time varying data for currents, voltages, torque, losses etc is obtained.

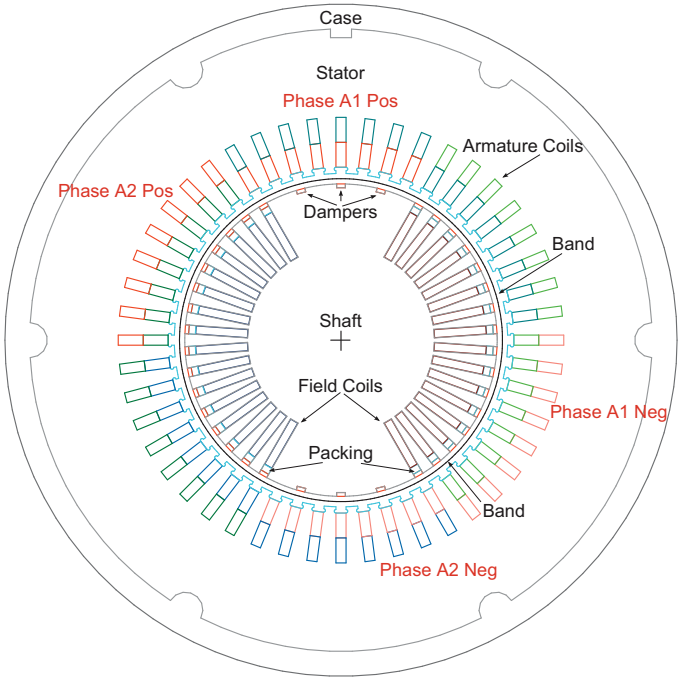


Figure 3.1: Completed 2D drawing of the generator in Maxwell's 2D Modeller

3.3 Drawing the mini-gen in 2D

The model can be drawn in two different co-ordinate systems either Cartesian (XY) or asymmetric (RZ) as in Figure 3.3. The asymmetric plane is symmetric about the z-axis. The XY plane is chosen to model the mini-gen from the axial perspective. This is the usual case for rotating machines as they are symmetric in the axial direction and the field components are assumed to be parallel to the XY plane.

Cross sections of the generator, which are needed to define the machine in Maxwell 2D, are provided in Figures 3.4 and 3.5. Photo's of the rotor and stator during construction are included in Figures 3.6, 3.7 and 3.8 to aid in visualising the real

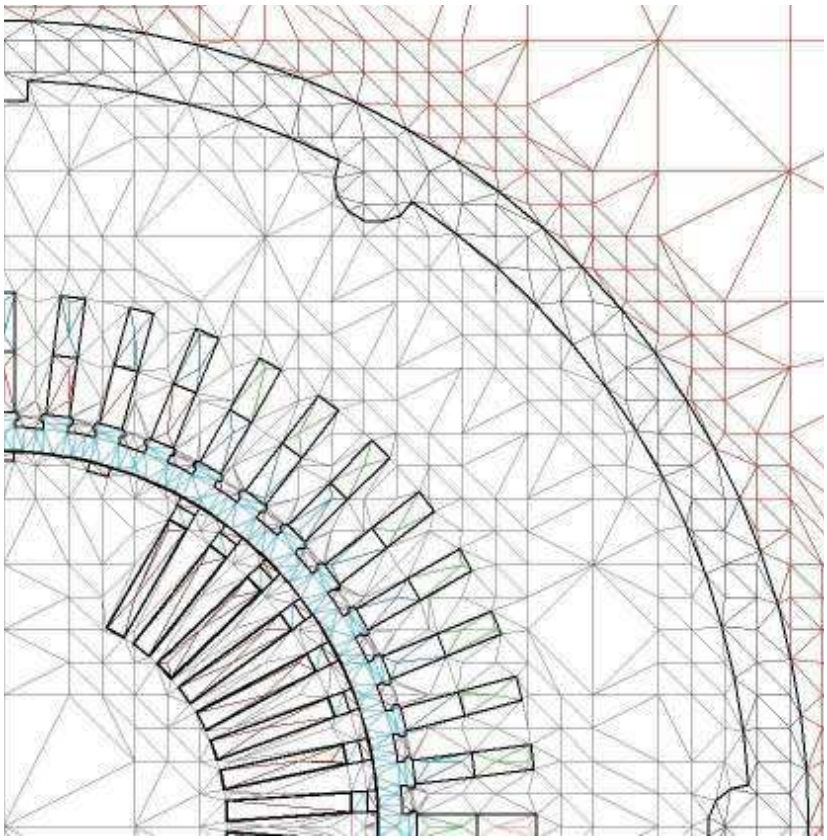


Figure 3.2: Mesh generated with the quadtree seeding algorithm with a seed value of 6

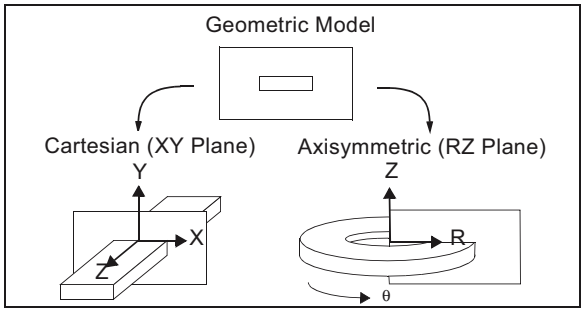


Figure 3.3: Possible drawing planes for Maxwell 2D

machine. Figure 3.9 is the side view of the machine. Table 3.1 contains other information necessary to setup the model.

In the xy-plane all objects are viewed as being uniform along the z-axis. Figure 3.1 is the completed drawing using the 2D Modeller. As can be seen the machine is modelled as a combination of simple closed shapes. All shapes must be closed

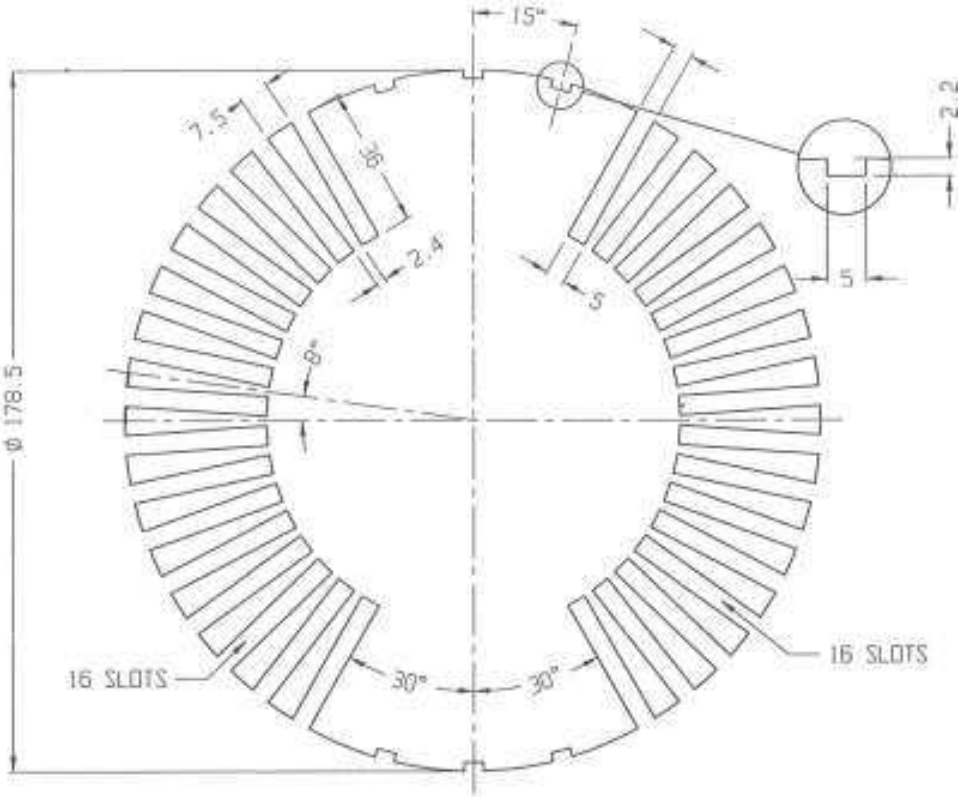


Figure 3.4: Drawing showing dimensions of the rotor of the mini-generator

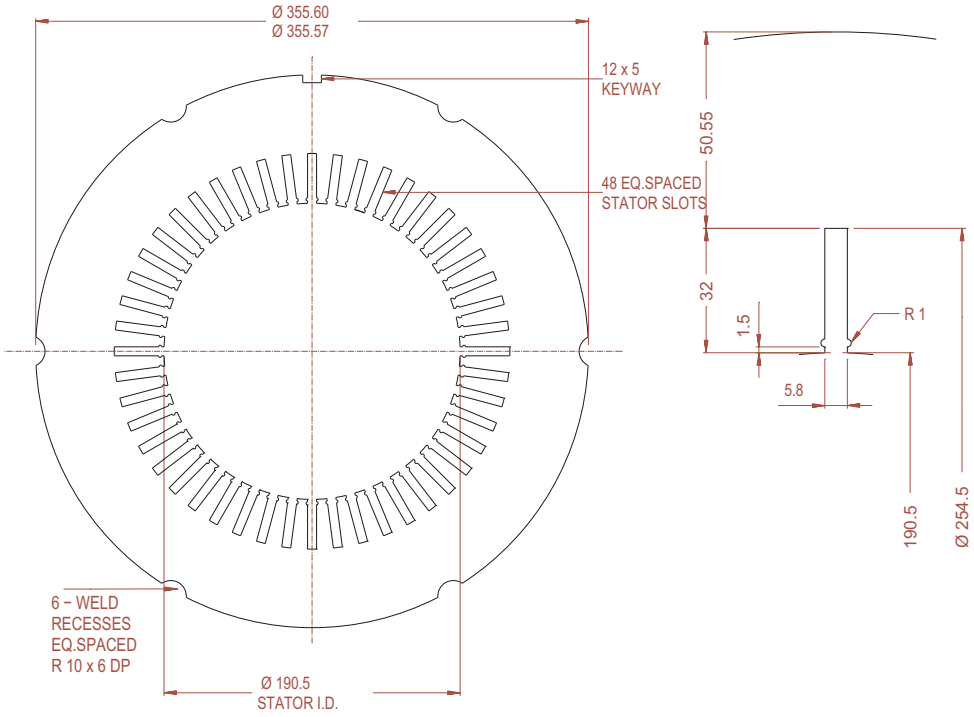


Figure 3.5: Drawing showing dimensions of the stator of the mini-generator



Figure 3.6: Photo of the rotor during construction with empty slots

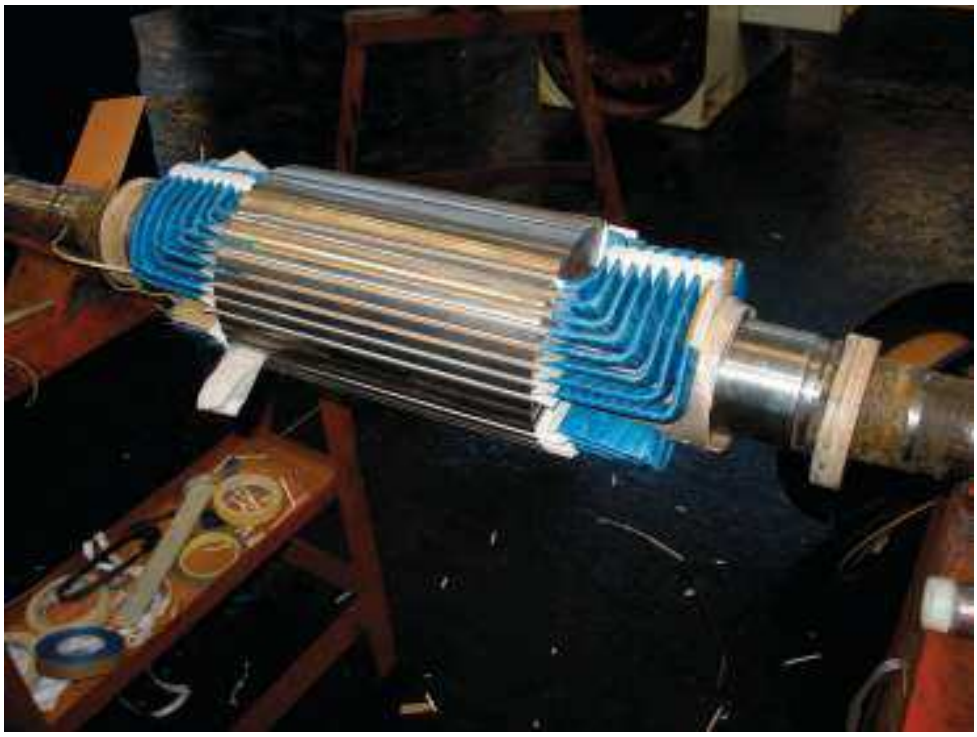


Figure 3.7: Photo of the rotor during construction with field winding



Figure 3.8: Photo of the stator during construction with casing

Table 3.1: Miniature Synchronous Generator Ratings

Parameter	**Value**	**Units**
General Data		
Rated Power	20	kW
No. of poles	2	
Synchronous Speed	3000	rpm
Air-gap	6	mm
Frequency	50	Hz
Stator		
Output Voltage	340	V
Output Current	35	A
Core length	280	mm
No. of slots	48	
Wires in parallel	6	
Pitch	1-17	
Conductors per slot	6	
Parallel circuits	2	
Connections	star	
Stacking factor	0.95	
Phase group DC resistance	53	mΩ
Rotor		
No slots	32	
No. of turns per slot	10	
Excitation Current at rated load	60	A
Total Resistance	500	mΩ
Damper Bars		
No. of Damper Bars	24	

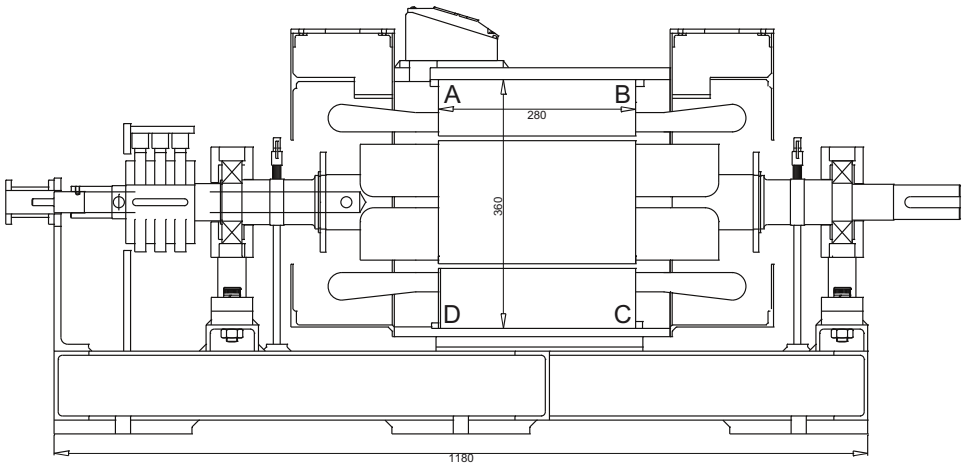


Figure 3.9: Cross section of the mini-generator

and may not overlap. Where a shape is completely enclosed by another, an inner boundary will be created and the properties of the inner shape will supersede those of the outer shape.

When modelling in 2D several assumptions are implicit:

- Currents only flow in the z direction
- Magnetic fields are parallel to the x-y plane
- The lengths of the rotor and stator cores are equal
- End-effects are negligible

Thus only the section ABCD in Figure 3.9 is modelled. The various contours of the rotor, winding overhangs, bearings, mounting frame and slip rings cannot be modelled in 2D. Since section ABCD is where the windings and the bulk of the magnetic material are located, the model has significance and if end-effects are known to be negligible then an accurate model can be obtained too.

Figure 3.10 shows the various stages in creating a 2D drawing of the model. First the case and outline of the stator are drawn as circles. Next a circle is drawn with its centre on the circumference of the stator. This circle represents one of the weld recesses. It is recommended that shapes be drawn by entering co-ordinates using the number keypad rather than clicking on grid points since this method is far more accurate and efficient. For example one weld recess has polar co-ordinates $(r, \theta) : (177.8, 120\,^{\circ})$ and a radius of 10 mm. The weld recess is then duplicated along

an arc in increments of 60°. A square shape is added for the keyway as in 3.10(a) with co-ordinates $(x, y) : (-6, 172.8)$ for the bottom left corner and $(6, 177.8)$ for the top right corner. The stator outline, weld recesses and keyway are then subtracted from one another using the Boolean Subtract function. The resulting shape is shown in Figure 3.10(b).

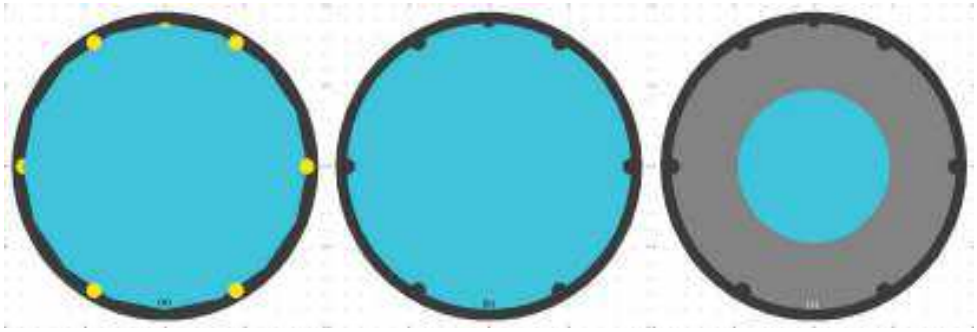


Figure 3.10: (a) Casing and outer part of stator with shapes for weld recesses and keyway, (b) subtraction of shapes in (a), (c) first shape for inner part of stator

The inside of the stator, where the rotor, and coils will sit, must be defined. A circle is defined with the inner diameter of the stator. Shapes are made for the stator slots and distributed equally over the inner circumference. A Boolean union is performed. The result is the combination of objects on different layers seen in Figure 3.11(c). The outer part of the stator will be assigned a steel material while the inner part vacuum. In this way the hollow cylindrical shape of the stator can be defined. The steel section of the stator behind this vacuum piece is ignored by the transient solver.

Rectangular shapes are added as in Figure 3.11(c) which represent the area occupied by the windings in the stator slots. These areas are later assigned a conducting material such as copper and external connections. Since currents only flow in the z direction it is not necessary to draw insulating materials between copper windings and steel sections. It is possible to draw an air-gap between the copper and steel if necessary. However one usually makes the assumption that these air-gaps are negligibly small and need not be included, to reduce computation times. It should also be noted that the conductors in each slot and layer are not drawn individually but as closed shapes. Maxwell allows for the definition of turns and parallel connections when defining excitations and this is discussed below. Defining each wire/conductor in a slot with individual air-gaps representing insulation layers would result in very long simulation times. It is therefore usually assumed that the current is distributed evenly between different conductors, of the same group.

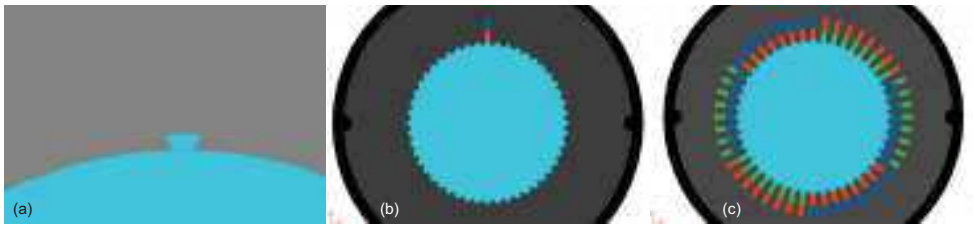


Figure 3.11: (a) Shapes for stator slots , (b) Shapes in (a) duplicated & first coils added for armature winding , (c) complete armature winding showing phase groups

The rotor is drawn in a similar manner to the stator. First a circle is drawn as in Figure 3.12(a). Rectangles representing slots are drawn and Boolean subtracted from the original circle as in Figure 3.12(b). The damper bars and field coils are then drawn with dimensions (0.1 mm) smaller than the slots to allow for air-gaps between the copper and steel to account for the affect of the insulation layers as in Figure 3.12(c).

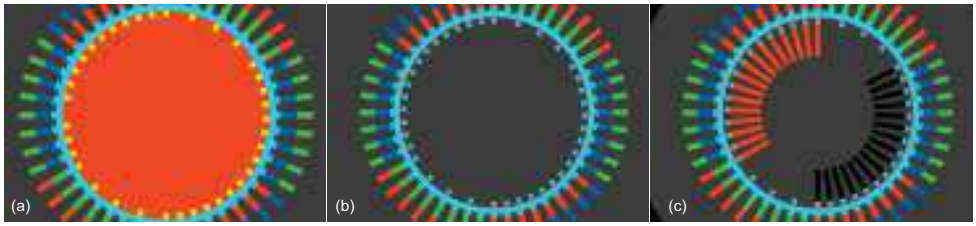


Figure 3.12: (a) Round shape for rotor with cut-outs for packing and dampers, (b) subtraction of shapes in (a) also showing damper bars, (c) completed rotor with field winding

Figure 3.13 shows how a search coil around a stator tooth can be drawn in the 2D Modeller.

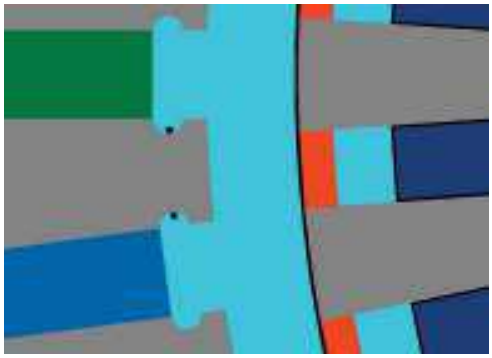


Figure 3.13: Location of one search coil in the 2D model

The Maxwell 2D Modeller allows one to select the level of detail in a model by

defining the number of segments making up a shape. Sensible values need to be chosen in order to represent the shapes accurately. The meshing algorithms use these segments to generate seed points which determine how the finite elements are defined and spaced. Too many segments may result in very dense meshes which may increase the simulation time unnecessarily [20].

Objects should be coloured and named intelligently so that consequent procedures are made easier. Objects can also be grouped to allow for easier selection in the different editors in Maxwell 2D.

3.4 Materials Setup

Table 3.2 is a table of the various materials assigned to the objects defined in the 2D Model.

Table 3.2: Table of Materials assigned to different objects in 2D Model

Object	Material
Casing	Steel_1008
Stator Outer	Steel_M400
Stator Inner	Vacuum
Rotor	Steel_1008
Band	Vacuum
Damper Bars	Copper
Phases	Copper
Rotor Packing	Vacuum
Background	Vacuum
Rotor Windings	Copper

Steel M400 is a custom steel added to Maxwell's library. It is recommended that at least 20 data points are entered for the BH curve in Maxwell, including data points well into saturation. Steel M400 was defined as having zero conductivity since it is laminated and is non-conducting in the z-direction. This is normal practice for 2D FEM packages since there is a limited concept of depth. If Steel M400 had a finite conductivity large eddy currents would be induced in the stator. Therefore the assumption is made that the eddy currents in the stator are negligible. All the other materials are part of the Maxwell 2D material database.

3.5 Boundaries

Boundaries define the behaviour of magnetic or electric fields at object interfaces and at the edges of the problem region.

By default all outside edges are defined as having Neumann boundaries. A Neumann boundary forces the magnetic field to be tangential to the surfaces of an object. The normal component of H is zero at the surfaces of these objects [27].

All object interfaces are defined as natural boundaries by default. This means that the tangential component of H and the normal component of B are continuous across the object surface [27].

The border of the problem region is assigned a balloon boundary which means that the region outside the drawing space is nearly infinitely large - the background object extends to infinity along the edges of the balloon boundary. The flux at infinity is zero and in this way Maxwell 2D obtains conditions for the solution of the problem. It is recommended that the drawing size be 3-5 times larger than the model size. In some problems where there are significant fringing effects the drawing size may need to be 10-20 times the model size [27]. It was found that a drawing size extending 250mm from the origin in the X and Y directions was suitable.

In order to reduce computation times the outer surface of the casing could be assigned a vector potential boundary of 0 Wb/m and fewer finite elements would be needed in the background object. Either a vector potential boundary on the outside edges or a balloon boundary on the border must be defined for a solution to be possible.

3.6 Sources

Sources define how charges, voltages and currents are distributed in a model. In the transient solver various types of sources are available; stranded or solid voltage sources or current sources and external connections. The documentation on these sources is comprehensive and should be consulted [27–29].

3.6.1 Stranded vs. Solid Sources

The voltage, current and external sources can be either stranded or solid. In a stranded source the current density is assumed to be uniformly distributed through the cross-sectional area of the object [27]. Thus no eddy or skin effects are taken into account. The assumption that the eddy effects are negligible in conductors is usually made in order to reduce simulation times. All the sources in this model were stranded except for that of the shaft voltage.

3.6.2 External Connections

An external source refers to the representation of a winding in the model by an inductor in an external circuit. The magnetic fields and inductances are computed at each time step and then passed onto the SPICE based circuit solver. The inductor in the external circuit is just the representation of the winding not a real inductor. The inductance is computed for each time step and the default value of 1 H is meaningless. These "inductors" (windings) can then be connected to voltage and current sources with arbitrary waveforms. Resistors, capacitors, real inductors and diodes can also be connected to the windings. At least one passive component with a resistive element must be connected to a winding. Figure 3.14 shows the external circuit with many "inductors" representing the phase groups, shaft voltage loop and search coil.

Field Winding

The field winding was created by selecting the field conductors and assigning an ideal stranded voltage source. The conductors on one side of the shaft are assigned a positive polarity while those on the other side of the pole face a negative polarity. The total number of turns as seen from the terminal is 160 (10 conductors/slot $\times$ 32 slots$\div$2). The terminal resistance was set at 0.5 Ω. Setting the initial current at the desired steady state value will save a great deal of computing time since the current will gradually increase from zero over several cycles if it is left at the default 0 A.

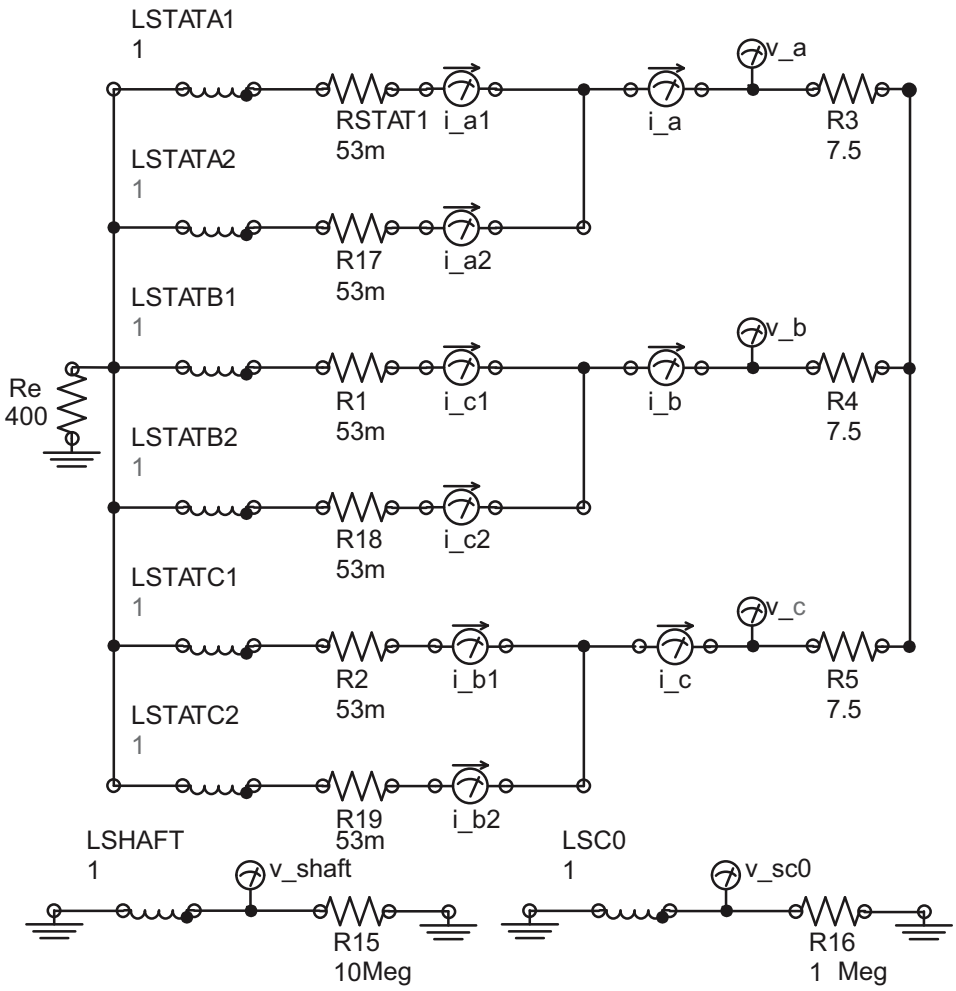


Figure 3.14: External SPICE circuit showing armature, shaft voltage and search coil windings

Armature Winding

The phase groups are assigned individual external sources as can be seen in Figure 3.14. The phase groups consist of two sets of eight conductors each. Therefore there are 12 groups of conductors, 4 per phase, with each phase group having 2 sets with opposite polarity as shown in Figure 3.1. Care needs to be taken when setting the polarity of the phase group sets. The phase groups have 24 turns as seen from the terminal (8 slots $\times$ 3 turns).

In the external circuit a resistance of 53 m$\Omega$was connected in series with the winding, which is the measured DC resistance of a phase group. The phase groups are connected in parallel star with an earthing resistor Re at the neutral point and a three phase resistive load. Voltage and current probes are added to create outputs for important node voltages and currents.

Shaft Winding

The shaft voltage winding was created by assigning a solid external source to the casing and shaft objects. The casing was assigned a negative polarity while the shaft a positive polarity. The number of turns as seen from the terminal was left at the default: 1.

In the external circuit the shaft winding is connected to a high impedance (10 MΩ) which represents the input impedance of the signal conditioning system used in the lab setup. The shaft winding is also grounded as in the lab setup.

Search Coils

Each search coil was assigned an external source with the conductors on either side of the stator teeth having opposite polarities. The number of turns was set at 1. The search coil windings are grounded at one end and connected to a high impedance (1 MΩ) at the other which represents the input impedance to dSpace.

Damper Bars

The damper bars were assigned a passive end connected conductor with a resistance of 0.002$\Omega$and an inductance of 0 H. It was found that since the simulations are all

in the steady state these parameters had a negligible effect on the results.

3.7 Solver Setup

3.7.1 Mesh Setup

To obtain accurate results from FEM simulations in a reasonable time period it is crucial to use the optimal mesh. The mesh is that structure which contains and ties together the finite elements into which the system has been divided. Having too few elements will result in the simulation not being accurate while having too many finite elements will waste time, money and computing resources.

Considering that the transient solver does not include the automatic mesh adoption of the static solvers it evident that a mesh of sufficient density must be created manually for accurate transient solutions.

Figure 3.2 is a screen capture of the recommended mesh for the mini-gen.

Automated Seeding Algorithms

The above mesh was generated using Maxwell 2D's quadtree seeding algorithm. The quadtree seeding algorithm subdivides the areas around the outside edges of objects into a grid and adds seed points to this grid. The seed points and object points then form the vertices of the triangles once the mesh is made. This algorithm is good for generating dense meshes in the air gaps of rotational machines and less dense meshes in areas with less contours such as the centre of the shaft.

The density of the mesh generated using this algorithm can be set by changing the seed value between 1 and 8. The seed value determines the number of divisions created near the edges of objects, a value of 1 results in a sparse mesh and 8, a very dense mesh. The mesh in Figure 3.2 was produced with a seed value of 6.

Manual Mesh Refinement

There are various other methods to refine the mesh manually. For example it is possible to create meshes with a desired number of triangles for each object using

the object refinement option. Various meshes are evaluated in the next Chapter including the curvilinear mesh.

Curvilinear Elements

One of the sources for the errors in the transient solver is the overlap of triangles in the air gap as the shaft rotates. The overlap between triangles can be avoided by using triangles with curved edges or 'curvilinear' elements. The curvilinear elements are implemented in the band object when the curved_element environment variable is set to 1.

3.7.2 Motion Setup

Motion is provided for by defining a band object. The band object tells Maxwell which parts of the model are moving and which parts are stationary. The band object in Figure 3.1 is drawn in the centre of the air gap thus dividing the stationary and rotating parts. For rotational motion the band object must be circular, have at least 100 line segments and its centre must coincide with the centre of rotation.

Maxwell makes the following assumptions regarding motion:

- No motion occurs outside the band object
- The motion is either translational or rotational
- The moving parts move as one rigid body

Therefore no vibration will occur between the field winding and shaft for example. Furthermore no vibrations or motion of any kind can occur outside the band. If the rotor and band are centred at the geometric centre of the model then the motion will be purely rotational. If the band is centred at the geometric centre of the model but the rotor is offset then a whirling or wobbling type of motion will be simulated. A static eccentricity can be simulated by offsetting both the band and rotor by the same distance.

The band object is assigned in the Motion Setup module under Solution Setup. Maxwell automatically determines which objects are moving and which are stationary. The mini-gen is assigned a constant angular velocity (3000 rpm) and in this sense the model is a steady state one with motion and time varying voltages etc.

The model is not a transient one in the usual sense, i.e. response to an instantaneous load change. Theoretically it is possible to simulate such a condition. The motion setup allows for the assignment of a damping factor and a moment of inertia for the rotating parts. The external circuit also allows for many different types of sources or switches with step functions.

3.7.3 Time Step Setup

The time step should be chosen so that all frequencies of interest are reliably simulated. The time step must give a sampling frequency of at least double the highest frequency of interest. For example the highest frequency of interest in the mini-gen is 2450 Hz (48 slots $\times$ 50 Hz) so the time step is set at 0.2 ms. It may be necessary to choose a time step which results in over sampling to ensure that adequate resolution in the frequency domain is obtained. It was found that the lower the time step the denser the mesh required for an accurate solution. The affect of the time step is illustrated in [20].

The stop time also needs to be selected to be long enough to reach a steady state operating point. It was found that the initial conditions took 60 ms to settle in the mini-gen. The stop time was set at 360 ms so as to ensure a large number of data points from the steady state are obtained. When simulating induction motors it may be necessary to set a much longer stop time in order to capture the slip frequency and slip modulated harmonics.

3.8 Simulation Outputs

3.8.1 Open and Short Circuit Characteristics

The classic short circuit and open circuit tests were performed and the results are compared in Figure 3.15 and Figure 3.16. The simulated curve was obtained from data from separate simulations with the armature winding either open circuited or short circuited with different levels of excitation.

The FE model enters saturation faster than the real machine. The generated voltage is also lower in the model. It was expected that the model would generate a higher voltage since eddy effects in the stator are assumed to be negligible and the coils are drawn as though the slot fill factor is 1. This discrepancy may be due to the use of

a built in material definition for the rotor core and shaft rather than the actual B-H curve. Nevertheless the curves are a good fit.

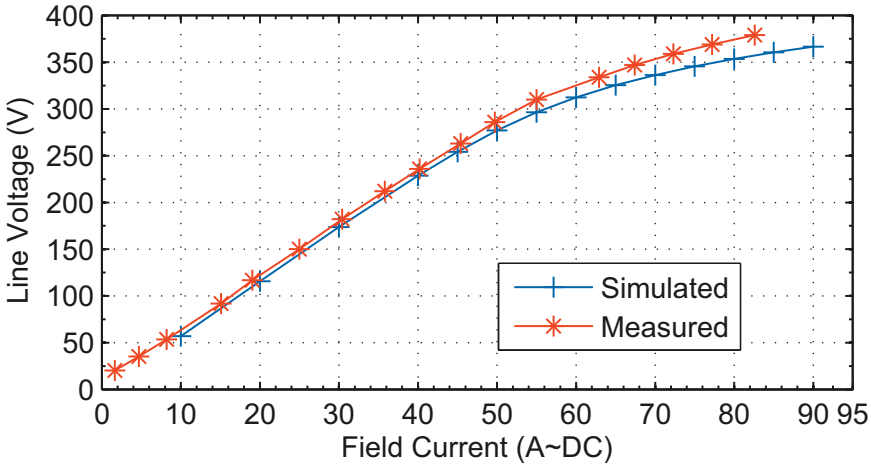


Figure 3.15: Open Circuit Characteristic

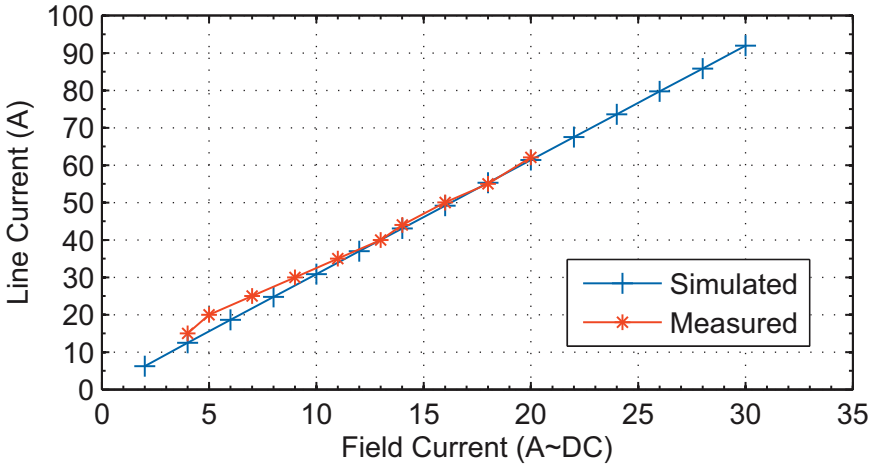


Figure 3.16: Short Circuit Characteristic

3.8.2 Search Coils

Figure 3.17 shows the simulated voltage from one of the search coils included in the Maxwell model. Figure 3.18 is the measured waveform. Good agreement is obtained between the measured and simulated waveforms. There is a 10% difference between the simulated and measured RMS values. This can be explained by a difference in the excitation levels of the measurements and simulations. The simulations were

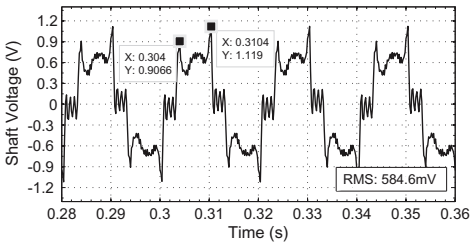


Figure 3.17: Simulated search coil voltage

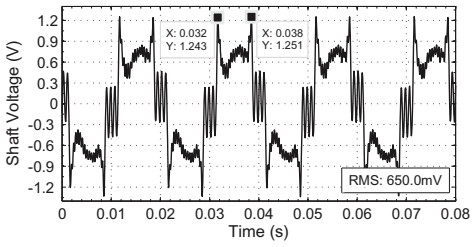


Figure 3.18: Measured search coil voltage

run with 60 A excitation while the measurements were taken with an excitation of 64 A.

3.8.3 Field Plots

The field plots are available through the usual method of opening the fields post processor. Figure 3.19 is an example of a flux density plot. Lines and shapes can be added to the fields post processor to obtain the various field quantities in a particular region.

3.8.4 Time Stamped Data

Various waveforms are available from the Transient Post Processor including:

1. Voltages
2. Currents
3. Torque, RPM, Position
4. Power Loss and Core Loss
5. Back EMF
6. Flux Linkages

This data can be analysed using the Transient Post Processor and calculator. The time stamped data is stored in *.dat files in the project folder and can be imported into MATLAB. Some of the other important file types for Maxwell are listed in Appendix D along with suggestions for choosing the best computer hardware for running FEM applications.

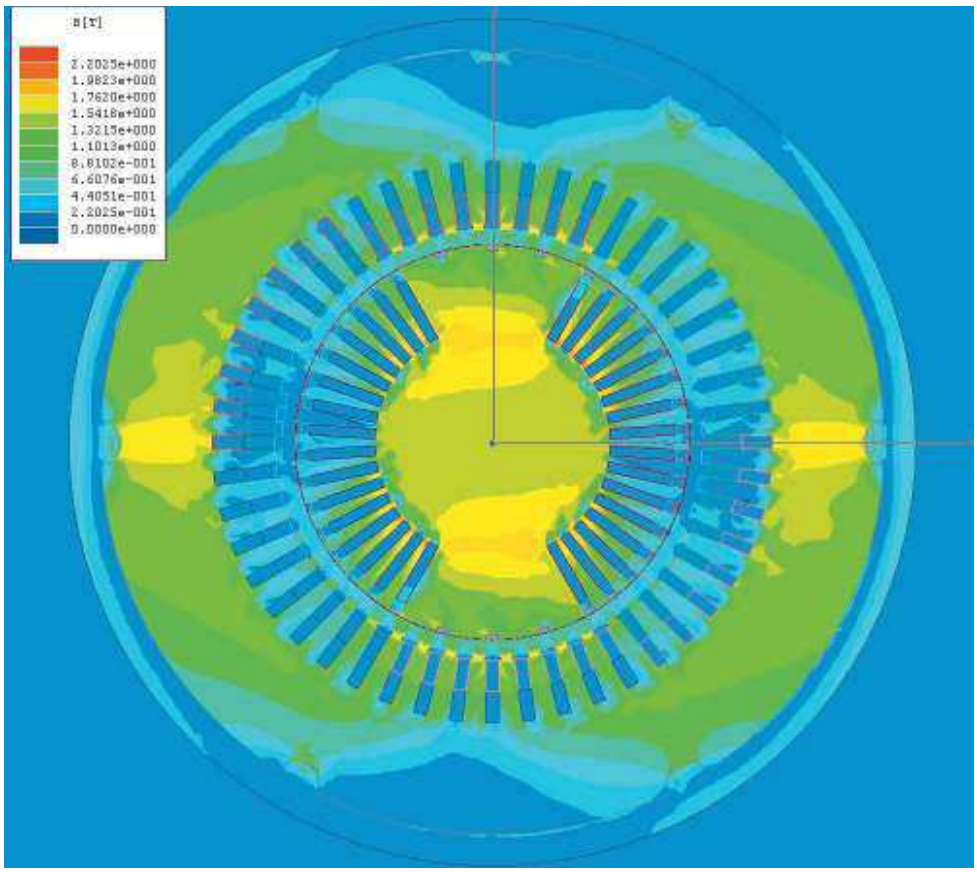


Figure 3.19: Magnetic Flux Density (T) field plot

3.9 Conclusion

The procedure for creating a Maxwell 2D transient simulation has been presented for the mini-gen. First a 2D model of the machine is drawn. Materials are then assigned to the various objects in the 2D drawing. Next the boundaries and sources are assigned and linked with an external SPICE circuit. Finally the mesh, motion and time step are entered and the problem can be solved. Field plots and time varying waveforms are available through the Maxwell 2D interface or from the text files in the project folder once the simulation has completed.

The Maxwell 2D FEM model has been evaluated by comparing the simulated and measured open and short circuit characteristics and search coil voltages. The FEM model parameters were found to be within a 5% of those measured which is acceptable considering that not all the magnetic material parameters are available. The shaft voltage from the FEM model is compared with measurements in the next chapter.

Chapter 4

Effect of the Mesh on the Shaft Voltage

4.1 Introduction

In [5] it is shown that the shaft voltage of the mini-gen can be simulated in Maxwell 2D. However it was found that the simulated shaft voltage RMS was much lower than that measured. The frequency components above 1 kHz in the simulated waveform were also out of proportion with those measured.

Bearing in mind the importance of the mesh and time step in any FEM simulation the effect of various meshes and time steps were investigated in order to explain the error in the simulations. Manually refined meshes, automatically generated meshes and a curvilinear mesh are evaluated in terms of which gives the most accurate shaft voltage with the shortest computation time.

Figure 4.1 is a screen capture of one of the meshes tested. As can be seen the cross section of the machine is divided into many small triangles of various sizes. These triangles are the finite elements and together form the mesh. The magnetic components of Maxwell's equations are solved at the vertices of these triangles. The field solutions between the vertices are interpolated using shape functions [24, 27].

Besides the different meshes, the simulations are identical in all other respects. The residuals, time steps, initial conditions and geometry were kept constant unless otherwise stated.

The number of elements contained in each object for the various meshes are shown

in Figures 4.2 and 4.3. Table 4.1 includes the number of elements in each mesh, the simulation time, the quality ranking of the result and an alias for each mesh.

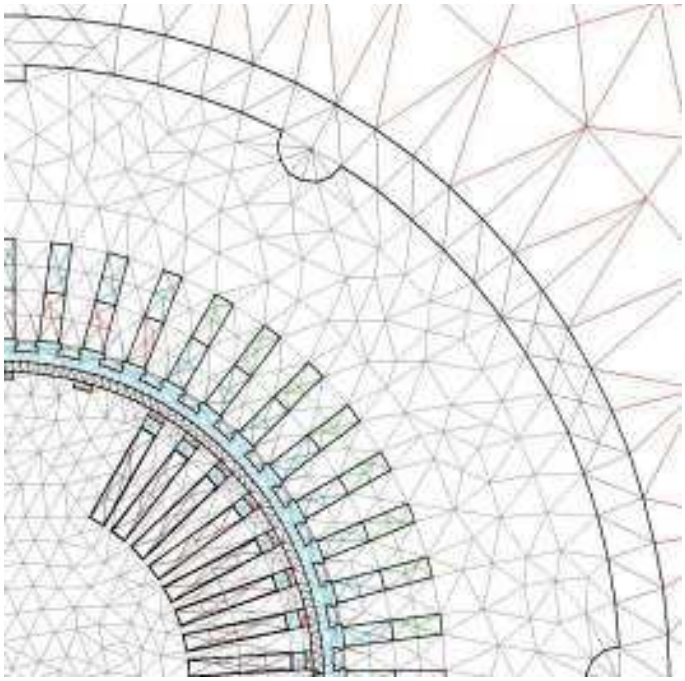


Figure 4.1: Mesh generated by refining each object individually - user1

4.2 User Generated Meshes

4.2.1 Object Refinement

One method to generate a mesh manually is to start with the initial mesh and refine the mesh by assigning a certain number of triangles for each object. The mesh generated using this technique is shown in Figure 4.1. Only a quarter of the machine is shown here to allow for the finer details to be seen clearly, however the entire machine was simulated - no symmetry boundaries were used. As can be seen the mesh is dense in the air gap while it is less dense but evenly distributed in areas with fewer contours such as the middle of the shaft.

Figures 4.6 and 4.7 show the shaft voltage obtained with this mesh. The time waveform includes many large spikes which are not found on the real machine. It was thought that these are the result of some sort of quantisation error. These spikes result in a noisy frequency spectrum above 1000 Hz which differs significantly

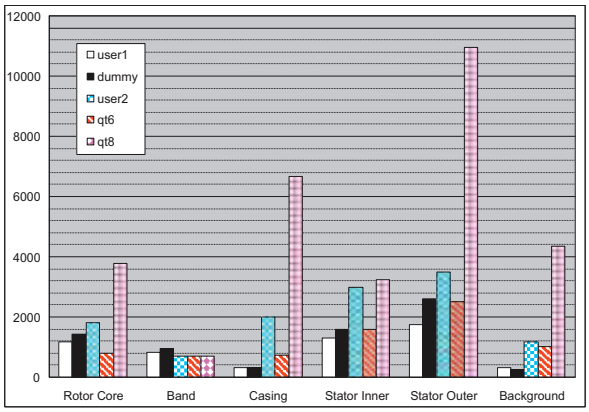


Figure 4.2: Number of elements for the larger objects

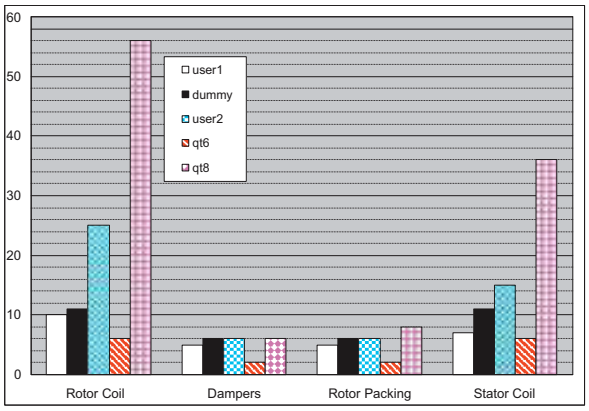


Figure 4.3: Number of elements for the smaller objects

Table 4.1: Details of various meshes and simulation times in Maxwell 2D

Alias	Mesh Type	No. △'s	Curvilinear	Time	RMS	Rank
qt8	qt8	35676	no	80h	15.5	1
qt6ls	qt6	8554	no	7h48min	11.4	2
qt6	qt6	8554	no	16h	12.8	3
qt6cl	qt6	8554	yes	17h58min	13.0	4
user2	object refinement	16164	no	39h08min	16.9	5
user1	object refinement	7674	no	12h30min	21.3	6
dummy	dummy object	11544	no	23h38min	52.1	7

from that measured. This simulation also calculates that the 5th harmonic was the largest instead of the fundamental.

It was found that reducing the band object in size so that it only just extends beyond the shaft and having a large number of elements in the case resulted in less glitches. It was initially thought that a dense mesh in the case would not be necessary since the fields are low there. Considering that the shaft flux path loop includes the case and shaft it can be seen why it is necessary to have a dense mesh in the case to acquire an glitch free shaft voltage. A second attempt was made at refining the mesh using object refinement this time with twice as many elements in total. This mesh (user2) is presented in Figure 4.4 and the waveforms in Figures 4.8 and 4.9.

4.2.2 Using Dummy Objects as Meshing Aids

It was thought that the mesh could be improved by adding dummy objects to the drawing. For example circles with various radii were added to create a dense mesh in the air gap. These circles have the same material as the air gap - vacuum. Square objects were added to the stator teeth to try and improve the aspect ratio of the triangles there. The squares were assigned the same material as the stator. Figure 4.5 clearly shows the dummy objects or mesh helpers.

It was found that this simulation resulted in the worst shaft voltage in terms of the number of quantization errors and relative proportions of the harmonics as in Figures 4.10 and 4.11.

4.3 Automatically Generated Meshes

Maxwell 2D has an automatic mesh generation option based on the “quadtree” seeding algorithm. The quadtree seeding algorithm subdivides the areas around the outside edges of objects into a grid and adds seed points to this grid. The seed points and object points then form the vertices of the triangles once the mesh is made. This algorithm is good for generating dense meshes in the air gaps of rotational machines and less dense meshes in areas with less contours such as the centre of the shaft.

It was found that these meshes gave good results with a relatively short simulation time. It was later determined that the good results were due to the dense mesh in the case which resulted from this algorithm.

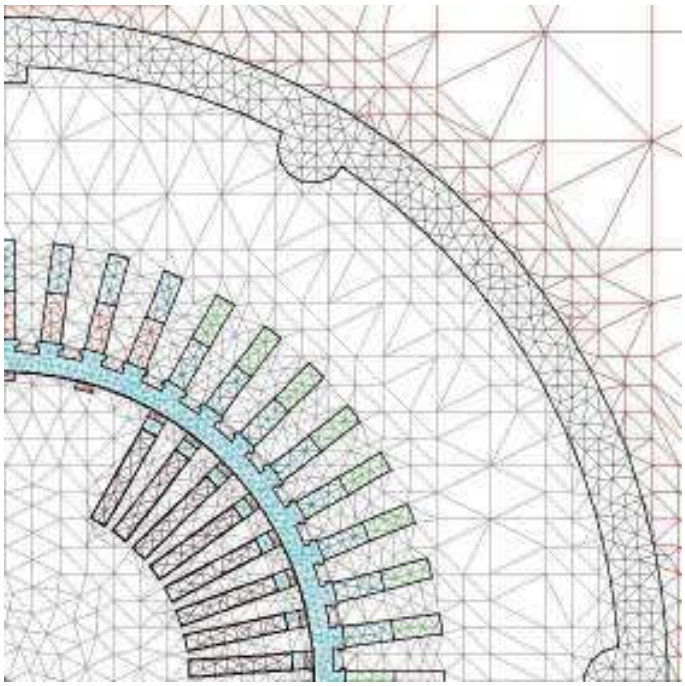


Figure 4.4: Dense manually refined mesh - user2

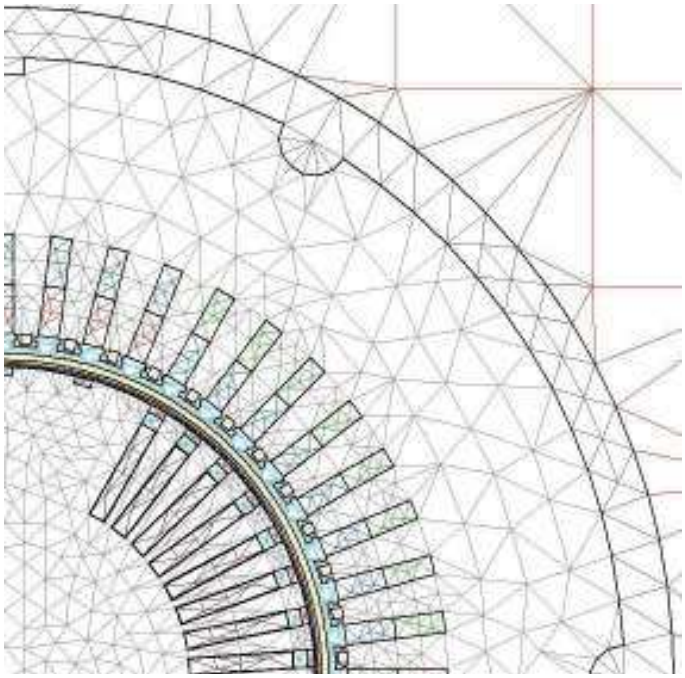


Figure 4.5: Mesh generated with dummy objects and individual object refinement - dummy

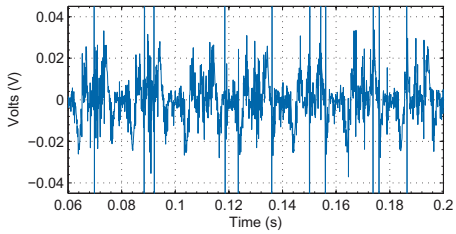


Figure 4.6: Calculated shaft voltage waveform using a manually refined mesh - user1

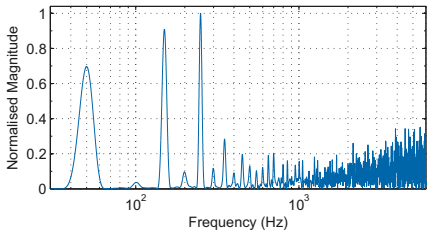


Figure 4.7: Calculated shaft voltage frequency spectrum using a user refined mesh - user1

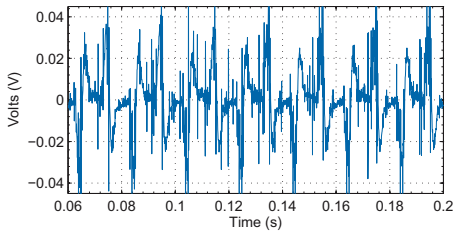


Figure 4.8: Calculated shaft voltage waveform using a dense manually refined mesh - user2

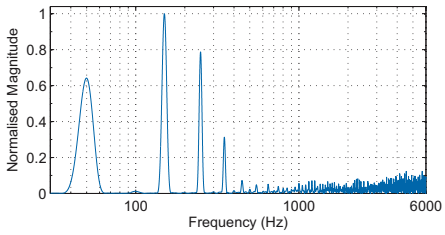


Figure 4.9: Calculated shaft voltage frequency spectrum using a dense manually refined mesh - user2

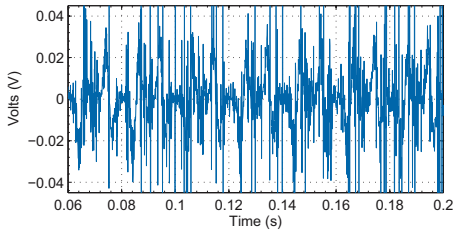


Figure 4.10: Calculated shaft voltage waveform using a mesh generated with dummy objects - dummy

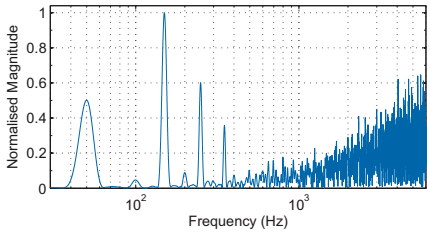


Figure 4.11: Calculated shaft voltage frequency spectrum using a mesh generated with dummy objects - dummy

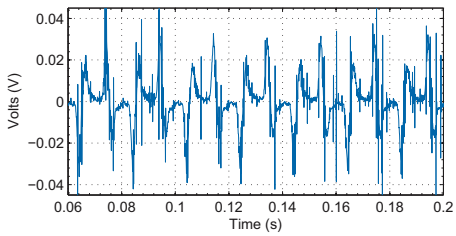


Figure 4.12: Calculated shaft voltage waveform using a mesh generated from the quadtree 6 algorithm - qt6

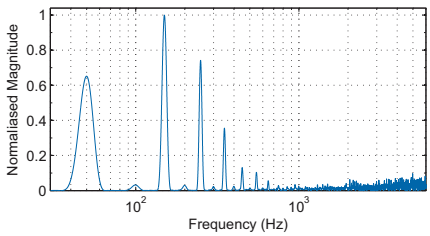


Figure 4.13: Calculated shaft voltage frequency spectrum using a mesh generated from the quadtree 6 algorithm - qt6

Results from two different versions of the quadtree algorithm are presented here. The density of the mesh generated using this algorithm can be set by changing the seed value between 1 and 8. The seed value determines the number of divisions created near the edges of objects, a value of 1 results in a sparse mesh and 8, a very dense mesh.

Values of 6 and 8 were chosen for the seed values. A value of 6 results in a similar number of triangles to the first manually refined mesh but a vastly different distribution as is evident in Figure 4.14. A value of 8 results in the densest mesh and produced the most glitch free time signal but also took the longest time to simulate. The mesh from quadtree 8 is shown in Figure 4.15.

The waveforms for the two quadtree meshes are shown in Figures 4.12, 4.13, 4.16 and 4.17.

The advantages of the quadtree algorithm are:

- it is the quickest mesh generation technique
- it produces a consistent mesh for different simulations with the same geometry
- it produces a dense mesh in the air gap
- it produces a mesh with larger triangles in areas with few contours or shapes
- it can produce sufficiently dense meshes for accurate results
- the density of the mesh can be controlled easily

The disadvantages of the quadtree algorithm are that it will produce a dense mesh on the outermost surfaces of objects where the fields may be close to zero and have little effect on the overall machine operation. For simulations where the case is not included in a shaft voltage measurement the quadtree algorithm may not produce the optimal mesh.

4.4 Curvilinear Mesh

One of the sources for the glitches in the shaft voltage is the overlap of triangles in the air gap as the shaft rotates. The overlap between triangles can be avoided by using triangles with curved edges or “curvilinear” elements. The results of these

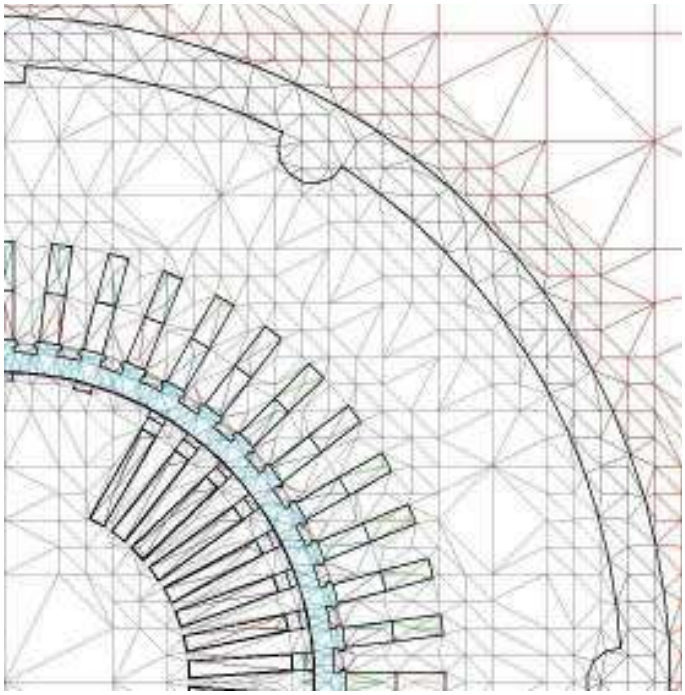


Figure 4.14: Mesh generated using the quadtree 6 algorithm - qt6

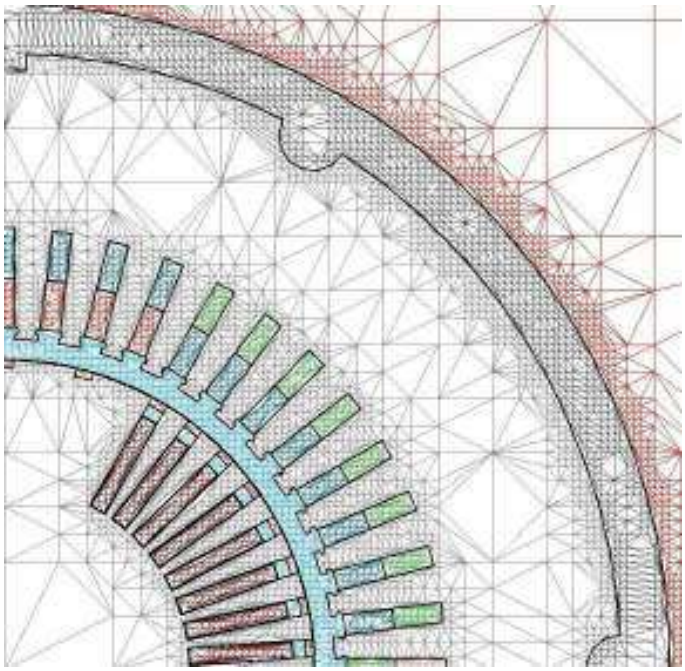


Figure 4.15: Mesh generated using the quadtree 8 algorithm - qt8

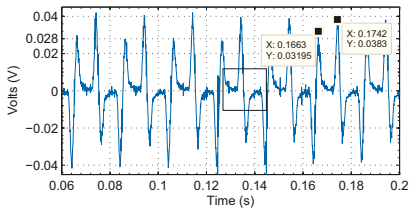


Figure 4.16: Calculated shaft voltage waveform using a mesh generated from the quadtree 8 algorithm - qt8

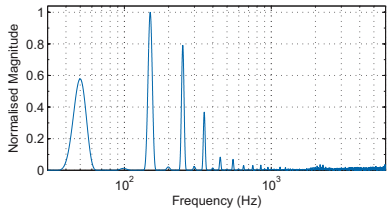


Figure 4.17: Calculated shaft voltage frequency spectrum using a mesh generated from the quadtree 8 algorithm - qt8

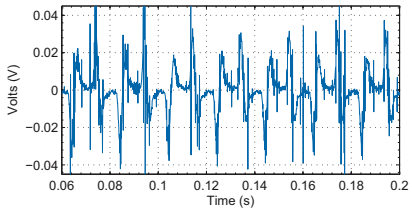


Figure 4.18: Calculated shaft voltage waveform using a curvilinear mesh generated from the quadtree 6 algorithm - qt6cl

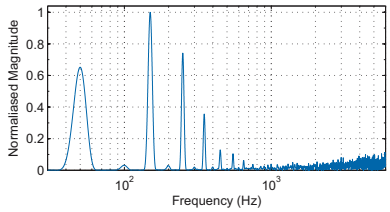


Figure 4.19: Calculated shaft voltage frequency spectrum using a curvilinear mesh generated from the quadtree 6 algorithm - qt6cl

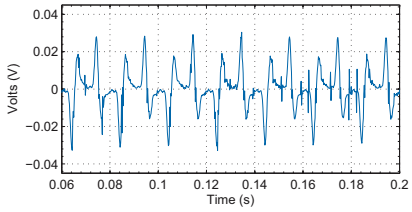


Figure 4.20: Calculated shaft voltage waveform using a 0.2 ms time step - qt6ls

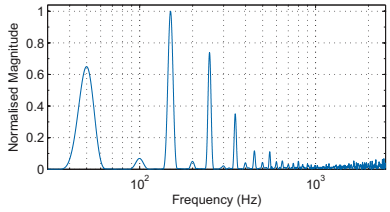


Figure 4.21: Calculated shaft voltage frequency spectrum with a 0.2 ms time step - qt6ls

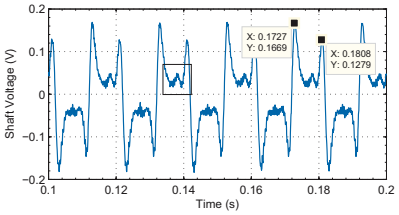


Figure 4.22: Measured shaft voltage waveform

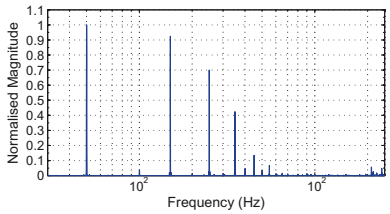


Figure 4.23: Measured shaft voltage frequency spectrum

simulations are presented in Figures 4.18 and 4.19. It was found that there wasn't a significant decrease in the number of glitches in the shaft voltage. The quadtree algorithm with a seed value of six was used to generate the mesh.

4.5 Effect of Time Step

The time step was initially set at $0.8\dot{3}$ ms (20 ms/(5steps/tooth×48 teeth)). An integer number of steps per tooth was chosen to ensure that no artefacts were obtained in the frequency spectrums of the various signals. This time step gave glitch free results with the qt8 mesh.

It was found that a large time step (0.2 ms) resulted in less glitches in the qt6 mesh as well as simulating in half the time. The highest harmonic of interest in the measured shaft voltage is the 50th. This time step satisfies the Nyquist criterion but the simulation would have to have a longer end time to obtain as good a frequency resolution.

4.6 Measured Shaft Voltage

Figures 4.22 and 4.23 show the measured shaft voltage time and frequency signals [5]. This data was captured under the same load and excitation conditions as the simulations. The RMS value is 78.5 mV.

It must be noted that the RMS magnitude of the measured shaft voltage is much higher than those of the simulations. Some more differences in the time signals are highlighted in Figures 4.16 and 4.22. The peaks in the simulated signal are not of equal magnitude and there appears to be some additional harmonic content in the measured signal. These discrepancies may be due to several reasons:

1. The asymmetries, due to manufacturing tolerances, in the real machine are larger than those of the 2D drawing which is drawn with as high a numerical accuracy as the program will allow.
2. Small (< 0.1 mm) dynamic or static eccentricities may be present in the real machine.
3. It not possible to simulate features such as the weld recesses perfectly, in 2D.

4. End effects are ignored in the model.

However it should also be noted that the frequency content is very similar. The frequency spectrums are normalised to their own maximums since the measured data is obtained from a much higher sampling frequency and sample length than is feasible with the simulations. Any affects in the simulated shaft voltage due to a fault can be correlated with the measured signal by comparing the percentage changes between the healthy and unhealthy frequency spectrums.

4.7 Conclusion

Results from seven different meshes have been presented and evaluated in terms of which gives the most realistic shaft voltage frequency spectrum with the least glitches in the time waveform. The following conclusions were drawn:

- Results can vary significantly with the mesh
- A denser mesh produces better results but takes longer to simulate
- Maxwell 2D's quadtree algorithm produced the best results
- The curvilinear mesh did not reduce the glitches in the shaft voltage significantly
- Simulations with small time steps require denser meshes than simulations with larger time steps

It was decided that the qt6 mesh with a time step of 0.2 ms was the optimal setting since it gives glitch free results with a relatively short computation time, thereby maximising the use of the available computing resources.

Chapter 5

Causes of the Shaft Voltage

5.1 Introduction

The common causes of shaft voltages according to [5, 11–13, 16–18, 30] are:

1. Asymmetry effects e.g. due to:
   (a) segmented stator laminations
   (b) joints in stator laminations
   (c) rotor eccentricity e.g. rotor sagging
   (d) stator eccentricity e.g. stator ovality
   (e) static eccentricity
2. Axial shaft flux e.g. due to:
   (a) residual magnetization
   (b) asymmetrical rotor or stator windings
   (c) saturation
   (d) rotor eccentricity
3. Homo-polar flux
4. Electrostatic charge effects e.g. due to
   (a) charge build up on steam turbines
5. External voltages on the rotor e.g. due to

(a) static excitation equipment

(b) voltage source and/or rotor winding insulation asymmetries

(c) active rotor winding protection

Considering constructional asymmetries, there are asymmetrical features in the mini-gen which would be expected to have a significant effect on the shaft voltage. In the stator, two of these features, the key way and weld recesses, have been modelled in Maxwell 2D in order to quantify their effects on the shaft voltage. Rotor asymmetries including a missing damper bar and distorted rotor slots, have also been simulated.

While a large turbo-set would have contributions to its shaft voltage made by electrostatic charge effects and possibly external voltages on the rotor these are not of concern in the mini-gen. The mini-gen is driven by an induction motor not a steam turbine, the excitation source is isolated from the test bed and no faults are suspected of being present in the field winding.

Homo-polar flux and axial shaft flux may well be present too, but as yet have not been fully investigated.

5.2 Stator Asymmetries

5.2.1 Weld recesses and key way

Small machines such as this once commonly have weld recesses and key ways in their laminations in order to align and bind them together. The weld recesses and key way can be seen in Figure 5.1. Considering that small asymmetries can cause a net flux to encircle the shaft it was decided to investigate the effect of the presence of the key way and weld recesses on the shaft voltage using the FEM simulations. The FEM simulations have the advantage that the key way and weld recesses can be removed individually from the model and the effect on the shaft voltage investigated. This obviously cannot be performed on the real machine.

Figure 5.2 shows the simulated shaft voltage with the key way and weld recesses removed from the model. Figs. 5.3 and 5.4 show the shaft voltages with either the weld recesses or key way present. Figure 5.5 shows the shaft voltage with both the key way and weld recesses modelled. Table 5.1 includes the RMS values of the shaft

voltage with all the combinations of weld recesses and the key way being present or not in the model.

As can be seen the shaft voltage is almost zero without the key way and weld recesses present. The 2D FEM model is drawn with as high a numerical accuracy as the program will allow and is almost perfectly symmetrical, however a small shaft voltage is still predicted. This may be due to the homo-polar flux or the way the program models curves - as a combination of many straight line segments. Once the weld recesses are added the shaft voltage increases by almost two orders of magnitude. When the key way is added the shaft voltage increases by almost 3 orders of magnitude! The weld recesses are in symmetrical positions and any disturbance in the flux encircling the shaft due to one weld recesses is very nearly cancelled by the flux disturbance due to the diametrically opposite weld recess. Since there is only one key way an asymmetry is present and it has a much larger effect on the shaft voltage than the weld recesses.



Figure 5.1: Cross section of the synchronous generator showing key way, weld recesses, missing damper and shaft based search coil

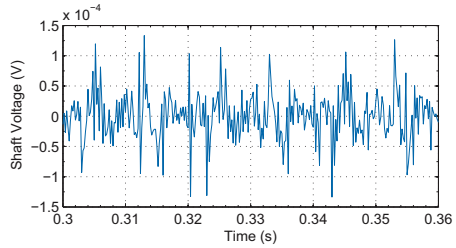


Figure 5.2: Simulated shaft voltage with no key way or weld recesses (note the voltage scale)

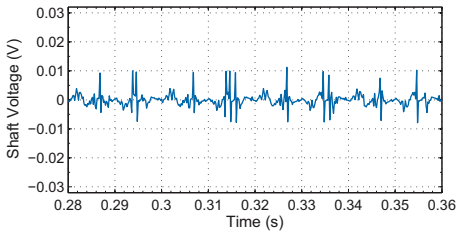


Figure 5.3: Simulated shaft voltage with weld recesses but no key way

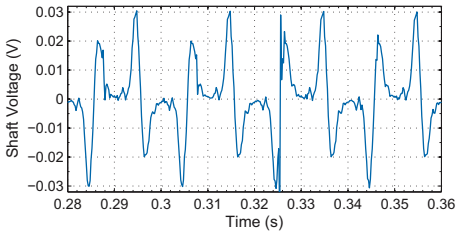


Figure 5.4: Simulated shaft voltage with a key way but no weld recesses

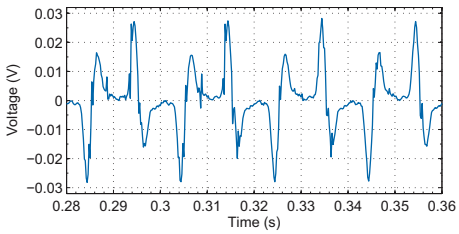


Figure 5.5: Simulated shaft voltage with a key way and weld recesses

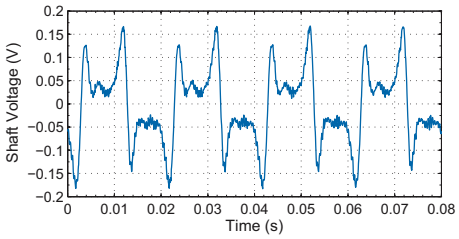


Figure 5.6: Measured shaft voltage

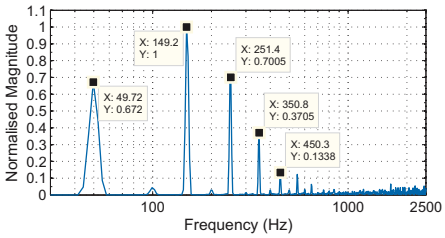


Figure 5.7: Simulated shaft voltage frequency spectrum with a key way and weld recesses

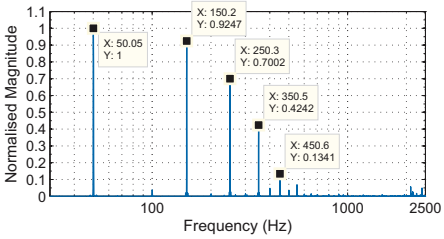


Figure 5.8: Measured shaft voltage frequency spectrum

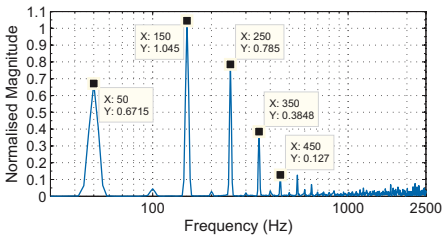


Figure 5.9: Simulated shaft voltage frequency spectrum with a key way, weld recesses and a missing damper bar

Table 5.1: Shaft voltage with combinations of the weld recesses and key-way

key way	weld recess	Shaft Volts (RMS)
n	n	44.2 μV
n	y	2.6 mV
y	n	13.3 mV
y	y	11.0 mV

5.3 Rotor Asymmetries

5.3.1 Effect of a missing damper bar

This generator has a damper winding similar to those of the 660 MW sets. The damper bars help to improve the transient performance of the generator but have negligible effect on the steady state condition. There were meant to be 38 damper bars (32 in the rotor slots and 6 on the pole faces) however it was discovered that that one of the damper bars was not inserted by the manufacturer. It is thought that the insertion of the other damper bars bent some of the teeth, which are relatively narrow, and as a result the last damper could not be inserted. This is an example of an asymmetry which can come about during the manufacturing process. The missing damper can be seen in Figure 5.10.

The simulated shaft voltage frequency spectrum is depicted in Figure 5.7, the simulated frequency spectrum with the missing damper is depicted in Figure 5.9. Both these frequency spectrums are normalised with respect to the maximum value of the healthy frequency spectrum (Figure 5.7). Even in the steady state the missing damper has an effect on the shaft voltage. The 3^{rd} and 5^{th} harmonics increase by approximately 5% and 12% with a missing damper, as can be seen from the frequency spectrums. At the slot with the missing damper, the magnetic flux lines cross the air gap differently to those slots with dampers, this is due to the difference in the permeability of copper and air. Thus a small magnetic asymmetry is present which affects the shaft voltage.

5.3.2 Rotor with distorted/wrong size slots

Apart from the missing damper there are rotor slots which appear to have been machined poorly. Noting the width of rotor tooth number 35 in Figure 5.10, in comparison to the adjacent teeth, makes this clear. Since the rotor is covered in



Figure 5.10: Upon removal of part of the resi-glass covering on the rotor, a slot without a damper bar and various other slot distortions were discovered

resi-glass and wound with coils it is not possible to get the exact dimensions of these slots in order to simulate their effect on the shaft voltage. Furthermore it would be a very tedious task entering such a detailed model of the mini-gen in Maxwell 2D! Therefore only two different simulations with distorted rotor slots have been completed.

Table 5.2 presents the RMS shaft voltages from two simulations with distorted rotor slots. In the first the missing damper occurs in a slot which is 1 mm too narrow and lastly another simulation is run with a slot which is 1 mm too wide as an additional distortion. Figures 5.11 and 5.12 present the effects of these distortions on the shaft voltage. Although the effects of the narrow slot are small, the addition of a slightly widened slot results in a large 6th harmonic which does not appear in the measured signal. Perhaps the combinations of many distorted rotor slots have a larger effect on the shaft voltage than just two such distortions. The FEM model neglects these distortions which could be another reason why there is a large difference in the measured and simulated shaft voltage RMS values.

Table 5.2: Shaft RMS voltages for simulations with differently distorted rotor slots

Simulation	Shaft Volts (mV)
Perfect Rotor	11.0
Missing damper	11.2
Missing damper in narrow slot	10.7
Missing damper in narrow slot + 1 wide slot	13.3

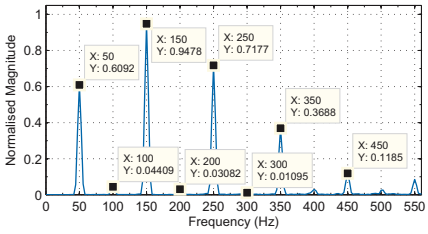


Figure 5.11: Shaft voltage with a missing damper in a slot which is 1mm too narrow

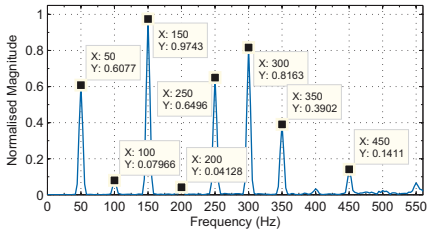


Figure 5.12: Shaft voltage with a missing damper in the narrow slot and one slot which is 1mm too wide

5.4 Shaft based search coil

In [30] it was found that the voltage obtained from a wire passing through the centre of the shaft was approximately equal to the shaft voltage. In [30] a hole was drilled through the centre of the shaft of an induction motor and a wire threaded through. The wire was wrapped round one half of machine back to the starting point. The voltage induced in this loop was measured and compared to the shaft voltage obtained from the shaft brushes.

It is not possible to drill a hole through the shaft of the miniature generator being tested, but a shaft based search coil or flux probe can be simulated in the FE package. Figure 5.1 shows conductors at the centre of the shaft and near the outside of the stator case which were used to define the coil in the FE package.

Figure 5.13 shows the simulated voltage from the shaft based search coil. Comparing it to Figure 5.5 we see that this search coil also produces a voltage similar to the shaft voltage. Therefore it can be concluded that when measuring shaft voltages using the above technique one is really using the shaft as part of a search coil or flux probe. This shaft based search coil also provides an equivalent shaft flux path/loop since the induced voltages are approximately equal.

5.5 Conclusion

A review of the common causes of shaft voltages has been given and through the use of the FE simulations it was found that the weld recesses and key way are examples of constructional asymmetries which can lead to a shaft voltage being generated. They are major causes of the shaft voltage in this machine. Once the key way and

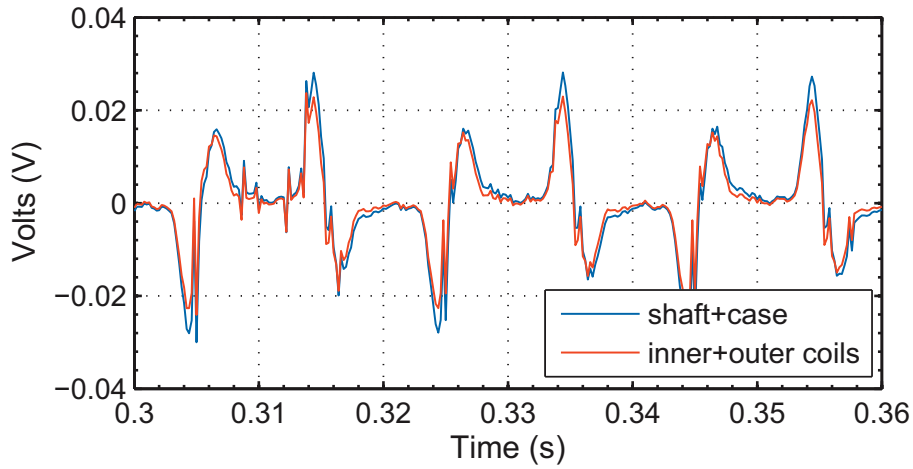


Figure 5.13: Simulated voltages from the shaft based search coil and from the shaft-case based 'winding'

weld recesses were added to the FE model the shaft voltage increased by 3 orders of magnitude. Therefore the following suggestions for avoiding potentially destructive shaft voltages in rotating machinery are made:

- Machine designers should try to avoid the use of constructional techniques which lead to magnetic asymmetries and minimise the number of asymmetries present.
- If certain features (e.g. weld recesses) are unavoidable they should be placed in symmetrical positions.

Another example of an asymmetry, which came about during manufacture, is that of the missing damper bar and its effect on the shaft voltage was also investigated using the FE model. Considering that small asymmetries such as the weld recesses, key way and a missing damper bar have significant effects on the shaft voltage it is anticipated that future investigations, where actual faults are induced in the generator, will yield positive results in terms of being able to uniquely identify the fault using the shaft voltage.

Chapter 6

Further Investigations into Eccentricity

6.1 Introduction

Recent works [11–13, 16–18] have explored using shaft signals as a tool for diagnosing faults in synchronous generators. Success in diagnosing eccentricity in machines with four or more poles and salient pole machines has been reported using shaft signals. Vibration based methods were not included in the above works and two pole non-salient machines are of interest here.

It was verified that no eccentricity exists in the machine and a capture of the shaft voltage and other quantities was taken as a reference for the healthy condition. Three different eccentricities were then induced in the machine and the measurements repeated so as to provide a comparison between the healthy and eccentric states. The eccentricities were all vertical and were of magnitudes: 0.3 mm (downwards), 0.6 mm (upwards) and 0.9 mm (downwards) where a downwards oriented eccentricity reduces the air gap near the bottom of the machine and vice versa. The air gap is 6 mm and it was carefully verified that the air gap was not disturbed in the horizontal direction using air gap feelers. It is possible to measure the air gap from both the drive end (DE) and non-drive end (NDE) of the machine so as to ensure that no skew exists.

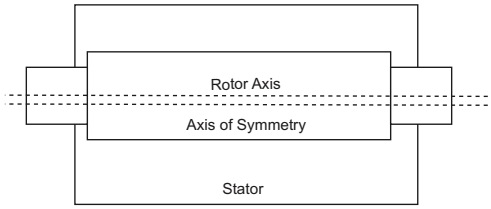


Figure 6.1: Static eccentricity where the axes of symmetry of the stator and rotor are offset but parallel

6.2 Effect of eccentricity on the shaft voltage

6.2.1 Simulated Shaft Voltage

Figs. 6.2, 6.3, 6.4 and 6.5 show the shaft voltage frequency spectrums and Table 6.1 shows the RMS values of the shaft voltage obtained from the simulations. As can be seen in the figures the FEM simulations predict a change in the frequency spectrum of the shaft voltage when eccentricity is present. The most significant changes occur in the 5th harmonic (250 Hz) and the RMS values also change with eccentricity. For the downwards oriented eccentricities (0.3 mm and 0.9 mm) the 5th harmonic increased while for the upward oriented eccentricity (0.6 mm) the 5th harmonic decreased.

After numerous simulations with eccentricity were run it was observed that the increase or decrease in the 5th harmonic is dependent on the orientation of the eccentricity relative to the key way in the stator laminations. The key way sits near the vertical top of the stator in both the 2D FEM model and the actual machine. If the eccentricity is upwards (smaller air gap at top of stator) the 5th harmonic decreases for small eccentricities ($\leq$0.6 mm) and again starts to increase for larger eccentricities. When the eccentricity is horizontal or downwards the 5th harmonic was found to simply increase with increasing eccentricity.

Table 6.1: Simulated shaft RMS voltages with various eccentricities

Eccentricity	Shaft Volts (mV)	% Change	% Eccentricity
none	11.0		0
0.3 mm	14.8	34.5	5
0.6 mm	13.1	19.1	10
0.9 mm	26.1	137	15

6.2.2 Measured Shaft Voltage

Figs. 6.6, 6.7, 6.8 and 6.9 are the measured shaft voltage frequency spectrums. As can be seen from the figures the FEM simulations correctly predicted an increase or decrease in the 5th harmonic depending on the orientation of the eccentricity relative to the key way. Since both the simulations and measurements exhibit similar changes in the 5th harmonic it can be concluded that static eccentricity can be diagnosed by identifying changes in the 5th harmonic of the shaft voltage.

Table 6.2: Measured shaft RMS voltages with various eccentricities

Eccentricity	Shaft Volts (mV)	% Change	% Eccentricity
none	79.0		0
0.3 mm	88.9	12.5	5
0.6 mm	73.2	-7.3	10
0.9 mm	100.1	26.7	15

6.3 Circulating currents and eccentricity

This generator has parallel connected phase groups as in Figure 6.10 and it was expected that circulating currents would be induced as shown in the figure when an eccentricity is present as predicted by the 2D FEM simulations and as observed in [13].

Measurements of the phase group currents were taken with the generator running on no load and full load and are presented in Tables 6.3, 6.4 and 6.5. It was found that small circulating currents exist even when there is no eccentricity suggesting that there are small asymmetries in the machine e.g. small ovality in stator or small differences in the phase group impedances. The armature is mush wound and not impregnated which also contributes to the asymmetries in the machine. However these circulating currents, with no eccentricity, are not significant compared to the full load current of 34 A.

As the level of eccentricity increases the circulating current increases significantly on both no load and full load. The percentage circulating current for the full load condition is defined as $i_{circ_a}\% = \frac{i_{a1}-i_{a2}}{i_{a1}+i_{a2}} \cdot 100$ where i_{a1} and i_{a2} are phasors. The magnitude of the circulating current is very sensitive to the air gap and large phase shifts (ϕ) between phase group currents were observed in both the simulations and measurements.

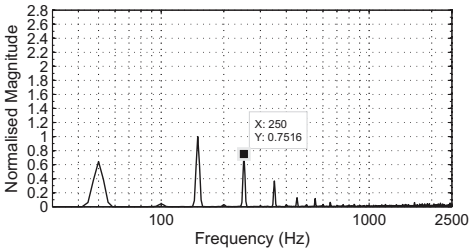


Figure 6.2: Simulated shaft voltage frequency spectrum with no eccentricity

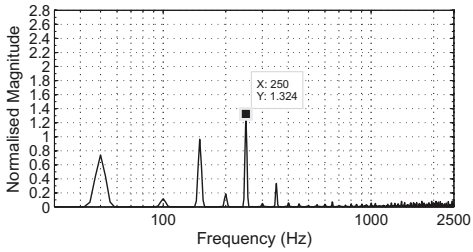


Figure 6.3: Simulated shaft voltage frequency spectrum with 0.3 mm eccentricity

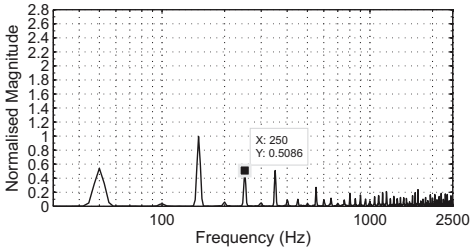


Figure 6.4: Simulated shaft voltage frequency spectrum with 0.6 mm eccentricity

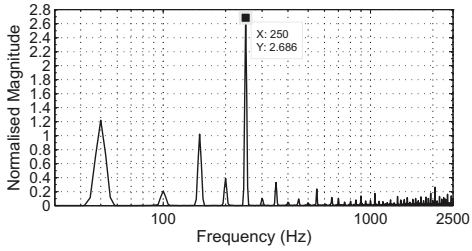


Figure 6.5: Simulated shaft voltage frequency spectrum with 0.9 mm eccentricity

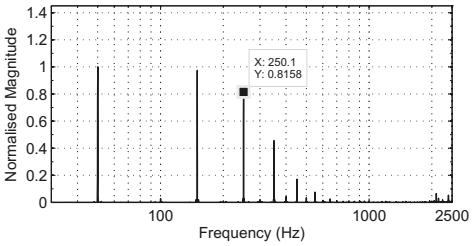


Figure 6.6: Measured shaft voltage frequency spectrum with no eccentricity

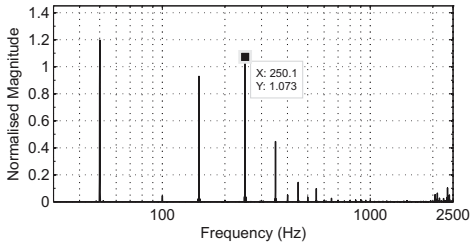


Figure 6.7: Measured shaft voltage frequency spectrum with 0.3 mm eccentricity

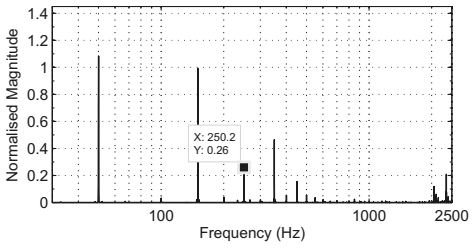


Figure 6.8: Measured shaft voltage frequency spectrum with 0.6 mm eccentricity

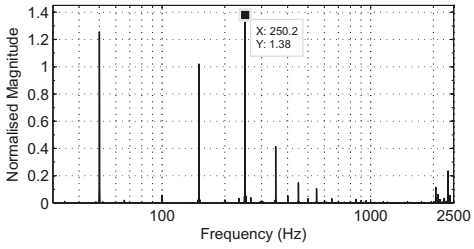


Figure 6.9: Measured shaft voltage frequency spectrum with 0.9 mm eccentricity

Other faults such as shorted stator laminations, earth and inter-turn shorts may cause circulating currents in machines with parallel circuits. However given the sensitivity of the circulating current to eccentricity it would be advisable to check for eccentricity if other faults are unlikely or haven't been detected by the protection system!

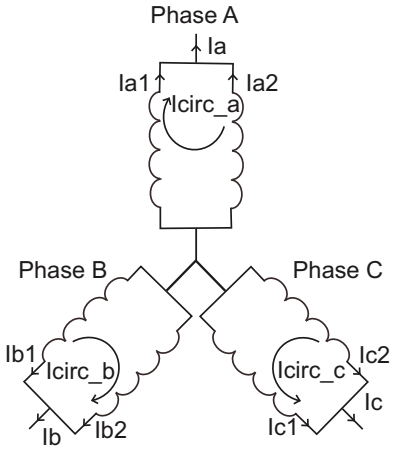


Figure 6.10: Parallel star connection of armature phase groups showing path for circulating currents

Table 6.3: Measured circulating current in **Amperes** (A) with no load

Eccentricity	Phase A (A)	Phase B (A)	Phase C (A)
none	0.47	0.68	0.54
0.3mm	3.31	4.2	4.23
0.6mm	6.8	9.4	8.71
0.9mm	7.5	9.9	9.43

Table 6.4: Simulated **percentage** (%) circulating current on full load

	Phase A		Phase B		Phase C	
Eccentricity	%	ϕ	%	ϕ	%	ϕ
none	0.52	0°	1.14	-2.9°	0.77	0.5°
0.3mm	31.8	-27°	31.9	-16°	32.5	39°
0.6mm	63.2	53°	64.3	35°	63	-69°
0.9mm	95.1	-93°	96.1	-92°	96.2	92°

Table 6.5: Measured **percentage** (%) circulating current on full load

	Phase A		Phase B		Phase C	
Eccentricity	%	ϕ	%	ϕ	%	ϕ
none	2.94	4°	4.92	5°	3.97	3°
0.3mm	21.6	-9°	28.3	-17°	28.7	-34°
0.6mm	47.8	8°	65.1	63°	60.0	62°
0.9mm	51.7	-14°	68.2	-60°	66.6	-68°

6.4 Vibrations and eccentricity

The vibrations were measured from the drive end bearing as in Figure 6.11 as it was noted that they are of largest magnitude in this location.



Figure 6.11: Placement of the vibration probes to measure radial and axial vibrations on the drive end bearing

6.4.1 Axial vibrations

Figs. 6.12, 6.13, 6.14 and 6.15 show the frequency spectrums of the axial vibrations with increasing eccentricity. Similar to the shaft voltages there is a large increase in the 5th harmonic with increasing eccentricity. There is also a large increase in the 4th harmonic.

6.4.2 Radial Vibrations

Figs. 6.16, 6.17, 6.18 and 6.19 show the radial vibrations, no significant increase in any particular harmonic is present.

It is interesting that the eccentricity caused an increase in the axial vibration levels and in particular the 5th harmonic which correlates with the trend noticed in the shaft voltage. It is unclear why the eccentricity manifested itself in the axial vibration. The lack of an increase in the radial vibrations could possibly be explained by the presence of the parallel connected phase groups and large circulating currents when eccentricity is present. The unbalanced magnetic pull (UMP) which is created when an eccentricity is present can be mitigated by the unbalanced currents in the phase groups [31].

The generator is driven by an inverter fed induction motor and it must be born in mind that the vibrations observed on the NDE bearing are dependent on vibrations from the induction motor transmitted through the coupling to the shaft of the generator.

6.5 Conclusion

The results of an investigation into using shaft voltages, vibrations and armature currents as a means of diagnosing eccentricity in a non-salient 2 pole synchronous generator have been presented. The following conclusions are drawn:

- It was found that when an eccentricity is present the 5th harmonic in the shaft voltage increases or decreases depending on the orientation of the eccentricity relative to the key way.
- Shaft voltage monitoring has potential for use as a condition monitoring method but the relationship between the healthy and eccentric signatures is complex in this machine.
- Constructional asymmetries can have a large effect on the shaft voltage and could cause complications in terms of using shaft voltages as a condition monitoring tool.
- When investigating the use of shaft signals as a condition monitoring tool many variations of a single fault should be implemented to ensure that there

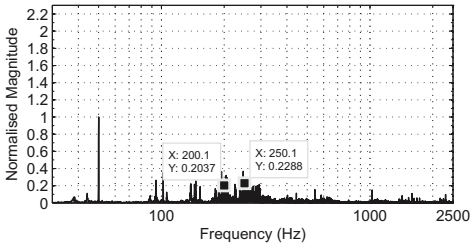


Figure 6.12: Measured axial vibration frequency spectrum with no eccentricity

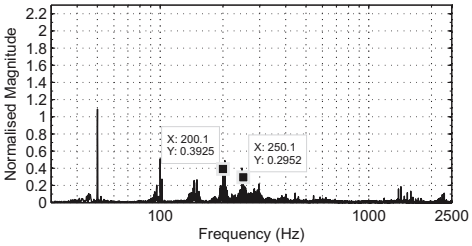


Figure 6.13: Measured axial vibration frequency spectrum with 0.3 mm eccentricity

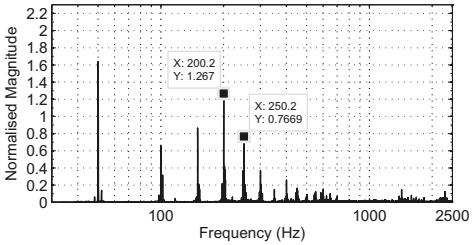


Figure 6.14: Measured axial vibration frequency spectrum with 0.6 mm eccentricity

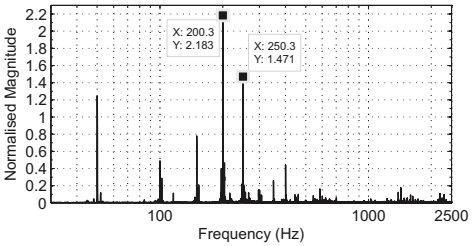


Figure 6.15: Measured axial vibration frequency spectrum with 0.9 mm eccentricity

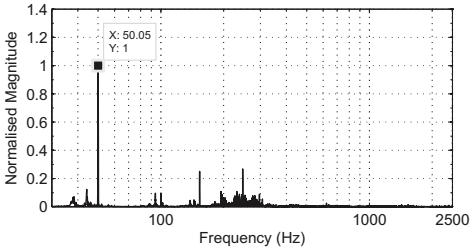


Figure 6.16: Measured radial vibration frequency spectrum with no eccentricity

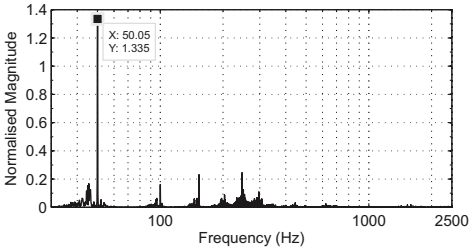


Figure 6.17: Measured radial vibration frequency spectrum with 0.3 mm eccentricity

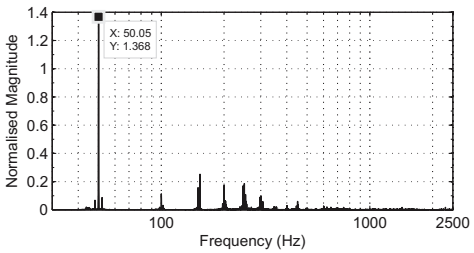


Figure 6.18: Measured radial vibration frequency spectrum with 0.6 mm eccentricity

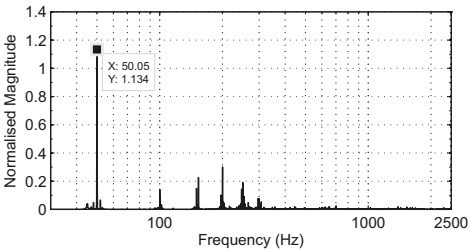


Figure 6.19: Measured radial vibration frequency spectrum with 0.9 mm eccentricity

are no complex relationships between the shaft voltage and the fault as was observed here. For example, if horizontal eccentricities had been investigated exclusively, the possibility of a decrease in the 5th harmonic with eccentricity present would not have been discovered.

- It was found that large circulating currents exist between the parallel connected phase groups when an eccentricity is present.
- The magnitudes of the circulating currents are very sensitive to the distortion of the air gap due to eccentricity. For example with 0.3 mm (5%) eccentricity the percentage circulating current on full load is 28% for phase B.
- The axial vibrations show large increases in the 4th and 5th harmonics with eccentricity, and could possibly be used to diagnose eccentricity.

Chapter 7

Simulation Based Fault Study

7.1 Introduction

The FEM model has not only been used to simulate static eccentricity, but other types of faults too. Simulating faults before they are induced in the mini-gen has several advantages. It helps one understand the fault better, since the fault must be represented in either the external circuit or in the drawing itself. Knowing which faults to induce first is also useful since we would rather start with faults which the FEM model predicts will affect the shaft voltage. Inducing a fault in the mini-gen can take several weeks because the job may be scheduled in with various other projects the lab staff are conducting. Many variations of a particular fault can be simulated much quicker than they can be induced in the mini-gen. Therefore a great deal of knowledge can be gathered before the fault is actually induced using the FEM model.

Various field and armature winding faults which can occur in a large 660 MW set have been simulated and their effect on the shaft voltage quantified. It is hoped that these simulations will be of use to future work.

7.2 Field Faults

7.2.1 Simulation Techniques

Before faults in the field winding can be simulated it is necessary to adapt the Maxwell FEM simulations so that the faults can be induced in the external circuit.

The field circuit was originally defined in the winding editor in Maxwell not in the external circuit. Figure 7.1 shows the adapted FEM model with the field winding included in external circuit. The field winding is excited by means of a current source instead of a voltage source as was the case when the field winding was defined in the winding editor. It was found that Maxwell broke down when the current source was used so a large resistance was added in parallel with the current source in order to simplify the solution for the circuit solver. It is suspected that certain circuit conditions result in the need for infinite rates of change for the current output by the source which makes the ideal current source very difficult to simulate. The field winding circuit includes a resistance of 500 mΩ which represents the DC resistance of the field coils. The Maxwell circuit solver requires that all sub-circuits are connected to ground. Since the field winding is obviously insulated from the shaft, this connection does not exist in the mini-gen so a large resistance was used to connect the field sub-circuit to ground. C_g is the capacitive coupling between the field winding and the shaft which was measured at 1 kHz. It was decided to include this capacitance even though capacitive coupling would only be expected to be significant at higher frequencies because it is more representative of the actual machine.

Figure 7.7 shows the shaft voltage generated when a voltage source is used in for the field excitation in the winding editor and Figure 7.8 is from the field circuit in the external circuit. The shaft and phase voltages are tabulated in Table 7.1. The spectrums and RMS values show that the field circuit based simulations are valid and that the differences between the two methods for simulating the mini-gen are negligible.

As explained in Chapter 2 the field coils are not drawn individually, in order to simulate an inter-turn short circuit it is necessary to separate some of the coils as in Figures 7.2 and 7.3. In Figure 7.2 the coils in the rotor slots nearest the pole faces are separated into 3 groups, 2 individual turns and one large group for the remaining 8 turns. The coils are similarly divided in Figure 7.3 except in slots equidistant from the pole faces in order to determine whether the location of the inter-turn short in the rotor has an effect on the shaft voltage.

In Maxwell the inter-turn shorts are implemented in the external circuit which now must include the individual coils as they were grouped in Figures 7.2 and 7.3. Figure 7.4 is the corresponding circuit showing only the field winding (the armature and shaft winding remain unchanged) with a single inter-turn short. LField1 and LField2 represent the first 2 turns in the 1st rotor slot, while LField3 represents turns 3-10.

LField4 is for the remaining 150 turns. An approximation is made in that the resistance of each turn is made equal and Rfield1 is the resistance of the shorted turn while Rfield is the resistance of the remaining turns.

Figure 7.5 is the field sub-circuit with 2 inter-turn shorts and Figure 7.6 has an earth fault in the field winding. In Figure 7.5 Rfield1 and Rfield2 are the resistances of the shorted turns and Rfield is the resistance of the remaining turns. Likewise in Figure 7.6 Rfield1 is the resistance of the first 2 coils and Rfield the resistance of the remaining coils. The earth short has occurred on the 2nd turn in this circuit. All these circuits were tested without the faults present and the results of the simulations were validated.

7.2.2 Effect of inter-turn shorts on the shaft voltage

Figures 7.9 and 7.10 are the shaft voltage frequency spectrums for the inter-turn shorts occurring in the 1st and middle slots respectively. For the fault in the first slot there is a doubling in the magnitude of the 6th harmonic while for the fault in the middle slot there is a 7 fold increase in that harmonic. This suggests that an inter-turn short may be detectable independent of the slot in which it occurs, however the effect on the shaft voltage may be pronounced when it occurs in certain slots. It is not understood why the 6th harmonic is affected by an inter-turn short and it would seem more promising if the 6th harmonic was larger in proportion to the other harmonics, but the increases in this harmonic are very large indeed!

To further investigate the increase in the 5th harmonic with the presence of inter-turn shorts a simulation was run with 2 of these faults present in the same slot between consecutive coils. The 6th harmonic in Figure 7.11 exhibits an increase of 13 times compared to that of Figure 7.8 which makes the trend clear: The presence of an inter-turn fault in the field winding causes the 6th harmonic to increase.

Table 7.1: Shaft and Phase voltages for simulations with various field winding faults

Simulation	Shaft Volts (mV)	Phase Volts (V)
Field winding in winding editor	11.0	179.2
Field winding in external circuit	10.7	178.0
Inter-turn short 1st slot	10.7	177.6
Inter-turn short middle slot	10.4	177.2
2x Inter-turn short 1st slot	10.5	176.5
Short to earth in middle slot	10.7	178.7

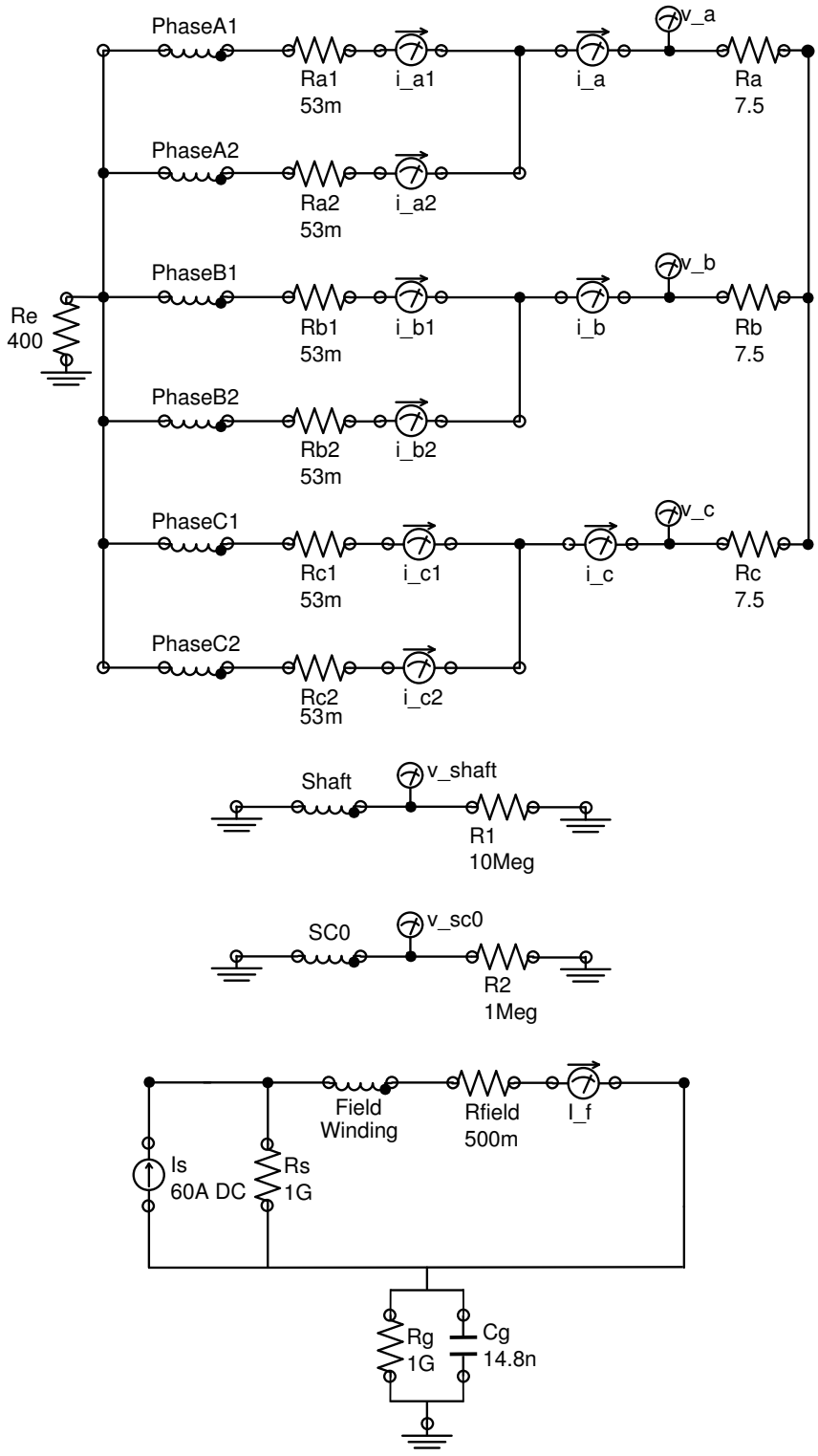


Figure 7.1: Maxwell 2D external circuit including the field winding

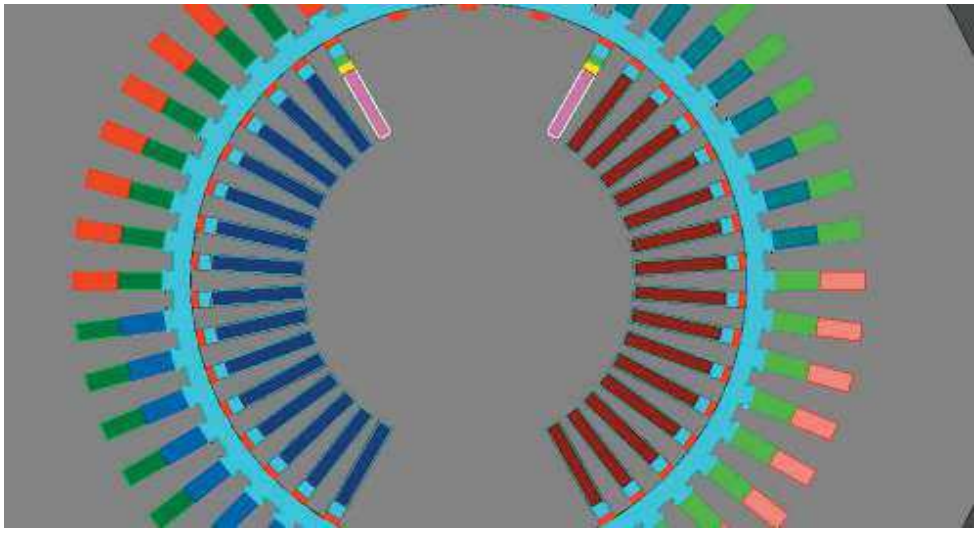


Figure 7.2: Boundaries and Sources editor in Maxwell 2D showing how the field coils are split up to simulate an inter-turn short in the top slots of the rotor

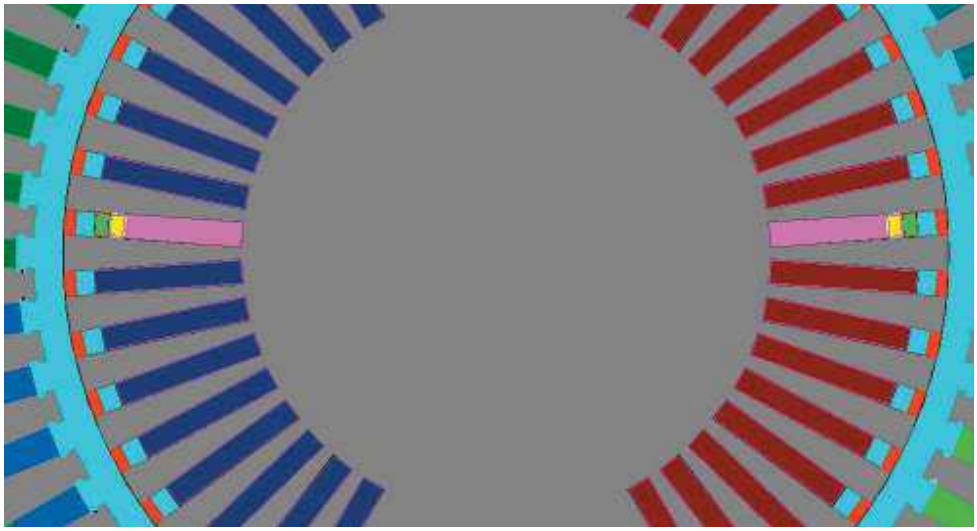


Figure 7.3: Boundaries and Sources editor in Maxwell 2D showing how the field coils are split up to simulate an inter-turn short in the middle slots of the rotor

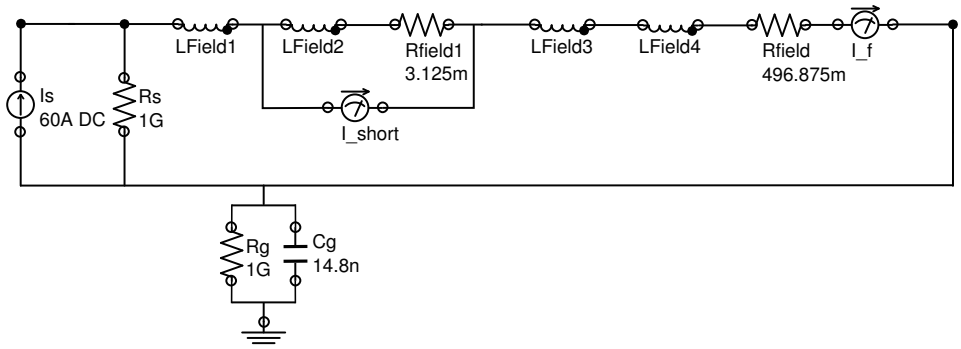


Figure 7.4: Maxwell 2D external circuit showing how an inter-turn short is induced in the field winding

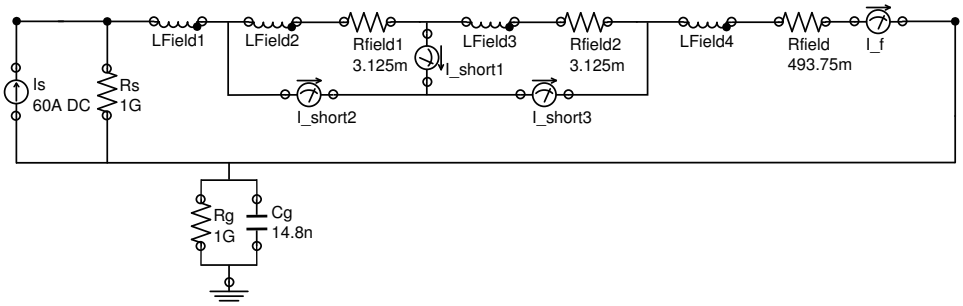


Figure 7.5: Maxwell 2D external circuit showing how 2 inter-turn shorts are induced in the field winding

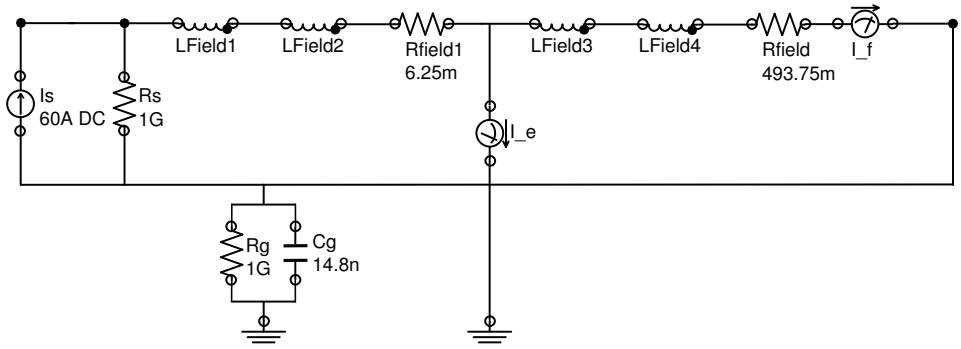


Figure 7.6: Maxwell 2D external circuit showing how a short between the field winding and the shaft (earth) is simulated

7.2.3 Effect of a single earth fault on the shaft voltage

It would be very desirable to be able to detect a single field to earth fault since a double earth fault could effectively remove a large number of turns from the field winding. If the fault could be detected then it would provide a warning that a double earth fault might present itself if repairs are not carried out in good time.

A simulation with a short between the 2nd turn in one of the middle rotor slots and the rotor core was run. The shaft voltage frequency spectrum from this simulation is depicted in Figure 7.12. Unfortunately there does not appear to be any noticeable differences between this spectrum and the healthy one.

It may be worthwhile to attempt to simulate this fault in Flux using a different technique. The coil where the short has occurred could form part of both the field and shaft windings in the external circuit. In this way it would not be necessary to insert the connection between the coil and earth in the field winding sub-circuit, the coil and the shaft would already be connected by definition.

It seems as though the asymmetry created by the fault is too small to affect the shaft voltage significantly. Considering the high impedance path of the fault current, this is understandable. Even at higher frequencies where the capacitive coupling between the shaft and winding is more significant the impedance of that loop is high (4 kΩ at 2.5 kHz). It may be necessary to run the simulations with a smaller time step to look for frequencies which can couple to the shaft capacitively more easily.

A 3D FEM application could aid in modelling the fault more accurately. Real conduction paths are taken into account in 3D and a fault between the field winding and shaft could be modelled as 2 conductors actually contacting.

7.2.4 Inducing field winding faults in the mini-gen

In the mini-gen only inter-turn shorts in the middle rotor slots can be induced since the resi-glass prevents access to the other coils in the overhang as can be seen in Figure 7.13. To make inserting an inter-turn short in these coils easier less insulation was applied to these coils on the outside of the overhang.

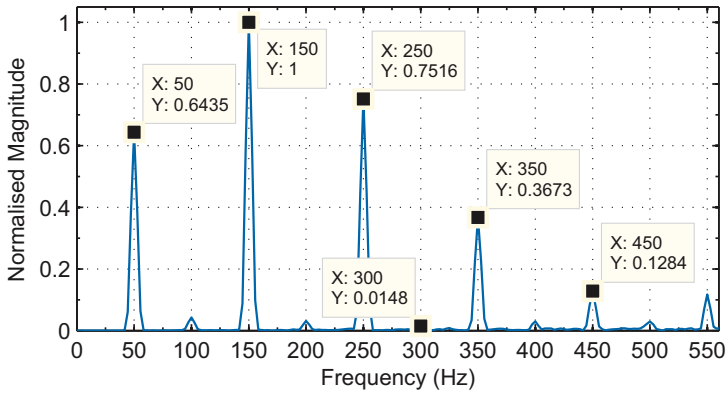


Figure 7.7: Shaft Voltage with the Field Winding excited by a voltage source in the winding editor

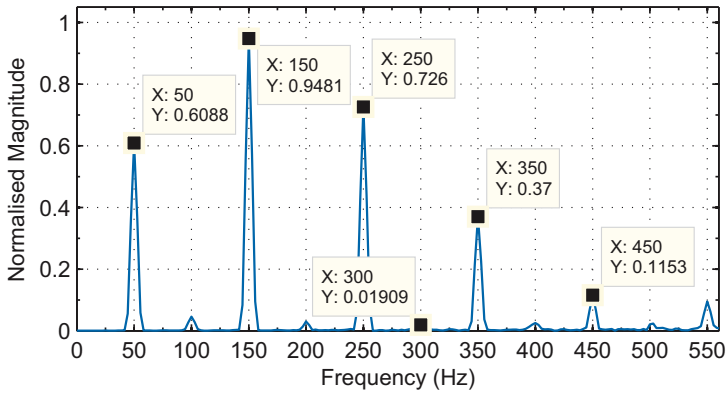


Figure 7.8: Shaft Voltage with the Field Winding excited by a current source in the external circuit

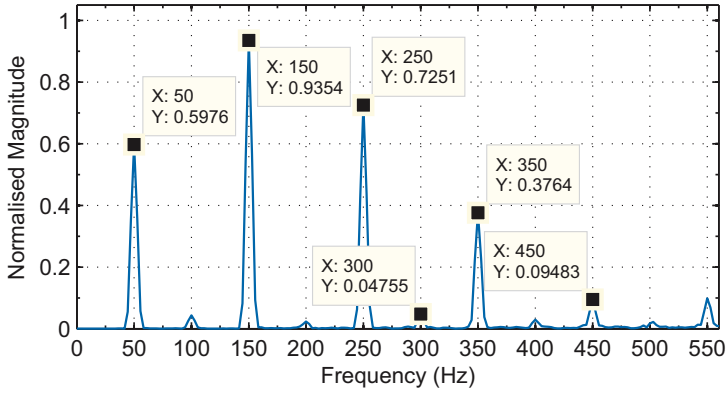


Figure 7.9: Shaft Voltage with one inter-turn short in the field winding in the 1st rotor slot

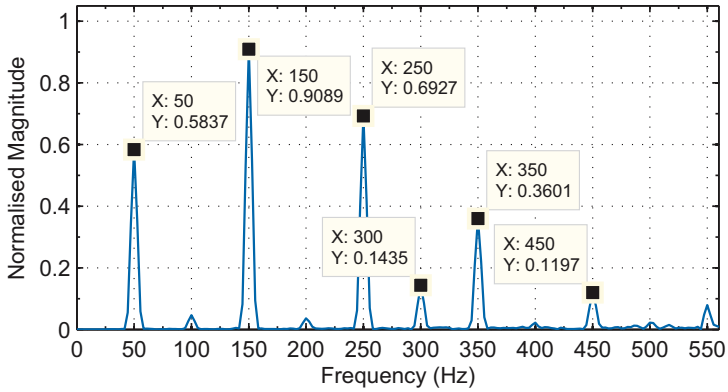


Figure 7.10: Shaft Voltage with one inter-turn short in the field winding in the middle rotor slot

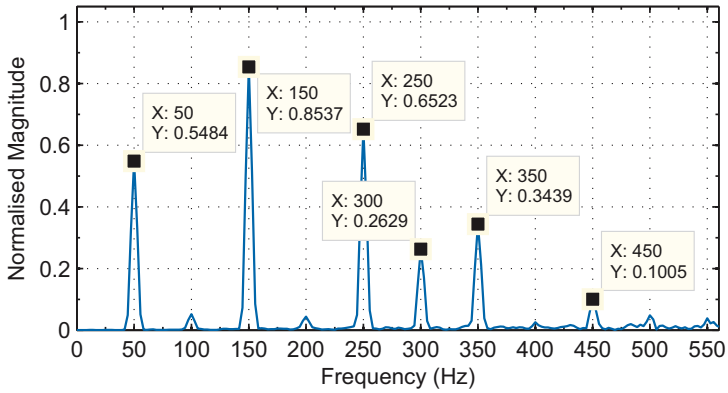


Figure 7.11: Shaft Voltage with two inter-turn shorts in the field winding in the middle rotor slot

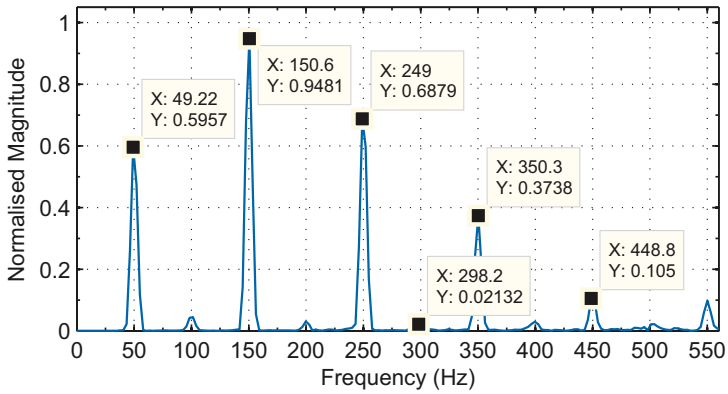


Figure 7.12: Shaft Voltage with a short between the field winding in the middle rotor slot and earth

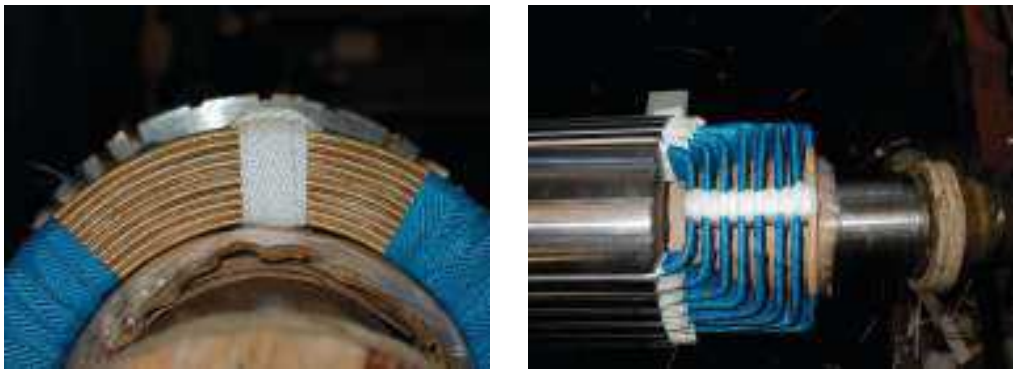


Figure 7.13: Insulation on the outermost rotor coils in the field winding overhang was deliberately removed during construction to allow for inter-turn shorts to be induced in the mini-gen

7.3 Exciter Faults

Exciter faults such as a failed rectifier would be a fault well suited to simulation with an FEM application. It is also particularly easy to induce in the lab by connecting one of the auto-transformers with a built in rectifier to the mini-gen as the excitation source. One of the diodes could be removed from the rectifier to mimic the effects of a failed rectifier in one of the rotating exciters that the larger 660 MW sets.

In the external circuit of the FEM application a diode based exciter could be connected to the field winding and various combinations of faults investigated. Both Flux and Ansys, two new FEM applications now available, can link with Matlab Simulink where a more realistic exciter could be modelled.

It would be expected that certain harmonics related to the structure of the exciter transfer to the shaft by means of capacitive coupling. An exciter with a failed rectifier would probably generate a different shaft voltage frequency spectrum from that of a fully operational one.

7.4 Armature Faults

One would imagine that faults such as earth faults in the armature winding or a phase group open circuit could be reliably detected by the protection equipment installed with each large turbo-set. Interestingly earth faults are not always detected by some protection systems as described in [32]. It has also been reported that a phase group open circuit was undetected by a protection system for a sustained

period of time on a 660 MW set. Indeed these faults going undetected may seem somewhat unlikely but having more than one means of detecting them could be advantageous for those occasions of uncertainty.

Both earth faults and a phase group open circuit have been simulated in Maxwell and the effects on the shaft voltage are significant as will be expanded on below.

In order to simulate earth faults some of the coils of the phase in which the fault is to occur need to be drawn individually as was done with the rotor coils in which inter-turn faults were to be simulated. Two different types of earth faults have been simulated; an 1/8th of phase group shorted to earth and 1/2 of a phase group shorted to earth. The armature circuits with the induced earth faults are included in Figures 7.14 and 7.15. It has also been assumed that the resistance of the individual turns is equal for the armature winding. An earthing resistor has been connected to the star point of the armature winding in order to limit the fault current and more accurately simulate the extent of the asymmetries created by such faults. The value of this resistor was chosen based on information obtained about the sizing of the earthing resistors the 660 MW sets. R_e is sized such that the ratio of the fault current to the full load current is equal in both the large 660 MW sets and the mini-gen for a given fraction of a phase group being shorted to earth. After the simulations were already run it was discovered that many generators use isolation transformers and a split star configuration to limit the current caused by earth faults. Therefore it is recommended that those configurations also be simulated and the mini-gen lab setup modified to more realistically model that of a 660 MW generator. The shaft voltage with the earthing resistor in the external circuit is presented in Figure 7.16 and was used as the reference with respect to which the spectrums with faults are normalised. There are no significant differences between this spectrum and the one obtained with no earth resistor.

The phase group open circuit was simulated by simply changing the value of one of the phase group resistances e.g. R_{a1} in Figure 7.14, to 1 GΩ to represent the open circuit. It was verified that the simulations produced the correct results without the faults present.

7.4.1 Earth Faults

The shaft voltage RMS values are recorded in Table 7.2 and there are some changes but no clear pattern emerges. For the fault in the 1st slot the shaft voltage increases but for the fault in the 4th slot (with a larger portion of the phase group shorted)

the shaft voltage decreases. The currents in the earth loop do increase as expected though.

The shaft voltage frequency spectrums of Figures 7.17 and 7.18 do exhibit consistent changes though. The harmonics between 400 and 2500 Hz increase significantly, the 17th, 27th and 43rd harmonics in particular.

Table 7.2: Simulated shaft voltages and earth currents with various armature faults

Simulation	Shaft Volts (mV)	Earth Current (mA)
Healthy	11.0	0
Earth fault: Phase A1 slot 1	11.3	24.4
Earth fault: Phase A1 slot 4	10.9	290
Phase Group Open Circuit	16.7	0

7.4.2 Phase Group Open Circuit

A phase group open circuit is an interesting but extremely uncommon fault. It can occur when and inter-turn fault causes the coils in a phase group to split somehow and effectively open circuits it. The parallel connection of the phase groups in these type of generators allows the undamaged phase group to continue supplying the full load current for the phase in which the fault occurred - a situation which could go undetected for a short time before the remaining phase group fails with the extra high current that it supplies.

The phase group open circuit has a large effect on the shaft voltage as would be expected. The RMS value increases by 52% and large changes in the harmonic content, shown in Figure 7.19. There are large increases in the fundamental and 3rd harmonics as well as a number of harmonics above 400 Hz.

7.5 Conclusion

The simulations of inter-turn shorts in the field winding, earth faults in the armature and the phase group open circuit indicate that there is potential for being able to diagnose these faults using the shaft voltage. Only measurements on the mini-gen can confirm this.

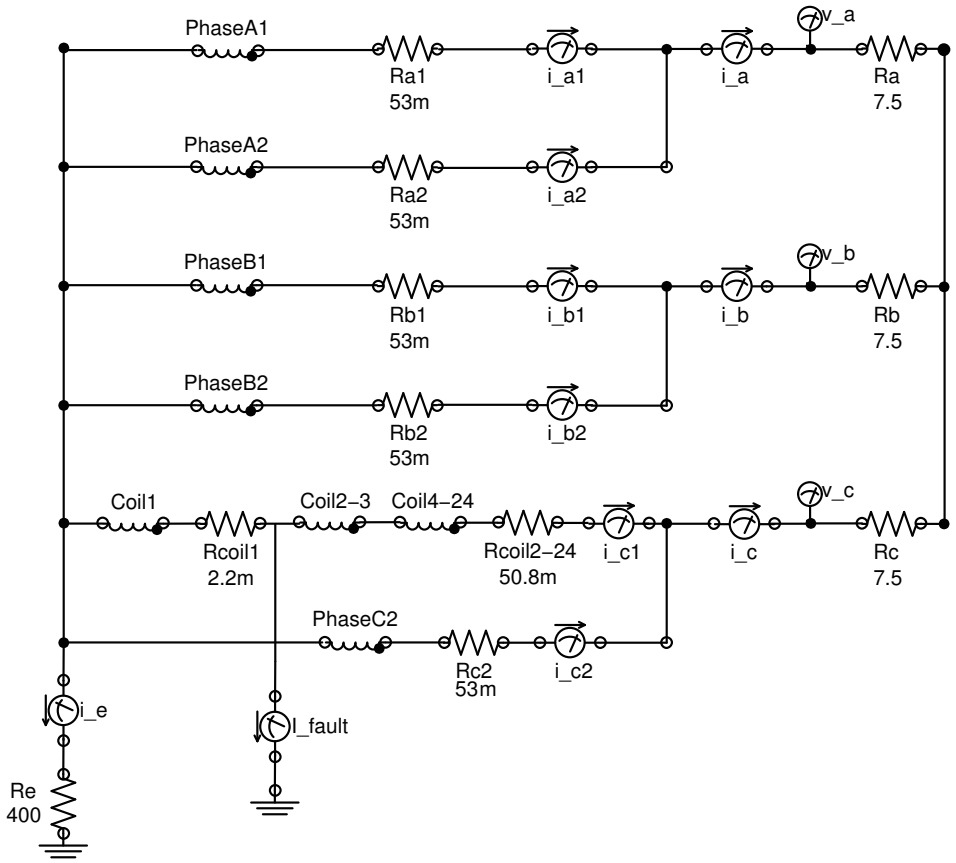


Figure 7.14: Maxwell 2D circuit with phase C partially separated into individual coils and a short between the first coil and earth

As was discovered while investigating the effects on eccentricity on the shaft voltage there may be complex relationships between the harmonics in the shaft voltage and the particular variant of a fault. Therefore it is recommended that when these faults are induced in the mini-gen as many variants as possible be investigated.

The single earth fault in the field winding does not produce a distinctive shaft voltage and some recommendations for investigating this further have been made.

The next chapter introduces the reader to the research group's new FEM package, Flux, which will be used for future FEM experiments. It would be interesting to see if the same results are obtained for the faults discussed above.

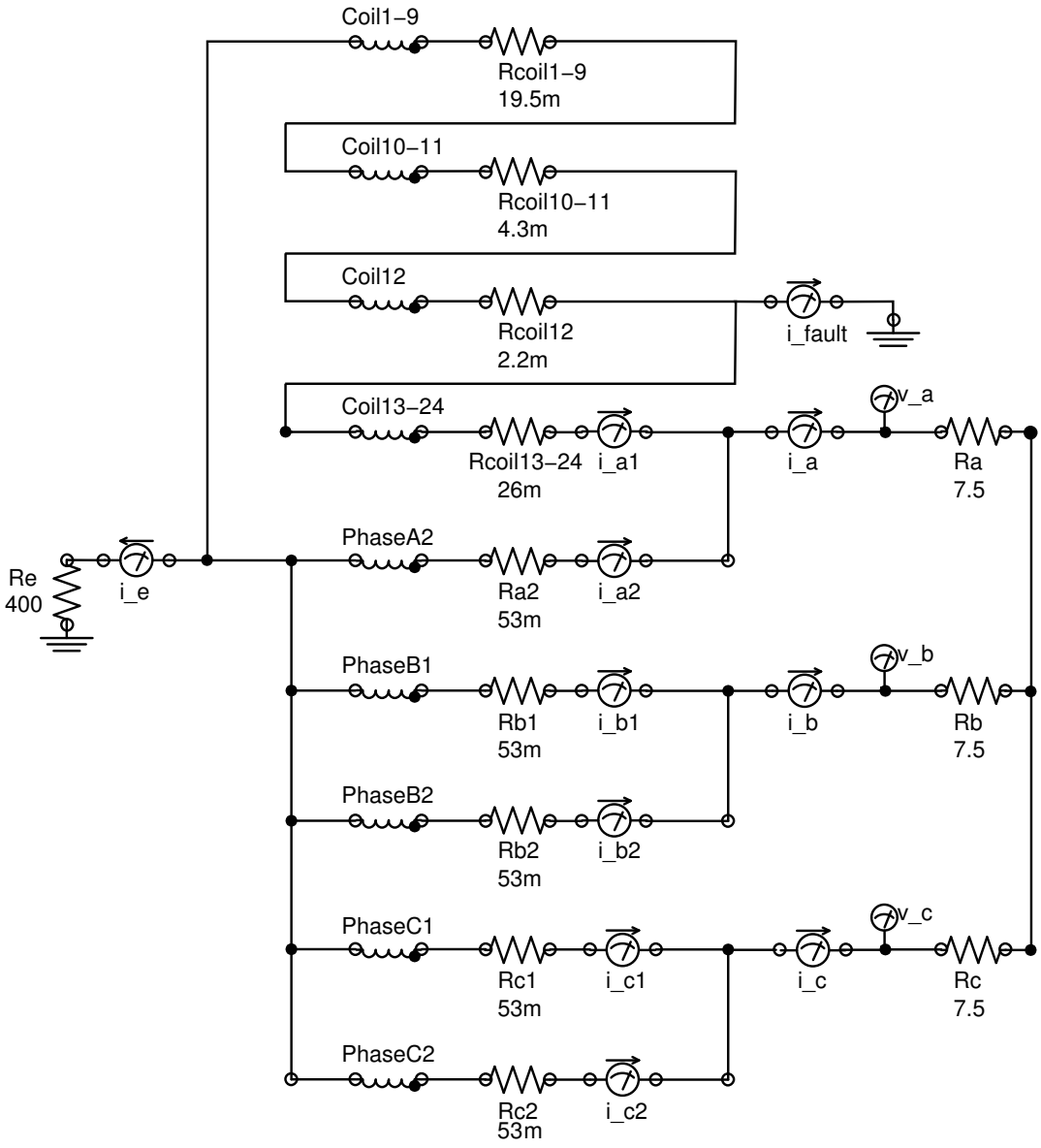


Figure 7.15: Maxwell 2D circuit showing how an earth fault is simulated in Phase A by separating the coils into various groups and connecting an individual coil from the 4th slot to earth

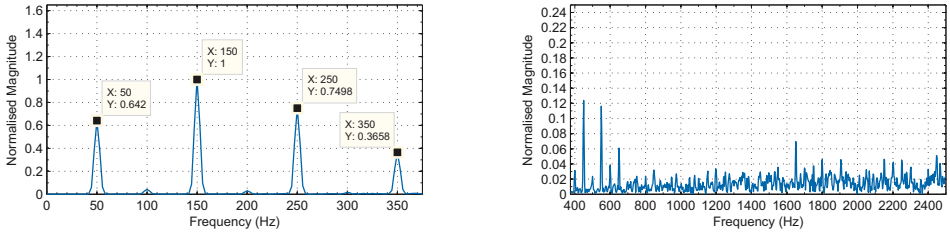


Figure 7.16: Shaft voltage frequency spectrum with an earthing resistor placed on the star point of the armature winding

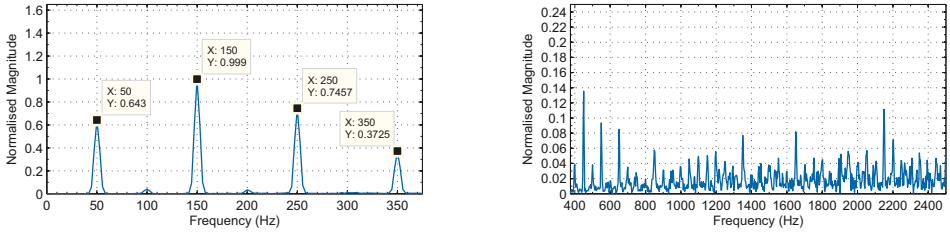


Figure 7.17: Shaft voltage frequency spectrum with a short to earth in the 1st slot of Phase group A1

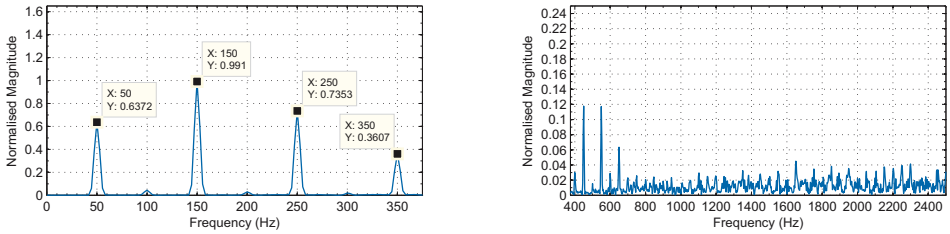


Figure 7.18: Shaft voltage frequency spectrum with a short to earth in the 4th slot of Phase group A1

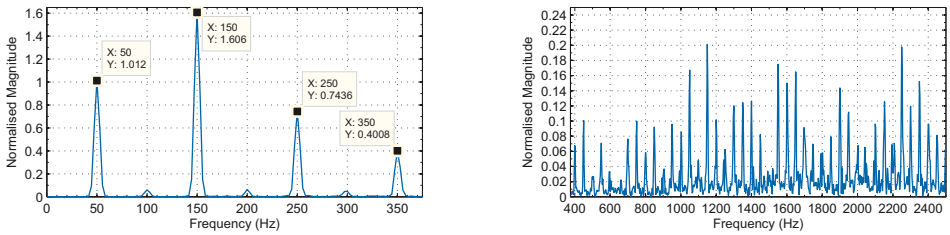


Figure 7.19: Shaft voltage frequency spectrum with a phase group open circuited

Chapter 8

Migrating from Maxwell to Flux

8.1 Introduction

After the expiration of the Maxwell license, the decision was taken to buy a perpetual Flux 2D license since it would be more economical than the annually renewable Maxwell license. Given the importance of the FEM simulations it was imperative that the mini-gen be modelled in Flux. This chapter serves as a migration guide for users starting with Flux who are acquainted with Maxwell. The mini-gen FEM model has been re-created in Flux and that process is documented here and used to highlight the differences between the two FEM programs.

Flux has a modern highly efficient user interface. It features multiple undo levels, comprehensive parameterisation, user definable co-ordinate systems, easy editing of arrays of objects and the option of scripting all or part of the model creation process.

In Maxwell 2D there are five contexts in which a model can be edited, as discussed in Chapter 2. In Flux these are reduced to three, namely, Geometry, Mesh and Physics and all are accessible from the same user interface as opposed to Maxwell where each editor is a separate program. The model creation process is laid out diagrammatically in Figure 8.1 and the contexts in which the model can be edited in the two programs are contrasted along with various other concepts in the Flux and Maxwell paradigms.

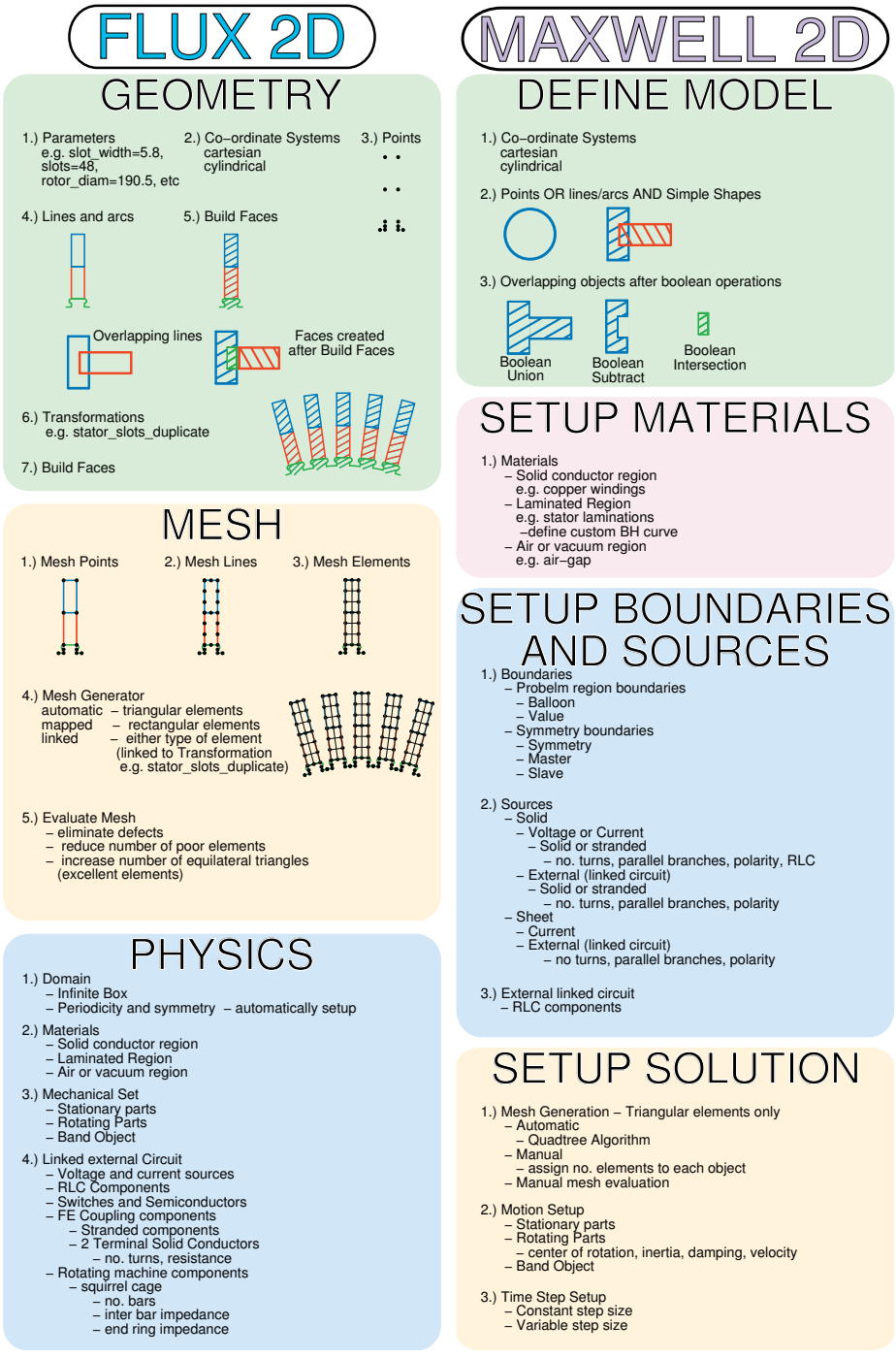


Figure 8.1: Comparison of Maxwell 2D and Flux 2D model creation

8.2 Geometry

The geometry creation process in Flux is vastly different from that of Maxwell. Referring to Figure 8.1, rather than using basic shapes such as rectangles and ellipses with a combination of Boolean operations all objects are created starting with points and then lines. Lines or arcs cannot be defined without first staring with points. These points can be defined in terms of parameters such as slot widths or diameters for example. They can also be drawn in local user defined co-ordinate systems. For example it might be advantageous for some slot shapes to define a co-ordinate system with its origin on a slot opening.

Once all points have been connected with lines/arcs the "Build Faces" can be run. This algorithm automatically creates shapes defined by the intersection of lines and arcs called "faces". Thus it is not possible to have any partially overlapping objects, similar to Maxwell.

To duplicate faces in Flux a transformation needs to be created and applied to the faces of interest. For example a transformation to duplicate a stator slot along an arc could be defined in terms of parameters for the number of slots and an angle. All the duplicated slots will inherit the properties of the original slot. So, the transformation is not just used in the geometry context as it would be in Maxwell, but also in the Physics and Mesh contexts for defining the mesh and materials etc.

Once the transformation is applied the Build Faces algorithm needs to be run to convert the duplicated lines and arcs into faces. This algorithm is run whenever new objects are drawn until the entire problem region is completed.

8.3 Mesh

In Maxwell the processes of drawing the model, assigning materials, boundaries and sources etc must be done in that exact order. In Flux these processes can be done in just about any order. For example after a stator slot has been drawn, the mesh for that region can be created straight away. This is particularly useful for creating good quality meshes. It enables one to focus on the mesh in one region at a time. In this way Flux's user interface is far more flexible than Maxwell's.

Mesh generation in Flux is significantly different from that of Maxwell. Flux generally requires much more interaction with the user to create a good mesh. The

automatic mesh generator most often cannot create a satisfactory mesh. A report is given on the quality of the mesh every time it is generated, listing the number of abnormal, poor and excellent quality elements.

Abnormal elements may have very high aspect ratios or may overlap. The solver cannot run with abnormal elements present. All abnormal elements have to be converted to better quality elements. Abnormal elements can be highlighted so as to provide an indication of the regions which need to be refined in order to remove them. Once all abnormal elements are removed all the "poor" quality elements can be highlighted so as to refine their regions and reduce their numbers. An ideal mesh would only have "excellent" quality elements (elements close to being equilateral triangles or squares) and in practice it is possible to create meshes with very high (above 90%) percentages of excellent elements.

To achieve an excellent quality mesh, mesh generators and lines must be assigned to individual regions. There are three types of mesh generators:

1. Automatic - uses △'ular elements
2. Mapped - uses rectangular elements
3. Linked - links to a transformation to duplicate a mesh from a particular region

The mapped mesh generator is well suited to rectangular shapes such as the stator and rotor slots. Mesh lines and points can be added to refine part of the mesh. For example, mesh lines can be added to the stator slots as in Figure 8.1 to define the number and size of the rectangular elements.

In order to create an excellent quality mesh it is recommended that important regions such as the air gap and stator teeth should consist of several faces. For example in Figure 8.2 the air gap consists of three layers. Each layer has its own mesh lines which results in a dense mesh in the air gap. The stator teeth in Figure 8.2 are composed of two faces as shown by the highlighted lines. The edges of the extra faces allow for extra mesh lines to be created in the stator teeth tips which results in a better mesh in those regions. Figure 8.3 shows how the centres of the rotor and stator were also split up into multiple disks each with mesh lines assigned to them. By setting the number of segments on these mesh lines appropriately the density of the mesh in these regions can be prevented from becoming too high.

Another advantage of using mesh lines extensively is that the overall size of the mesh can be easily adjusted by changing the number of segments on the mesh lines. The

meshes in Figures 8.4 and 8.5 were created by simply reducing a single parameter in the mesh of Figure 8.3.

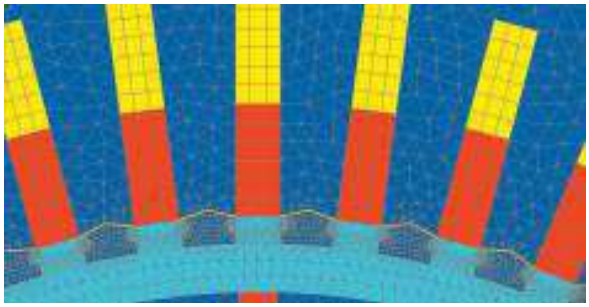


Figure 8.2: Flux 2D mesh 1 showing areas with very high element densities such as the air gap and stator teeth

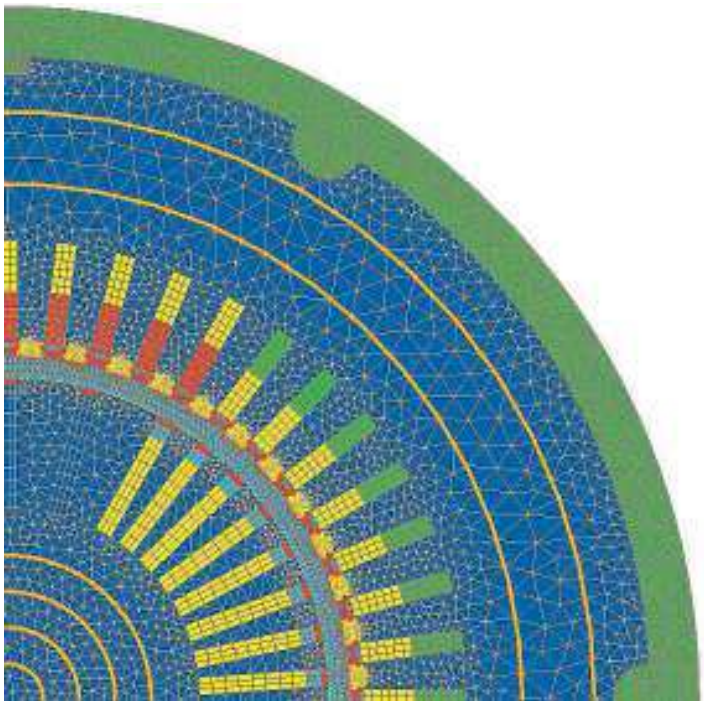


Figure 8.3: Flux 2D mesh 1. Important mesh lines which divide the stator and rotor into segments are highlighted in yellow

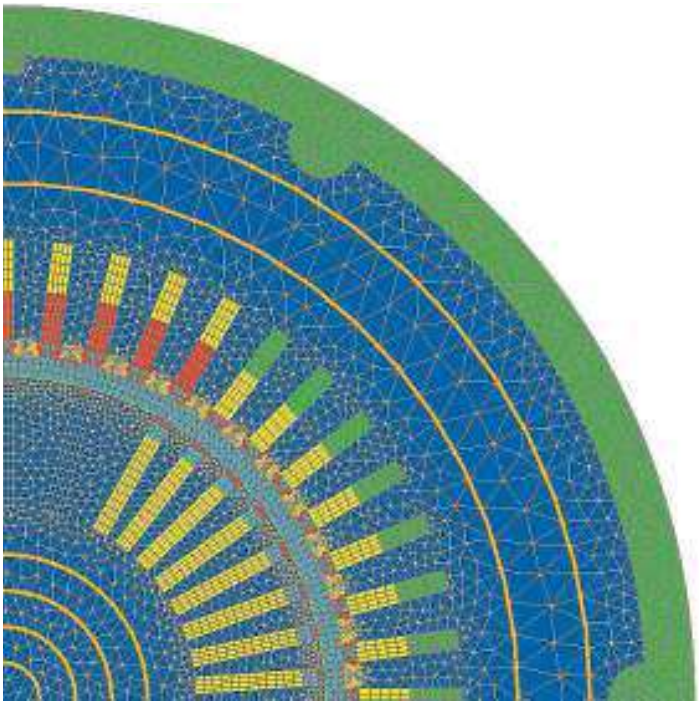


Figure 8.4: Flux 2D mesh 2, obtained by reducing the number of mesh points on the mesh lines as highlighted

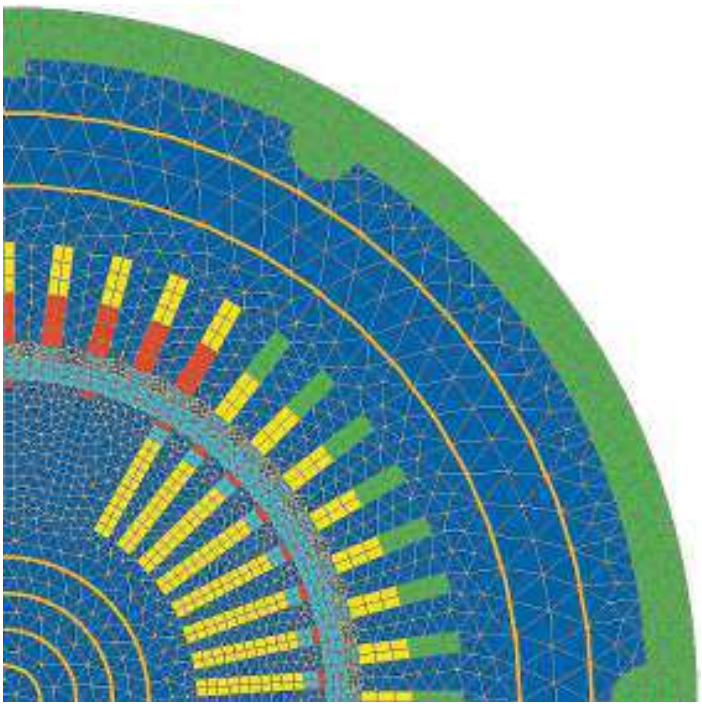


Figure 8.5: Flux 2D mesh 3, obtained by further reducing the number of mesh points on the mesh lines as highlighted

8.4 Physics

Once enough objects are drawn, they can be assigned materials, boundaries and sources etc under the "Physics" context. The materials, sources, motion and external circuit setup in Flux are very similar to those in Maxwell, however they are all accessed from the Physics tab of the user interface rather than from separate editors as in Maxwell. The order in which they need to be applied is also more flexible in Flux.

The boundaries and symmetry setup is a different matter altogether, it is for more automated in Flux. Flux can automatically detect and apply the correct symmetry boundaries which can be of great help.

8.5 Solver

After all the geometry, meshing and physics setup are complete a solver can be selected. There are four solvers, two "SuperLU" and two "CGBiCG" solvers. The "SuperLU" solvers are faster but less stable than the "CGBiCG" solvers, they may be unable to obtain a solution when the mesh is not very dense. All these solvers include a pre-solver which computes the initial conditions to arrive at the steady state before the computation using the fixed time steps begins. This is important, without the pre-solver simulations running for several cycles would have to be run just to arrive at the steady state which would increase the total simulation time significantly.

Apart from being able to select the solver and time step a number of accuracy settings can also be fine tuned. All the accuracy and precision settings were left at their defaults for the simulation results presented here, however it may be worth experimenting with these settings for future work.

8.6 Results

As mentioned above models with three meshes were created. In the same way that different meshes were evaluated in Maxwell, results from different meshes in Flux need to be investigated. The details of these meshes is given in Table 8.1 along with the RMS values of phase and shaft voltages which were obtained from them. The

Maxwell simulation was run with an excitation of 60 A and a load current of 30 A, but the Flux simulations were run with an excitation of 64 A and a load current of 33 A since these conditions are closer to those used with the lab setup. With 64 A excitation on full load (33 A) the mini-gen generates at its rated voltage of 340 V line (196 V phase). As we can see from Table 8.1, similarly to the Maxwell simulations, Flux produces a slightly lower (5%) output voltage which also seems to be due to the BH curves used in the model (both Maxwell and Flux use the same BH curves).

Table 8.1: Simulated Shaft and Phase RMS voltages from different meshes in Flux

FEM Package	Phase (V)	Shaft (mV)	No. Elements	Time (h)
Maxwell 2D	179.2	11.0	8 554	16
Flux mesh 1 (dense)	188.2	6.99	41 816	46.5
Flux mesh 2	188.2	6.01	31 242	24
Flux mesh 3 (sparse)	187.8	4.94	13 348	14

The shaft voltage RMS values in Flux are even lower than in Maxwell, which itself produces much smaller shaft voltages than those measured as was discussed in Chapter 3. The shaft voltages from Maxwell and the three Flux meshes are presented in Figures 8.6, 8.7, 8.8 and 8.9. The measured shaft voltage is included in Figure 8.10 once more for comparison sake. As can be seen from the time waveforms the Flux shaft voltage is significantly different from Maxwell and the measurements. The Maxwell shaft voltage looks like a scaled version of the real shaft signal, but the Flux version does not.

Considering the frequency spectrums, the Flux spectrums have numerous harmonics which are out of proportion with one another and with those of the measured spectrum. The Flux spectrums also differ greatly depending on which mesh was used, showing once again that for simulating such detailed phenomena as the shaft voltage, careful mesh generation is required.

It is suspected that it is the because of the different ways that Maxwell and Flux model curves that they produce different shaft voltages. In Maxwell the curves of weld recesses are modelled as being composed of many straight line segments whereas in Flux they are arcs. Considering the large effect that the weld recesses have on the shaft voltage it would be interesting to see if Flux can produce a better fitting shaft waveform with the weld recesses modelled in the same way that they are in Maxwell.

The Flux waveforms, although they are not as close to the real thing as those of

Maxwell, are still relevant. As was done with the Maxwell frequency spectrums, the shaft signals are normalised with respect to their own maximums and percentage changes in the proportions of the harmonics can be correlated with those from measurements in order to determine whether any particular fault can be diagnosed.

The fastest Flux simulation was 14 hours as can be seen in Table 8.1 which is 2 hours less than the Maxwell simulations which were derived from the mesh evaluation process in Chapter 3. Noting that this Flux simulation has almost 36% more elements it is clear that Flux relies on fast matrix solvers and carefully generated meshes. A mesh with equilateral or square elements results in sparse matrices which can be solved faster than other matrices. The shaft voltage frequency spectrum from this simulation has the same major harmonics present in the measured spectrums although they are of somewhat different proportion, for example the 5th harmonic is disproportioned by a factor of almost 7. It is however the only simulation which correctly predicts that the fundamental harmonic should be of largest magnitude. Considering that the other Flux simulations require considerably longer computation times, this is the optimum mesh to use with this mini-gen Flux model. There may yet be further enhancements which can be made as indicated above with modelling the weld recesses differently and experimenting with different precision settings.

8.7 Conclusion

Flux has been introduced to the reader by means of a direct comparison with Maxwell both in terms of creating a 2D FEM model but also by means of a shaft voltage comparison. The current mini-gen Flux 2D model does not produce as accurate a shaft voltage as Maxwell does. Possible reasons for this have been discussed. However the Flux produced shaft voltage is sufficiently representative of that measured to use it to further enhance the understanding of shaft voltages and for fault investigations.

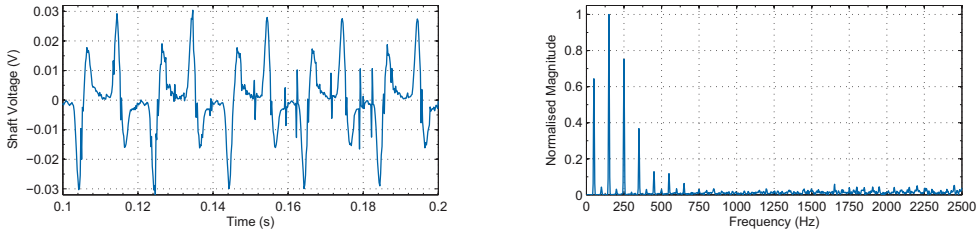


Figure 8.6: Maxwell 2D shaft voltage time and frequency signals

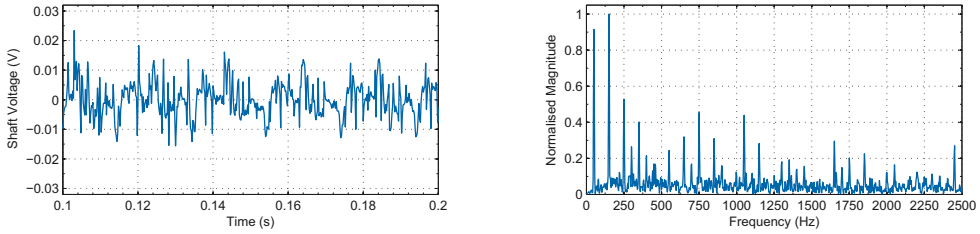


Figure 8.7: Flux 2D shaft voltage time and frequency signals using mesh 1 (dense)

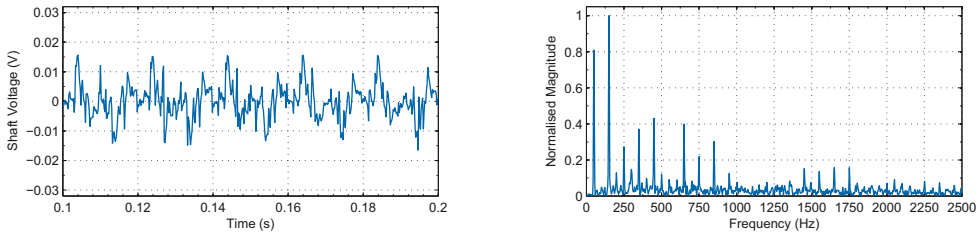


Figure 8.8: Flux 2D shaft voltage time and frequency signals using mesh 2

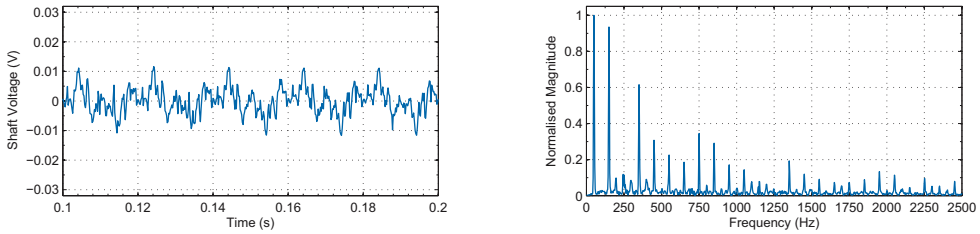


Figure 8.9: Flux 2D shaft voltage time and frequency signals using mesh 3 (sparse)

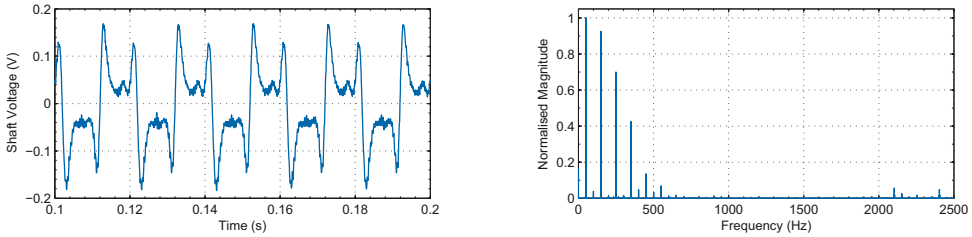


Figure 8.10: Measured shaft voltage time and frequency signals

Chapter 9

Conclusion

To conclude, recommendations for further work are made and the major outcomes of the project are re-iterated.

9.1 Recommendations for further work

9.1.1 Faults to be investigated

Some of the faults which could possibly be induced in the mini-gen include:

1. Field winding inter-turn shorts
2. Field winding to earth shorts
3. Rectifier failure
4. Armature winding to earth shorts
5. Armature winding inter-turn shorts
6. Foreign object failure
7. Bearing insulation failure
8. Stator lamination shorts

It is now necessary to decide which faults to induce in the mini-gen. There are several ways to choose between which faults to investigate, not least of which is how commonly each fault occurs in practice. Other criteria should include:

1. which faults are most easily induced in the mini-gen?
2. which faults are reversible easily?
3. which faults can not be diagnosed using other techniques?

9.1.2 Signal Processing

The means of analysing the healthy and faulty shaft signals has been the FFT and in some cases the power spectral density. The FFTs of the faulty and healthy shaft signals are calculated in Matlab, plotted on a normalised scale and then compared by eye for a change.

It is recommended that a more advanced signal processing technique be investigated, such as using Artificial Neural Networks (ANN) to identify the type of fault given a capture of the shaft voltage. A large number of faults have been simulated in Maxwell 2D and could possibly be used to train a neural network. These simulations could be repeated in Flux 2D and this data used to either test the ANN or provide further training before the ANN is tested on mini-gen data.

A further extension of the project could be to look at methods of identifying faults from data captured during transient conditions e.g. a step change in load or sudden onset of a fault. This may be worthwhile for faults such as broken damper bars which one would expect to have a negligible effect in the steady state operation. Wavelets could be a worthwhile tool to investigate in this regard.

9.1.3 FEM Simulations

A large number of FEM simulations were run, from which a great deal was learnt about the causes of the shaft voltage in the mini-gen as described in Chapter 7. It is likely that by setting up various simulations with many different combinations of rotor and stator slots, different numbers of weld recesses and key-ways, it will be possible to relate the harmonic numbers in the shaft voltage to physical characteristics of the machine such as the number and positioning of the weld recesses.

Concerning the simulation of various faults in Maxwell 2D as described in Chapter 7, it would be worthwhile duplicating those simulations in Flux 2D for the sake of training an ANN and comparing the two FEM packages. Furthermore the more corroborative data available the greater the confidence in the results. Some faults

were not simulated in Maxwell 2D such as exciter faults e.g. a failed rectifier. Simulating such an event in Flux 2D with Simulink would be relatively novel and provide a more complete database of fault simulations. Transient phenomena as discussed above have also not been simulated in the FEM applications.

Lastly the FEM simulations provide a means of comparing the shaft voltage of the mini-gen to that of the large 660 MVA turbo-gens. Considering the effect that the weld recesses and key way have on the shaft voltage as described in Chapter 5 one would expect that the types of constructional asymmetries in the 660 MVA generators, such as segmented laminations, would have their own effects on the shaft voltage which should be investigated and understood. Furthermore the only way of knowing whether the results obtained from the mini-gen are directly applicable is to simulate the faults on a turbo-gen FEM model.

Given the great decreases in RAM prices and large increase in DIMM sizes it could be argued that it is now no longer prohibitive to run 3D FEM simulations - at least using a magneto-static solver. Based on Maxwell 3D simulations which were attempted it is estimated that with 4GB RAM a static solution using 1/4 symmetry (1/2 radial, 1/2 axial) could be completed in reasonable time. So it seems that the computing resources required for 3D FEM simulations are not prohibitive anymore.

9.1.4 Mini-gen Lab Setup

As it stands the mini-gen lab setup doesn't have the ability to run loads of any arbitrary power factor. The full power output of the mini-gen can also not be achieved in the current setup. This will require connecting the mini-gen to a synchronous motor as a variable power factor load. The change in the shaft voltage with output power and power factor could then be investigated.

Further improvements could be made to the lab setup in terms of automation of the various machines using the dSPACE system. For example a dSPACE user interface could be created where the user enters a certain operating point (speed, terminal voltage, load etc) and the system automatically controls the drives and excitation systems to achieve and maintain those conditions.

9.1.5 Shaft Signals

To date no work has been done on measuring shaft currents. It would be interesting to ground both sides of the mini-gen and analyse the current in that loop to see if it is as effective/convenient to monitor the condition of the machine as it is to use the shaft voltage.

As mentioned above little is known of how the shaft signal changes with the operating point of the generator. To fully understand the shaft voltage a study should be done investigating how the shaft voltage changes with excitation, loading and power factor.

9.2 Major Outcomes

Mini-gen: It is possible to measure phase group currents now that the phase group coils have been made accessible. It was the measurement of the phase group currents which led to the discovery that the air-gap was eccentric when it was believed to be aligned. The air-gap has been corrected and the phase group currents are relatively balanced.

Maxwell 2D FEM model: The Maxwell 2D FEM model has been improved and a more realistic shaft signal is now obtainable from the simulations. The most important factor in this improvement was the refinement of the mesh.

Causes of the Shaft Voltage: Using the Maxwell 2D FEM model it was discovered that the key way and weld recesses in the mini-gen are asymmetries which are major causes of the shaft voltage. Other asymmetries such as a missing damper and distorted rotor slots were simulated but their effects on the shaft voltage are not well correlated with the measured shaft voltage. However the sensitivity of the shaft voltages to asymmetries such as the missing damper bodes well for future fault investigations. If such small asymmetries have an effect on the shaft voltage then certain faults may too!

In order to avoid shaft voltages, machine designers should try to avoid the use of asymmetrical features as far as possible.

Diagnosing Eccentricity: It was discovered that the effect of eccentricity on the shaft voltage is more complex than previously imagined, the 5th harmonic can increase or decrease depending on the magnitude and position of the eccentricity relative to the key-way. The increase or decrease is very sensitive to eccentricity even for small eccentricities e.g. 0.1 mm. This emphasises the significant role of constructional asymmetries in affecting the shaft voltage, once again.

Many variations of a single fault should be investigated in future to test for complex relationships like this which could complicate the identification of faults in a real application.

It was also found that vibration and detection of circulating currents are other methods which can be used to diagnose eccentricity.

Maxwell fault simulations: Various faults were simulated and the methods by which they were simulated have been discussed in detail. The simulations predict that inter-turn shorts in the field and armature windings, earth faults in the armature winding and a phase group open circuit can be diagnosed using the shaft voltage. Field to earth faults and exciter faults are yet to be investigated thoroughly using an FEM application.

The next step is to start inducing some of these faults in the mini-gen and simulating them using the newly acquired FLUX FEM application.

FLUX: The process of converting the Maxwell model to a FLUX model was documented in Chapter 8 and it was found that FLUX can also produce a sufficiently realistic shaft signal even though it was not as close to the measured shaft voltage as Maxwell was. The FLUX model may require further refinement as was done on the Maxwell model.

Considering that the only fault investigated so far has been static eccentricity there is still a way to go in determining the usefulness of shaft signals as a diagnostic tool. That said, a solid understanding of the operation of the mini-gen and the FEM applications has been gained and this serves as a solid base from which to start investigating more faults. The predictions of Maxwell with regard to inter-turn faults in the field winding and other faults bode well for future work.

Appendix A

Laboratory Setup Modifications

A.1 Earthing Resistor

Earthing resistors were added between the star points and earth as in Figure A.1. The earthing resistor limits the current in the case of an earth fault in the armature winding. The values were chosen so that the ratio of the fault current to the line current in the mini-gen is equal to that of a 660 MW generator.

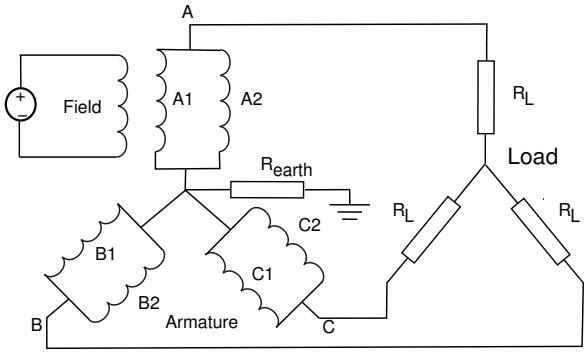


Figure A.1: Armature in parallel star with an earthing resistor

Appendix B

Series Star Configuration

The generator was tested in a series star configuration as in Figure B.1 after large circulating currents were found in the parallel star configuration of Figure B.2. Figures B.3 and B.4 show the break out board of the mini-gen for the series and parallel star configurations. The conventions for the labelling of the terminals of the armature winding are included in Figure B.5 for reference.

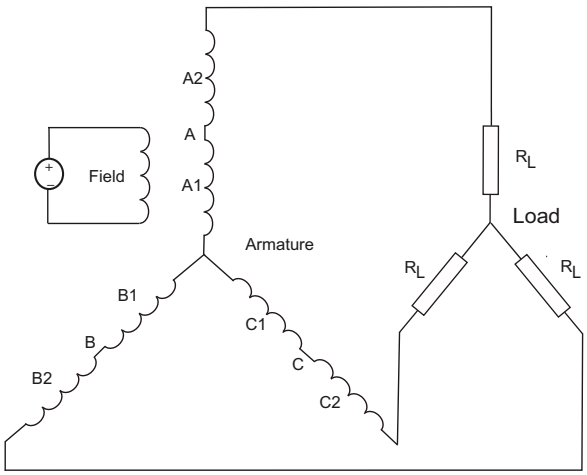


Figure B.1: Armature in series star

The line voltage simply doubles in the series star configuration. Operating at 680 V (62 A excitation) is inconvenient since most of the equipment (auto-transformers, motors) in the lab operates at 380 V to 400 V. Table B.1 shows convenient operating points in the series star configuration. As can be seen a lower excitation is required to produce approximately 400 V for the auto-transformer. The level of saturation will therefore be different from the parallel star-configuration.

Table B.1 shows that the power rating of the mini-gen was underestimated. Even

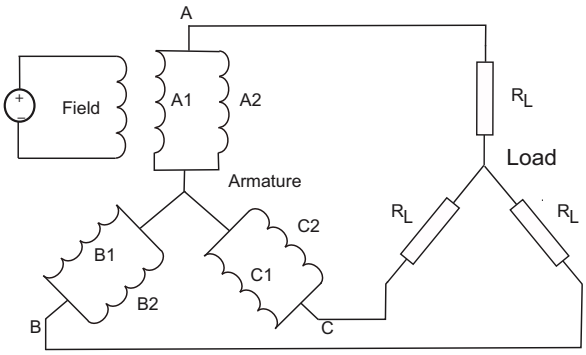


Figure B.2: Armature in parallel star



Figure B.3: Parallel star connection

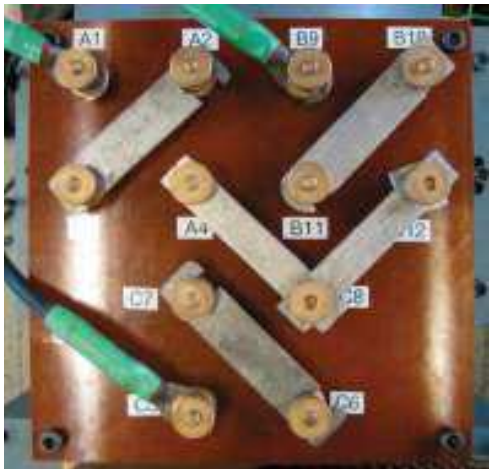


Figure B.4: Series star connection

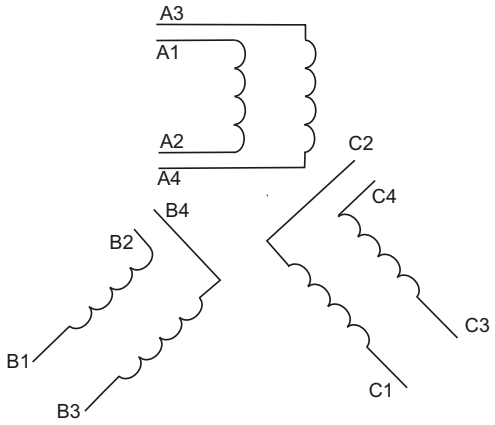


Figure B.5: Phase group winding conventions

Table B.1: Series and parallel Y operating conditions

	Line Volts	Line Amps	Field Amps	Load Angle (deg)	Output kW
series-Y	398	0	33	0	0
series-Y	395	35.2	41.2	36	24
parallel-Y	340	0	62	0	0
parallel-Y	340	33	64	21	19.4

at a low excitation the mini-gen can supply 24 kW. It should be noted that the mini-gen is a short run machine and after 20 min the field winding will over heat at 60 A excitation as discussed in [5].

The open and short circuit tests were performed as in [5] and are presented in Figures B.6 and B.7.

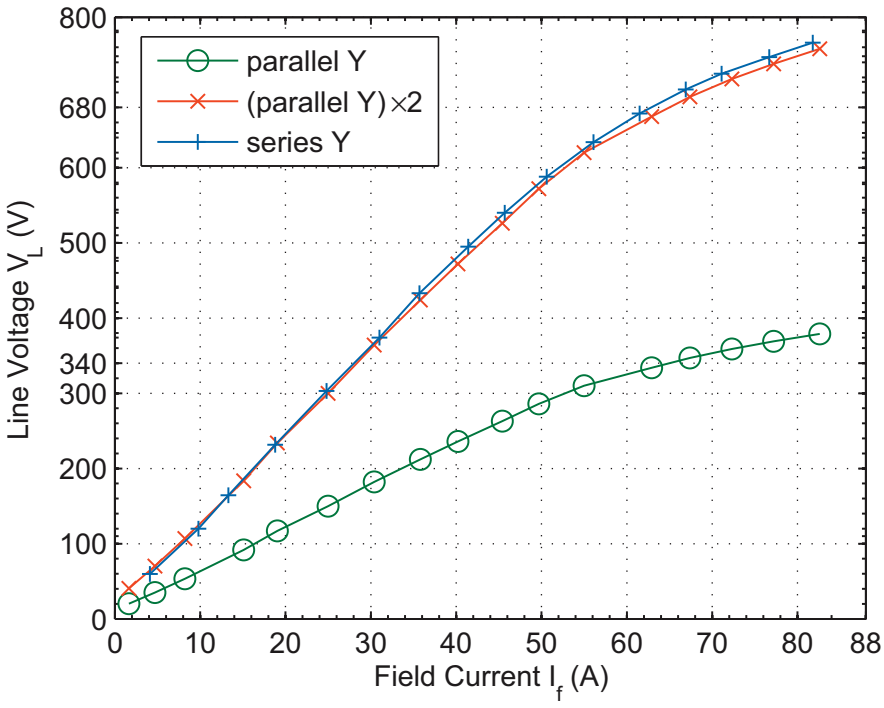


Figure B.6: Open Circuit Characteristic

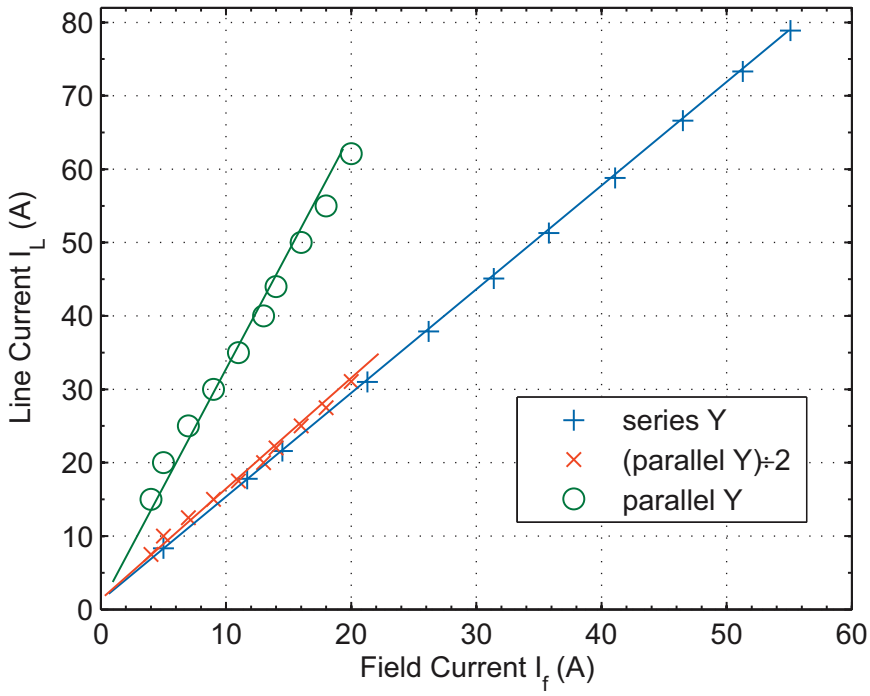


Figure B.7: Short Circuit Characteristic

Appendix C

Measurement of Load Angle

The load angle was measured using the setup in Figure C.1. A speedometer is setup to measure the speed of the shaft and its logical output connected to the scope. The speedometer outputs a square wave as in Figure C.2. Every time the reflective strip passes the speedometer the output goes low. The scope can be set to trigger on the falling edge of this signal. The phase voltage is also measured using the scope. As the line current is increased the phase voltage moves relative to the speedo output on the scope's screen. The load angle is the angle through which the phase voltage signal moves relative to the speedo reference signal. The load angle for two different loads is presented in Table B.1.

This technique was confirmed by performing the measurement using the traditional method. A tacho-generator was connected to one of the mini-gen phases to keep it in synchronism with the shaft speed. The tacho-generator was set to operate at 220V and 50 Hz. The relative angular displacement of a reference line on the shaft was measured as the line current was increased. The two techniques showed good agreement.

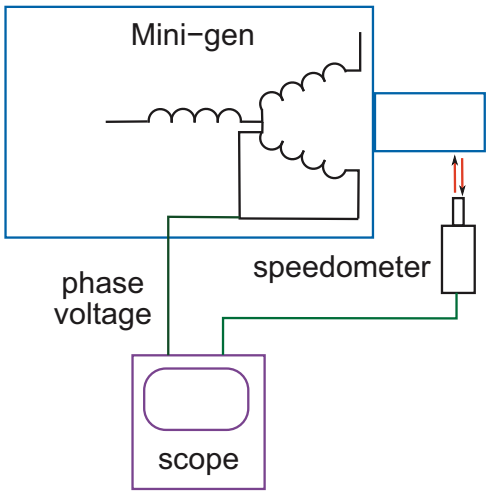


Figure C.1: Setup for load angle measurement

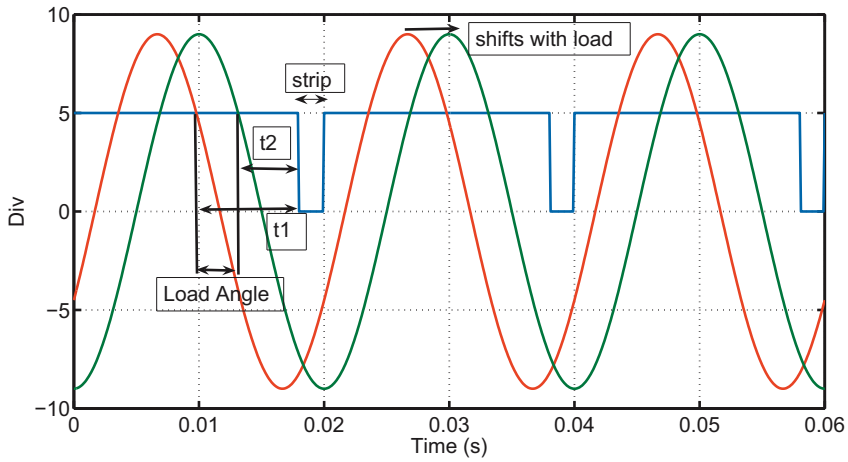


Figure C.2: Waveform displayed on scope

Appendix D

Additional useful information for Maxwell

D.1 Maxwell File Types

Some important file types are:

- *.sm2 - 2D drawing file
- *.ckt - external circuit file
- *.dat - text file with time stamped data
- out*.pjt - folders containing data for field plots
- *.pjt - project folder
- *.bh - text file with BH curve data
- *.mat - text file with material definitions

D.2 Simulation Times

For Maxwell 2D simulations to be feasible the simulation times must not be prohibitive. Working around long simulation times and having suitable hardware are an integral part of running these types of simulations. Thus some user experiences with simulation times and hardware are included here.

The simulation times for transient solutions are very long (hours) while static solutions are very short (minutes). On an Athlon 64 3700+ (socket 939), 1 GB DDR-400 RAM Windows XP x64 system, a transient simulation with 8500 elements, 0.2 ms time step and 360 ms stop time takes approximately 12 hours to complete. A static simulation with 35700 elements takes approximately 35 s to complete.

When choosing a system on which to run Maxwell 2D simulations the following list of components is prioritised in terms of the most important for achieving short simulation times:

1. Fastest 64 bit CPU (usually most GHz and cache)
2. Highest bandwidth between CPU and RAM
3. RAM with highest clock speed

Maxwell 2D uses the MKL (Intel) version of the LAPACK libraries, so it would be expected that Intel CPUs give the best performance. However Ansoft recommend that an Intel Xeon or an AMD Opteron processor be used. It should be noted that CPUs cannot always be rated by their clock speeds. For example an Intel P4 at 2.8 GHz (512 kB cache) was found to be approximately 40% slower than the AMD Athlon 64 3700+ at 2.2 GHz (1 MB cache) on Windows XP 32 bit.

Systems with multiple processors can also help reduce simulation times. Unfortunately a multi-processor license must be purchased separately to make full use of a PC with multiple CPUs. The multi-processor license could reduce the simulation times by 20-25%. Furthermore there is also the possibility of running several simulations at once on a multi-processor (or multi-core) machine without the multi-processor license.

As far as RAM is concerned enough must be free for Maxwell 2D to store the entire solution matrix there. For the above transient simulations Maxwell 2D only used 128 MB of RAM. Even if a small part of the solution matrix is cached on the hard disk the simulation times could be severely lengthened. High bandwidth between the CPU and RAM is also recommended. High frequency RAM is necessary to achieve a high bandwidth with the CPU but is not the only criterion. For example an AMD system with DDR-400 MHz RAM and a 128 bit bus can achieve a higher RAM to CPU bandwidth (14 GB/s) than an Intel system with DDR2-1066 MHz RAM and a 64 bit bus (8 GB/s).

Appendix E

MATLAB files

E.1 Introduction

The following MATLAB files have been used to compute FFTs e.g. of shaft voltages, analyse circulating currents and plot graphs in a format suitable for printing.

E.2 Computing and plotting FFTs

The following function plots FFTs. The user simply enters the magnitude data from a time signal and the sampling frequency which was used to gather the data. A window function is applied to the data and then the FFT is calculated and plotted with a normalised magnitude.

```
function out = plotfft(data,fs, s)
out = [];

%find a window function
window_fn = window(@blackman,length(data));

%multiply by window function
windowed_data = data.*window_fn;

%perform fft
fft_data = fft(windowed_data);
```

```
%find magnitudes
mag_data = abs(fft_data);

%find phase info
phase_data = angle(fft_data);

%plot normalised to 1 curve
max_val = max(mag_data)
%max_val = 10 - maxwell
norm_data = mag_data/max_val;
%norm_data = 20*log(mag_data/max_val);
axis([0 fs/2 0 1.1])
%axis([0 500 1.05*min(norm_data) 0])
hold on
xlabel = 'Frequency (Hz)';
ylabel = 'Magnitude';
grid on
f = 0:fs/(length(fft_data)-1):fs;
plot(f,norm_data, s)
hold off
out.mag = norm_data;
out.f = f;
out.max = max_val;
```

E.3 Analysing circulating currents

The MATLAB function below calculates the phase angle between 2 signals. By detecting the time difference between the zero crossings of the 2 signals and averaging these time differences over many complete cycles the phase difference can be calculated. The signals are first filtered using a zero phase Butterworth filter to eliminate any noise. This aids in detecting zero crossings reliably and improves the accuracy of the algorithm.

```
function out = phasediff(x1, x2, ts)

out = [];
index1 = 0;
```

```
index2 = 0;

%filter the signals
[b,a] = butter(6, 0.1);
x1f = filtfilt(b,a,x1);
x2f = filtfilt(b,a,x2);


%plot(t, x1f, t, x2f)

k=1;
u=1;
for i = 1:length(x1f)-1
        if (x1f(1,i) < 0) && (x1f(1,i+1)>=0)
            index1(1,k) = i*ts;
           k = k + 1;
        end
        if (x2f(1,i) < 0) && (x2f(1,i+1)>=0)
            index2(1,u) = i*ts;
           u = u + 1;
        end
end
%check that the vectors are the same lengths
l1 = length(index1);
l2 = length(index2);
if l1 > l2
    index2(1,l1)=index1(1,l1);
end
if l2 > l1
    index1(1,l2)=index2(1,l2);
end

out.index1 = index1;
out.index2 = index2;
out.f1 = 1/(sum(diff(index2))/length(index2));
out.f2 = 1/(sum(diff(index1))/length(index1));
out.phi = 360*sum(index1-index2)/length(index1)/(1/out.f1);
out.tdiff = sum(index1-index2)/length(index1);
plot(index1-index2)
```

```
function out = circI(i1, i2, ts)

out.line = rms(i1+i2);
out.circI = rms(i1-i2);
out.mag = abs(out.circI)/out.line*100;
phase_data = phasediff(i1, i2, ts);
out.f = (phase_data.f1+phase_data.f2)/2;
out.phi = phase_data.phi;
out.tdiff = phase_data.tdiff;
out
```

E.4 Plotting graphs for publishing

When preparing graphs for publishing it is important to keep their formatting consistent. The function below plots data according to a set template which is suitable for printing on an A4 page.

```
function plotfig(xdata, ydata, xtitle, ytitle,  xlim,
ylim, attr, width, height, xtick, ytick);

%set the default width and height
if not(exist('width'))
    width = 13;
end
if not(exist('height'))
    height = 6.5;
end
if not(exist('attr'))
    attr = 'b-';
end



hold on

%set the font and font size
plotFont = 'Arial';
plotFontSize = 10;
```

```
%create titles
%title(plottitle, 'FontName', plotFont, 'FontSize', plotFontSize)
xlabel(xtitle, 'FontName', plotFont, 'FontSize', plotFontSize);
ylabel(ytitle, 'FontName', plotFont, 'FontSize', plotFontSize);

grid on
box on

%plot the data
plot(xdata,ydata, attr,'LineWidth', 1);

hold off

hf = gcf;

%set the width and height
set(hf, 'Units', 'centimeters');
set(hf, 'Position', [10 10 width height]);

ha = findobj(hf, '-property', 'XGrid');

%some ticks etc
for h = [ha]
    set(h,...
        'FontName', 'Arial',...
        'FontSize', 10,...
        'XMinorTick','on',...
        'YMinorTick','on');
end

ha = gca;
set(ha, 'LineWidth', 0.75);

if exist('xlim')
set(ha, 'XLim', xlim);
end

if exist('ylim')
```

```
set(ha, 'YLim', ylim);
end

if exist('xtick')
set(ha, 'XTick', xtick);
end

if exist('ytick')
set(ha, 'YTick', ytick);
end
```

References

[1] P. L. Alger and W. Samson. "Shaft Currents in Electric Machines." *AIEE Trans.*, pp. 235–245, Feb 1924.

[2] C. Ammann, K. Reichert, R. Joho, and Z. Posedel. "Shaft Voltages In Generators With Static Excitation Systems – Problems and Solution." *IEEE Trans. Energy Conversion*, vol. 3, no. 2, pp. 409–419, Jun 1988.

[3] S. P. Verma, R. S. Girgis, and R. J. Fleming. "Shaft Potentials and Bearing Currents in Modern Turbogenerators: Damages and Means of Prevention." In *Spring Meeting of the Canadian Electrical Association*. Toronto, Ontario, Mar 1981.

[4] D. Busse, J. Erdman, R. J. Kerkman, D. Schlegel, and G. Skibinski. "System Electrical Parameters and Their Effects on Bearing Currents." *IEEE Trans. Ind. Applicat.*, vol. 33, no. 2, pp. 577–584, Mar 1997.

[5] S. J. Hoffe. *Synchronous Generator Fault Diagnosis using Shaft Signal Measurements*. Master's thesis, School of Electrical and Information Engineering, University of the Witwatersrand, Private Bag 3, 2050, Johannesburg, South Africa, 2006.

[6] P. I. Nippes. "Shaft Voltage Current Monitoring System for Early Warning and Problem Detection." *United States Patent No. 6460013 B1*, Oct. 1 2002.

[7] Z. Posedel. "Arrangement for detecting winding shorts in the rotor winding of electrical machines." *United States Patent No. 5006769*, Apr. 9 1991.

[8] R. C. Miller and M. Twerdochlib. "Core Monitor that uses Rotor Shaft Voltages." *United States Patent No. 5032826*, Jul. 16 1991.

[9] S. V. Bowers, K. R. W. Piety, and W. A. Davis. "Proactive Motor Monitoring for avoiding Premature Failures and for Fault Recognition." *United States Patent No. 5680025*, Oct. 21 1997.

[10] R. W. Piety, S. V. Bowers, and D. Q. Gaddis. "System and Method for Measuring and Analyzing Electrical Signals of the Shaft of a Machine." *United States Patent No. 6091236*, Jul. 18 2000.

[11] J.-É. Torlay, C. Corenwinder, A. Audoli, J. Hérigault, and A. Foggia. "Shaft Voltage Analysis: A New Generator Diagnostic Tool." In *Proc. ICEM '98*, pp. 396–401. Sep 1998.

[12] J.-É. Torlay, C. Corenwinder, A. Audoli, J. Hérigault, and A. Foggia. "Analysis Of Shaft Voltages In Large Synchronous Generators." In *Proc. IEEE IEMDC '99*, pp. 607–609. May 1999.

[13] J.-É. Torlay, C. Corenwinder, A. Audoli, J. Hérigault, and A. Foggia. "Analysis of Shaft Voltages and Circulating Currents in the Parallel-Connected Windings in Large Synchronous Generators." In *Electric Power Components and Systems*, vol. 30, pp. 135–149. Feb 2002.

[14] R. Ong, J. H. Dymond, R. D. Findlay, and B. Szabados. "Shaft Current in AC Induction Machine—An Online Monitoring System and Prediction Rules." *IEEE Trans. Ind. Applicat.*, vol. 37, no. 4, pp. 1189–1196, Jul 2001.

[15] P. I. Nippes. "Early Warning of Developing Problems in Rotating Machinery as Provided by Monitoring Shaft Voltages and Grounding Currents." *IEEE Trans. Energy Conversion*, vol. 19, no. 2, pp. 340–345, Jun 2004.

[16] J. S. Hsu and J. Stein. "Shaft Signals of Salient-Pole Synchronous Machines for Eccentricity and Shorted-Field-Coil Detections." *IEEE Trans. Energy Conversion*, vol. 9, no. 3, pp. 572–578, Sep 1994.

[17] J. S. Hsu and J. Stein. "Effects Of Eccenttricites On Shaft Signals Studied Through Windingless Rotors." *IEEE Trans. Energy Conversion*, vol. 9, no. 3, pp. 564–571, Sep 1994.

[18] D. R. Rankin and I. Wilson. "The use of shaft voltage to detect air gap eccentricity and shorted turns in salient pole alternators." *IEE Seventh International Conference on Electrical Machines and Drives, Conf. Publ. No. 412*, pp. 194–197, Sep 1995.

[19] D. de Canha, W. A. Cronje, S. J. Hoffe, and A. S. Meyer. "Construction of a synchronous generator 2D FEM model." *SAUPEC*, January 2007.

[20] D. de Canha, W. A. Cronje, S. J. Hoffe, and A. S. Meyer. "Finding the Optimal Mesh: Results from different meshes in Maxwell 2D." *SAUPEC*, January 2007.

[21] D. de Canha, S. J. Hoffe, A. S. Meyer, and W. A. Cronje. "The Use of an Electromagnetic Finite Elements Package to Aid in Understanding Shaft Voltages in a Synchronous Generator." *IEEE PES PowerAfrica Conference and Exhibition*, Jul 2007.

[22] D. de Canha, S. J. Hoffe, A. S. Meyer, and W. A. Cronje. "Methods for diagnosing static eccentricity in a synchronous 2 pole generator." *IEEE PES Powertech Conference*, Jul 2007.

[23] *Ansoft Corporation*. URL http://www.ansoft.com/. Last accessed: March 2006.

[24] S. J. Salon. *Finite Element Analysis of Electrical Machines*. Kluwer Academic Publishers, 1995.

[25] Ansoft Corporation. *Maxwell 2D Student Version - Getting Started: A 2D Magnetostatic Problem*. URL http://www.ansoft.com/maxwellsv/MaxwellSV_Magnetostatic.pdf. Last accessed: October 2006.

[26] Ansoft Corporation. *Maxwell 2D Student Version - Getting Started: A 2D Electrostatic Problem*. URL http://www.ansoft.com/maxwellsv/MaxwellSV_Electrostatic.pdf. Last accessed: October 2006.

[27] Ansoft Corporation. *Maxwell 2D Version 11 - Online Help*, 2006.

[28] W. N. Fu, P. Zhou, D. Lin, S. Stanton, and Z. J. Cendes. "Modeling of Solid Conductors in Two-Dimensional Transient Finite-Element Analysis and Its Application to Electric Machines." *IEEE Trans. Magnetics*, vol. 40, no. 2, pp. 426–434, March 2004.

[29] P. Zhou, D. Lin, W. N. Fu, B. Ionescu, and Z. J. Cendes. "A General Co-Simulation Approach for Coupled Field-Circuit Problems." *IEEE Trans. Magnetics*, vol. 42, no. 4, pp. 1051–1054, April 2006.

[30] K. Dhuness. *An investigation into aspects of the online detection of broken rotor bars in induction motors*. Master's thesis, Department of Electrical and Electronic Engineering, University of Johannesburg, 2006.

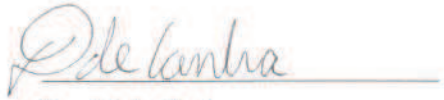
[31] D. G. Dorrell and A. C. Smith. "Calculation of U.M.P. in Induction Motors with series or parallel winding connections." *IEEE Trans. Energy Conversion*, vol. 9, no. 2, pp. 304–310, June 1994.

[32] G. J. Coetzee. "CIGRE Study Committee A1 - Current Activities and Long Term Objectives." *CIGRE Electra No. 233*, pp. 9–12, Aug 2007.

Declaration

I declare that this dissertation is my own, unaided work, except where otherwise acknowledged. It is being submitted for the degree of Master of Science in Engineering in the University of the Witwatersrand, Johannesburg. It has not been submitted before for any degree or examination in any other university.

Signed this 18th day of May 2012



Daniel de Canha